Thèse n° 9173

Mechanical Reinforcement of Hydrogels through Physical Crosslinks and Double Network Granular Architecture

Présentée le 5 avril 2022

Faculté des sciences et techniques de l'ingénieur
Laboratoire de la matière molle
Programme doctoral en science et génie des matériaux

pour l'obtention du grade de Docteur ès Sciences

par

Alvaro Lino Boris CHARLET

Acceptée sur proposition du jury

Prof. C. Hébert, présidente du jury
Prof. E. Amstad, directrice de thèse
Prof. C. Creton, rapporteur
Prof. N. Holten-Andersen, rapporteur
Prof. F. Stellacci, rapporteur

École
polytechnique
fédérale
de Lausanne

2022

Le destin bat les cartes mais c'est nous qui les jouerons.

La longue route, Seul entre mers et ciels
Bernard Moitessier

Acknowledgments

First and foremost, I would like to thank my advisor Prof. Dr. Esther Amstad for her continuous support and advice during my master and doctoral studies. She provided me with extraordinary freedom to explore new scientific subjects, while supporting my work with her strong expertise in soft matter. She always pushed our work to be presented and written at the highest academic level, which I greatly appreciated. She also generously funded any laboratory equipment or consumable that I desired to establish this work. Moreover, I would also like to acknowledge her strong support to prepare for my future entrepreneurial endeavour.

I would then like to extend my gratitude to Prof. Dr. Francesco Stellacci, Prof. Dr. Costantino Creton, and Prof. Dr. Niels Holten-Andersen for agreeing to be part of my thesis examination committee as well as Prof. Dr. Cécile Hébert for chairing the examination.

I want to thank all past and current members of the Soft Materials Laboratory, also know as the SMaL group. First, I would like to acknowledge Matteo Hirsch with whom I had the great pleasure to do research with, shared many fruitful discussions, and travel to foreign countries. I greatly appreciated the kind environment established by Antoine Vian and Gianluca Etienne in the early days of the lab, when I first joined as a semester student. I am delighted to see that all following members embraced the friendly and collaborative spirit, including Mathias Steinacher, Huachuan Du, Jui-Chia Chang, Michael Kessler, Aysu Okur, Amin Hodaei, Chuen-Ru Li, Ran Zhao, Eva Baur, Francesca Bono, Gaia De Angelis, Pauline Pradal, Alexandra Thoma, Tianyu Yuan and Lorenzo Lucherini.

I would like to warmly thank Mercedes Quintas, our secretary, with whom I had the pleasure to share an office the past 4 years, for her enormous support, constant availability, and joyful discussions.

I would also like to acknowledge all the students that worked with me, and helped in the

progress of my research. This includes Emilie Vuille-dit-Bille, Stella Laperrousaz, Camille Daganaud, Paolo Pedrazzini, Francesca Bono, Sanjay Schreiber and Joëlle Piot.

An indispensable acknowledgement goes to the EPFL staff who have made the PhD experience so pleasant. In the particular, the secretariat and the management of the Institute of Materials who work relentlessly to make this place so welcoming and promoting all of us to make the best of our time here. I would also like thank the staff of the shared characterization platforms of EPFL. Their valuable help and support greatly benefit our research community. This includes Dr. Arnaud Magrez for his expertise on Raman spectroscopy, Dr. David Bi for XRD crystallography, Danièle Laub and Fabienne Bobard for SEM imaging and Xavier Dutoit for taking care of the reception of chemicals.

Certainly, I want to thank my excellent collaborators. Dr. Viviane Lutz Bueno taught me a lot on SAXS characterization and helped me design experiments. Prof. Dr. Rafaelle Mezzenga greatly helped me in the drafting of a manuscript.

I would like to thank all my dear friends of Lausanne and beyond, that bring such happiness to my life. I would like to particularly thank Malika for the beautiful shared years of adventures and experiences, and for the discussion that led me to start a PhD.

Mainly, I want to thank my parents Barbara and Laurent for all the support they gave me ever since. They managed to triggering my curiosity for science in the natural world, that eventually led to pursue my academic studies. I warm thanks also goes to my sister, Anaïs, with whom I have spent so much fun time over the years. I have tremenduous gratitude also to my family in Basel, Ute and Daniel who I look to as my second set of parents; to my grandmother Margit for her kindness; and to my family in Ardèche, Blaise et Jocelyne for sharing with me their passion for arts and wine making.

And last but not least, I would like to thank Sedona, for her unconditional love in the past years. She has undoubtedly believed in me and I look forward to many more beautiful adventures together.

Abstract

Throughout nature, organisms fabricate a myriad of materials to sustain their lifestyle. Many of the soft materials are composed of water-swollen networks of organic molecules, so-called hydrogels. They generally contribute to the mechanical integrity of the organism, and act as scaffolds for living cells. The ability to fabricate synthetic hydrogels that mimic their natural counterparts would greatly benefit the biomedical field. In particular, synthetic hydrogels have the potential to revolutionize tissue engineering and to enable the fabrication of functional load-bearing soft implants. However, available hydrogels suffer from poor mechanical properties, as they are either too brittle or too soft. While great effort in the field of soft matter has been devoted to the development of hydrogels with improved mechanical properties, they are often not compatible with state-of-the art manufacturing techniques such as additive manufacturing.

In this thesis, I present the mechanical reinforcement of hydrogels using two distinctive strategies, and demonstrate their potential as 3D printable materials. I first investigate the use of high functionality crosslinks in metal-coordinated hydrogels. I show that this crosslinking strategy greatly improves the solid-like mechanical properties of viscoelastic gels. I then present the use of hydrogel microparticles to fabricate double network granular hydrogels. I discovered that these materials exhibit an extraordinarily high strength and toughness. Furthermore, the jammed microparticle precursor ink enables the extrusion and 3D printing of this material. This allows the fabrication of hydrogels with locally varying compositions, which can be utilized for example to design stimuli responsive materials. I leverage the granular structure to design recyclable double network granular hydrogels. This is achieved by forming a percolating network that has reversible covalent bonds. I show that this method can be extended to the fabrication of degradable hard plastics. Finally, I conclude by presenting the key findings, and I present a few possible follow-up ideas to further develop the field of load-bearing hydrogels.

In summary, I provide several solutions to combine mechanical reinforcement of hydrogels,

and state of the art 3D printing. I believe that soft material science will greatly benefit the development of complex materials for novel biomedical and soft robotic applications.

Keywords: *hydrogels, soft materials, double networks, 3D printing*

Zusammenfassung

In der Natur erzeugen Organismen eine Vielzahl von Materialien durch unterschiedliche Stoffwechselprozesse, um ihre Lebensweise zu sichern. Viele dieser weichen Materialien bestehen aus wassergesättigten Netzwerken organischer Moleküle, den sogenannten Hydrogelen. Sie tragen im Allgemeinen zur mechanischen Integrität des Organismus bei und dienen als Grundgerüst für lebende Zellen. Die Fähigkeit, synthetische Hydrogele herzustellen, die ihre natürlichen Gegenstücke nachahmen, wäre für die Biomedizin von großem Nutzen. Insbesondere haben synthetische Hydrogele das Potenzial, die Gewebezüchtung zu revolutionieren und die Herstellung funktioneller, tragfähiger weicher Implantate zu ermöglichen. Die verfügbaren Hydrogele besitzen jedoch bis jetzt schlechte mechanische Eigenschaften, d. h. sie sind entweder zu brüchig oder zu weich. Obwohl auf dem Forschungsgebiet der weichen Materie große Fortschritte gemacht wurden, um Hydrogele mit verbesserten mechanischen Eigenschaften zu entwickeln, sind diese oft nicht mit modernen Herstellungsverfahren wie der additiven Fertigung vereinbar.

In dieser Dissertation wird die mechanische Verstärkung von Hydrogelen mit Hilfe zweier unterschiedlicher Mechanismen vorgestellt und die Eignung der Gele als 3D-druckbare Materialien aufgezeigt.

Zunächst wurde der Einfluss von hochfunktionalen Vernetzungen auf die mechanischen Eigenschaften metall-koordinierter Hydrogelen untersucht. Dabei konnte gezeigt werden, dass diese Vernetzungsstrategie die festkörper-ähnlichen mechanischen Eigenschaften von viskoelastischen Gelen erheblich verbessert. Im Weiteren wurde die Verwendung von Mikropartikeln zur Herstellung von Hydrogele mit doppeltem Netzwerk erforscht, die diesen Materialien zu einer außergewöhnlich hohen Festigkeit und Zähigkeit verhelfen. Darüber hinaus ermöglicht die Vorläufer-Tinte aus gestauten Mikropartikeln die Extrusion und den 3D-Druck dieses Materials. Dies gewährleistet die Herstellung von Hydrogelen mit lokal unterschiedlichen Zusammensetzungen, die zum Beispiel für die Entwicklung von Materialien genutzt werden können, die auf bestimmte Anreize reagieren sollen.

Um wiederverwendbare granulare Hydrogele mit doppeltem Netzwerk zu erhalten wurden eine granulare Struktur angestrebt, die durch die Bildung eines perkolierenden Netzwerks erreicht wir, das reversible kovalente Bindungen besitzt. Dabei konnte gezeigt werden, dass diese Methode auch auf die Herstellung abbaubarer Hartkunststoffe erweitert werden kann.

Zusammenfassend stelle ich mehrere Lösungsansätze vor, um die mechanische Verstärkung von Hydrogelen und den modernen 3D-Druck zu kombinieren, dabei werden die wichtigsten Forschungs-Ergebnisse und einige mögliche weiterführende Ideen diskutiert, um den Bereich der tragenden Hydrogele weiterzuentwickeln. Ich bin davon überzeugt, dass die weiche Materialwissenschaft einen entscheidenden Beitrag zur Entwicklung komplexer Materialien für neuartige biomedizinische sowie weiche Roboter-Anwendungen leisten kann.

Stichwörter: *Hydrogele, weiche Materialwissenschaft, doppelte Netzwerke, 3D-Druck*

Résumé

Dans la nature, les organismes vivants fabriquent un grand nombre de matériaux pour survivre. Parmi eux, les hydrogels, qui sont des matériaux souples composés de réseaux de molécules organiques gorgés d'eau. Ils contribuent à l'intégrité mécanique de l'organisme et servent d'échafaudages pour les cellules. La capacité à fabriquer des hydrogels synthétiques qui imitent leurs homologues naturels serait très utile dans le domaine biomédical. En particulier, les hydrogels synthétiques ont le potentiel de révolutionner l'ingénierie tissulaire et de permettre la fabrication d'implants souples résistants aux contraintes, utiles à l'orthopédie. Cependant, les hydrogels ne sont actuellement que rarement utilisés faute de propriétés mécaniques suffisantes, car ils sont soit trop fragiles, soit trop mous. Alors que de grands efforts dans le domaine de la matière molle ont été consacrés au développement d'hydrogels aux propriétés mécaniques améliorées, ces derniers ne sont souvent pas compatibles avec les techniques de fabrication de pointe telles que l'impression 3D.

Dans cette thèse, je présente les résultats de mes recherches pour renforcer la mécanique des hydrogels à travers deux stratégies distinctes. Dans un premier temps, j'étudie l'utilisation de complexes organométalliques à haute fonctionnalité qui réticulent le réseau organique de l'hydrogel. Je montre que cette stratégie de réticulation améliore considérablement les propriétés mécaniques des hydrogels viscoélastiques. Par la suite, je présente l'utilisation de microparticules pour fabriquer des hydrogels à double réseau. J'ai découvert que ces matériaux présentent une résistance et une ténacité extraordinairement élevées. De plus, le précurseur de ce matériau, formé de microparticules concentrées, forme une pâte dont le comportement rhéologique permet l'extrusion et l'impression 3D. Cela permet de fabriquer des hydrogels dont la composition varie localement, ce qui peut être utilisé, par exemple, pour concevoir des matériaux réagissant à des stimuli. J'exploite ensuite cette structure granulaire pour concevoir des hydrogels recyclables. Ceci est réalisé en formant un réseau percolant les microparticules qui possède des liaisons covalentes réversibles. Je montre que cette méthode peut être étendue à la fabrication de plastiques

durs dégradables.

Je conclus en présentant les principaux résultats de mes recherches, ainsi que de nouvelles pistes pour développer plus encore la mécanique des hydrogels.

En résumé, je propose plusieurs solutions pour combiner le renforcement mécanique des hydrogels et l'impression 3D. Je pense que le développement de matériaux complexes pour des nouvelles applications biomédicales et robotiques souples profitera grandement de la science des matériaux souples.

Mots-clés: *hydrogels, science des matériaux souples, matière molle, doubles réseaux, impression 3D*

Contents

CHAPTER 1

Introduction

1.1 Length scale in material science

The field of material science aims at designing new materials with novel properties, or combinations thereof, by understanding the underlying physical and chemical mechanisms governing the material's response to external stimuli [1]. The invention of means to observe, and measure, the micro and nano-structure of a material has driven our understanding at those length scales. In materials composed of crystalline structures, the composition and arrangement of atoms down at the Angström scale directly reflects into its macroscopic properties, such as the resistivity or absorption of a material. The assembly of the crystalline domains at the micro scale into macroscopic materials is also key, in particular for the mechanical properties [2]. For example, the engineering of the grain structure of metals and ceramics has driven their use for load-bearing applications [3]. Similarly, the mechanical properties of hydrogels are governed by the arrangement of the polymer network, and how they are crosslinked and assembled into a macroscopic material [4]. In this thesis, we aim to build on the established knowledge at the nanoscale to explore the material's assembly at a larger scale. We first explore a physically crosslinked hydrogel with high functionality crosslinks that are several tens of nanometers in diameter. We will then study granular hydrogels composed of particles that are tens of micrometer in diameter. Finally, we will demonstrate the use of the these microparticles as building blocks for the fabrication of macroscopic recyclable materials.

1.2 Applications of hydrogels

1.2.1 Biomedical applications

Hydrogels are frequently used in biomedicine, for example for wound healing [5], as drug carriers [6], and in tissue engineering to support cell culture[7, 8] or cartilage replacements [9]. Hydrogels are intrinsically similar to many natural tissues, making them an ideal choice for biocompatible materials [10].

Tissue engineering applications often require the precursors to possess multiple functionalities, be biocompatible, degradable [11], and injectable [12]. Moreover, their processing into superstructures must be biocompatible [13]. The resulting superstructures must enable cells to proliferate through percolating pores such that they can populate the entire scaffold over time [14], and possess locally tunable chemistries, including biochemical and mechanical gradients [9, 15, 16], to direct cell differentiation and growth. In addition, they should have specific viscoelastic properties that drive proper cell fate and activity. These time-dependent mechanical properties, in particular stress relaxation and creep, impact cell behaviors such as cell spreading, proliferation, and differentiation [17, 18, 19] and are thus imperative to control if scaffolds are used for tissue engineering. Unfortunately, the design of hydrogels that meet all these requirements is challenging. Granular hydrogels, which we will discuss further in section 1.8, are increasingly often used as substrates for biological applications [20, 21], because they fulfill many of the above mentioned requirements. Hydrogels used for tissue engineering are typically soft and degradable such that cells can remodel them or grow their own extracellular matrix (ECM) within them. These features are especially important if hydrogels are used as scaffolds for the growth of functional organoids [22], neural interfaces [23] or cartilage [24]. The viability and fate of cells can be tuned through the addition of appropriate chemical receptors, growth factors, and nutrients [11]. This can be achieved by infiltrating these compounds into granular hydrogels, or by chemically linking them to well-defined microgels to locally vary their concentration.

In many biomedical applications, the mechanical properties of the material are key. Sometimes, the limited mechanics are even the main reaason that prevents a widespread use [25, 4]. As an example, in the field of orthopaedics, hydrogels have been explored as tissue replacement for damaged cartilage repair [26]. However, many of the reported hydrogels do not match the extraordinary high mechanical properties of natural human cartilage. The development of a tough, stiff, low hysteresis, low wear, yet fatigue resistant hydrogel would tremendously contribute to the development of cartilage repair materials, which would greatly benefit the lives of patients with articulation injuries or illnesses [27]. As

another example, the recent development of granular hydrogels with strong wet adhesion to tissues, combined with good mechanical properties show tremendous potential as surgery sealant glue [28]. More viable applications of this material emerge following the development of hydrogels with good mechanical properties. As a result, hydrogels are being envisioned beyond the biomedical field.

1.2.2 Soft robotics

Hydrogels have been effectively used in the fabrication of soft robots [29, 30, 31], for their intrinsic resemblance to water-based materials found in the natural world. Soft robots offer unique opportunities in areas were traditional rigid robots are not viable. They are composed of a mixture of soft sensors [32], actuators [33, 34, 35], controls and power systems [36]. Soft robots represent an emergent field of research aiming at bringing a closer interaction between humans and machines [37, 38]. For example, they are capable of mimicking the motion of organisms found in nature, unlike their rigid predecessors. As a result, they can safely interact with humans, to be used for example in assistive surgery [39], in prosthetics as artificials limbs [40], as wearable muscular support [41], or even as ocean exploring machines [36]. The development of soft robots requires several technological advances, among which material science plays a key aspect.

1.3 Common hydrogels

1.3.1 Natural polymers for hydrogels

Living organisms commonly manufacture hydrophilic polymers, often used as mechanical reinforcement of their tissues. Naturally derived polymers, or biopolymers, are therefore widely used in the synthesis of hydrogels, as they are highly biocompatible. In biological applications, many of them can be degraded and absorbed by the metabolism of the host organism. Furthermore, they generally provide plenty of reactive sites used to chemically functionalize them as new crosslinking sites for mechanical reinforcement, or to anchor biologically active molecules. Naturally produced structural polymers can be classified into polypeptides, which are assembled from amino acids, and polysaccharides, which are assembled from simple sugars.

Amid the plethora of biopolymers, hydrogels are often synthesized from polypetides such as collagen, gelatin, fibrin, or from polysaccharides such as alginate, hyaluronic acid, agarose, cellulose, and chitosan. However, a common limitation of biopolymers is the

limited tunability of their properties [42], and the batch to batch reproducibility issues arising from bio-sourced reagents [43].

1.3.2 Synthetic polymers for hydrogels

Well-defined hydrogels whose properties can be precisely tuned can be fabricated from polymers synthesized from small reactive synthetic molecules, known as monomers, as shown in Figure 1.1. Following the initiation of the reaction scheme, many monomers with single reactive groups assemble linearly into polymeric chains. Interconnecting these chains, known as crosslinking, establishes the polymeric networks. We will discuss in detail various crosslinking strategies in section 1.6. Additionally, chain entanglement can be used as reinforcement method to fabricate strong elastic networks [44].

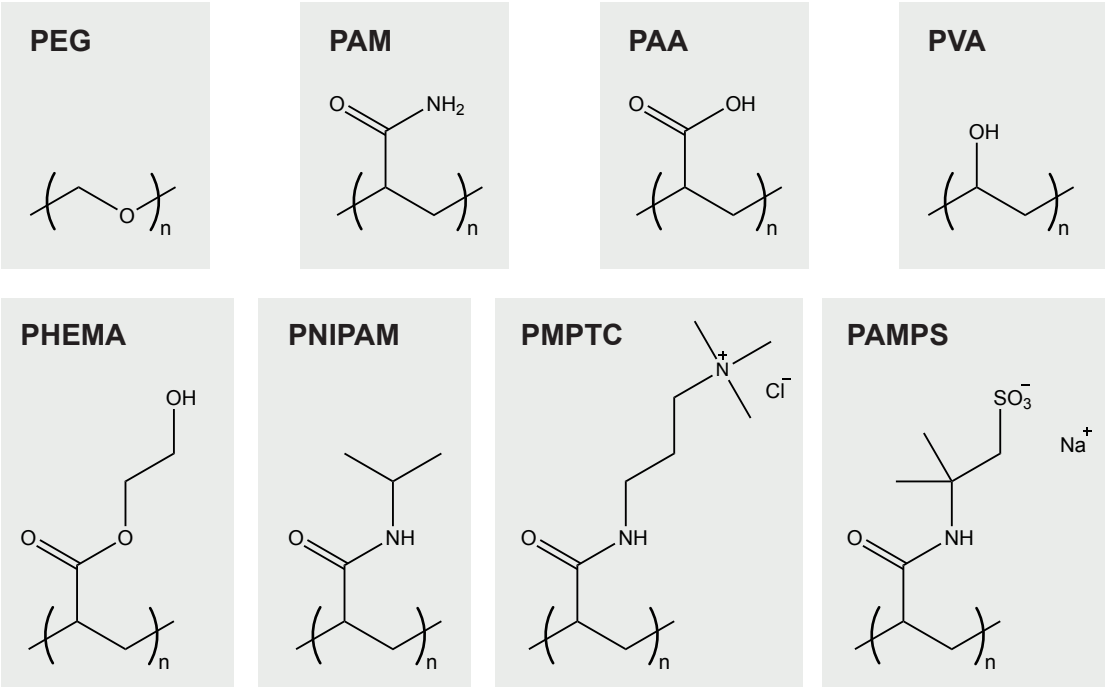

Figure 1.1: Chemical structure of common synthetic polymers used for hydrogel synthesis.

Pre-polymerized chains can be either crosslinked using chemical groups intrinsically present on the monomers, such as with poly(vinyl alcool) (PVA)[45], or by functionalizing the polymer specifically for this purpose. A prominent example of the latter is poly(ethylene glycol) (PEG), commonly used as a linear or multi-arm oligomer with molecular weights ranging from 700 Da to 20 kDa. The PEG chain is relatively inert, making it highly biocompatible. PEG can be end-functionalized with unsaturated groups, such as acrylates and methacry-

lates, to be used as reactive macro-crosslinker or as macro-monomer to form hydrogels by UV-induced polymerization[46, 47]. Alternatively, the end groups can be modified with various reactive pairs, such as N-hydroxysuccinimide/NH_2[48], maleimide/thiols[49], acetylene/azide[50]. These functional pairs have usually high reaction efficiency and fast reaction kinetics, such that the PEG chains are rapidly assembled into relatively well-defined network architectures[51]. PEG chains can also be functionalized with molecules to form physically crosslinked networks, such as nucleobase pairs[52], host-guest molecules[53], or ion-chelating molecules[54, 55].

Alternatively, monomers can be polymerized, and simultaneously crosslinked into a network. A molecule with multiple reactive sites referred as crosslinker is co-polymerized alongside the monomer, to form bridges between polymeric chains. Acrylates and methacrylates are commonly used as reactive groups for this method. Resulting polymers include poly(acrylamide) (PAM), poly(acrylic acid) (PAA)[56], poly(hydroxyethylmethacrylate) (PHEMA), poly(N-isopropylacrylamide) (PNIPAM), poly((3-(methacryloylamino)propyl)trimethylammonium chloride) (PMPTC) or poly(sodium 2-acrylamido-2-methyl-1-propanesulfonate) (PAMPS), as shown in Figure 1.1.

1.4 Basic concepts of mechanical reinforcement of hydrogels

The study of the mechanical performance of an engineered material is by far and away most usefully done using tensile tests. The mechanical performance is defined in terms of scalar-valued material properties extracted from the characteristic stress-strain response. Common measures include the stiffness and strength of a material. It is here important to point out that these properties are assumed to be time independent, and that they are extracted from a quasi-static tensile test. While this assumption is valid for classical engineered materials such as metals and ceramics, polymers and in particular gels are much more prone to have rate-dependent properties. In the case where time strongly affects properties, oscillatory tests can be done to further quantify rate-dependent mechanical properties.

In the case of hydrogels, we distinguish two regimes that define which tool is the more adequately fitted to measure the mechanical performance. On the one hand, covalently crosslinked hydrogels are fully crosslinked through permanent bonds, and have therefore a reduced tendency to have time-dependent properties. They are therefore often characterized as hookean solids using a quasi-static tensile test approach, as elaborated in sections 1.4.1 - 1.4.3. In particular, hydrogels with a Young's modulus superior to 10 kPa, can be reliably characterized. On the other hand, hydrogels with non-permanent crosslinks,

will display rate dependent mechanical properties. We will discuss in section 1.4.4 how to tackle the characterization of these soft materials.

1.4.1 Stiffness

The stiffness of a material is defined by the energy required to deform elastically the volume of a material along one axis, and is characterized by the Young's Modulus E in units of Pascal (Pa). In practice, E quantifies the linear relationship between stress, and the deformation of a material, according to Hooke's law:

$$E = \frac{\sigma}{\varepsilon} \tag{1.1}$$

where σ is the stress (force per unit area), and ε is the strain (proportional deformation).

1.4.2 Strength

The ultimate strength of a material is defined by the maximum stress it can withstand prior to failure. It is the intrinsic critical stress that will enable a crack to propagate through the material. Multiple types of strengths such as tensile strength, compressive strength, and shear strength have been used to characterize materials. We will focus in this thesis primarily on the tensile strength of hydrogels due to two main reasons. (1) The various types of strengths are correlated to each other. For example, the uniaxial compressive tension correlates to the bi-axial tensile tension of the sample [27]. (2) The tensile strength is easier to measure than the shear strength, and it is less affected by boundary conditions than the compressive strength [27]. The tensile strength σ_T is defined as:

$$\sigma_T = \frac{f_T}{a} \tag{1.2}$$

where f_T is the maximum tensile force the sample can withstand, and a is the cross section of the sample.

1.4.3 Toughness

The energy dissipation in a material dictates its resistance to sudden failure. Classically, the energy dissipation is described either by the fracture toughness, herein simply "toughness", or the fracture energy. The toughness is defined as the critical energy required to break a material, therefore in units of $\mathrm{J{\cdot}m^{-3}}$.

$$T = \int_0^{\varepsilon_f} \sigma \, d\varepsilon \tag{1.3}$$

where T is the toughness, ε_f is the fracture strain, and σ is the stress.

The fracture energy, is defined as the critical energy release required to cause a pre-cut crack to extend, in units of J·m^{-2}. This corresponds to the energy cost of breaking bonds at the crack tip. The Lake-Thomas theory predicts that the ideal fracture energy G_c, can be calculated as follows:

$$G_c = \rho \cdot n \cdot U \tag{1.4}$$

where ρ is the area density of polymer chains on fractured surfaces, U is the bond dissociation energy, and n is the average number of monomer units between crosslinks. Therefore, failure of the network scales with broken bonds at the crack tip.

1.4.4 Viscoelasticity

As mentioned in section 1.4, the mechanical properties of soft materials are often time-dependent. Unlike stiffer materials, whose mechanics are governed by the linear-elastic contribution of covalent bonds, many soft hydrogels have additionally a viscous contribution on the same order as the elastic contribution. So-called viscoelastic materials, are neither linear-viscous, or newtonian fluids, nor are they linear-elastic, or hookean solids. They represent a twilight zone, away from the ideal behavior of common engineered materials [57]. Therefore, scientists cannot rely on simple quasi static tensile tests, and have developed more complex time-dependent tests. Two of these tests are outlined in Figure 1.2: stress relaxation, and oscillatory strain. They are typically used to test soft hydrogels using a shear geometry on a rheometer.

In a stress relaxation experiment, a constant angular displacement is applied on a material while a shear cell measures its torque response, from which the constant strain γ_0 and the stress $\sigma(t)$ are calculated as a function of time. This data is combined to generate the relaxation modulus $G(t)$ of the material:

$$G(t) = \frac{\sigma(t)}{\gamma_0} \tag{1.5}$$

While a stress relaxation test provides a good analysis of the rearrangement mechanisms

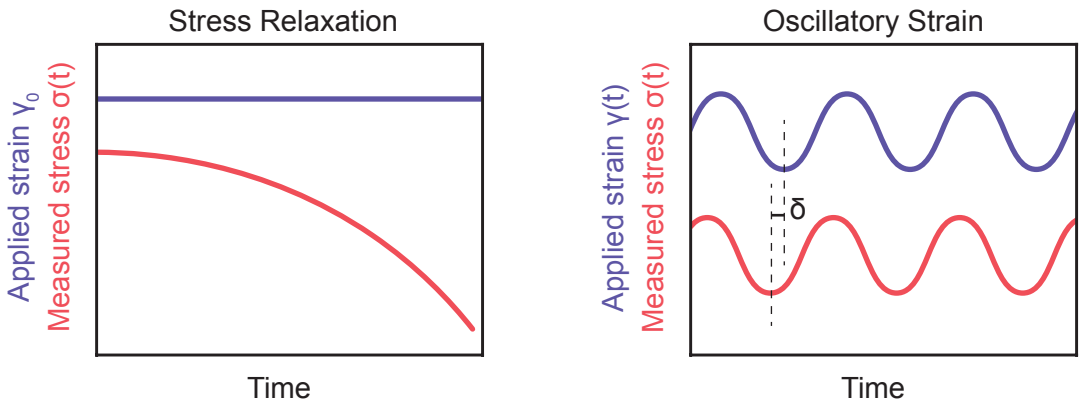

Figure 1.2: Two common mechanical tests performed on viscoelastic materials. (**left**) A stress relaxation test measures the shear stress upon an initial step strain applied to the material. (**right**) An oscillatory strain test measures the shear stress while an oscillatory strain is applied to the material.

in a polymeric network at long time scales, it fails to provide meaningful information at short time scales. Scientists have therefore developed an oscillatory test, in which the instrument applies a sinusoidal strain $\gamma(t) = \gamma_0 \sin(\omega t)$ with angular frequency ω, typically in the range of 10^{-2} - 10^{2} rad·s^{-1}. The instrument measures in the linear regime a sinusoidal stress $\sigma(t) = \sigma_0 \sin(\omega t + \delta)$ that has an identical frequency ω but which may be phase-shifted by an amount δ. This data is converted into a complex modulus $G^* = G' + iG''$ by separating the stress into two components: a part that is in phase with the applied strain, and an out-of-phase part:

$$\sigma(t) = \sigma_0 \sin(\omega t + \delta) \tag{1.6}$$

$$\sigma(t) = \sigma_0 \left(\sin(\omega t)\cos(\delta) + \cos(\omega t)\sin(\delta)\right) \tag{1.7}$$

$$G' \equiv \frac{\sigma_0}{\gamma_0}\cos(\delta); \quad G'' \equiv \frac{\sigma_0}{\gamma_0}\sin(\delta) \tag{1.8}$$

$$\sigma(t) = \gamma_0 \left(G' \sin(\omega t) + G'' \cos(\omega t)\right) \tag{1.9}$$

The in-phase part G', referred as storage modulus, originates from the elastic contribution of the network at each frequency, while the out-of-phase part G'', referred as loss modulus, arises from inelastic dissipation. In a typical frequency sweep oscillatory strain experiment, G' and G'' are reported as a function of the oscillation frequency ω. If $G'(\omega) > G''(\omega)$, the material elastically stores more energy than it dissipates, resulting in a solid-like behavior. On the contrary, if $G'(\omega) < G''(\omega)$, the material dissipates more energy than it stores, resulting in a fluid-like behavior. Some viscoelastic materials might be fluid-like at certain frequencies, but solid-like at others, such as metal-coordinated hydrogels. We

will discuss this further by focusing on the crosslinking mechanism in section 1.6.3. The reciprocal of the characteristic frequency ω_c, where $G'(\omega) = G''(\omega)$, is the characteristic relaxation time τ_c of such materials. However, some materials cannot be naively described by a single relaxation time. The full distribution of relation times can be described by a relaxation spectrum $H(\tau)$, which quantifies the amount of stored and dissipated energy under dynamic loading at frequency ω. It can be effectively seen as an infinite parallel series of Maxwell elements, along the time axis, as shown schematically in Figure 1.3. Each Maxwell element may be thought as a characteristic relaxation mode in a material, with a resonant frequency given by $1/\tau$ [55].

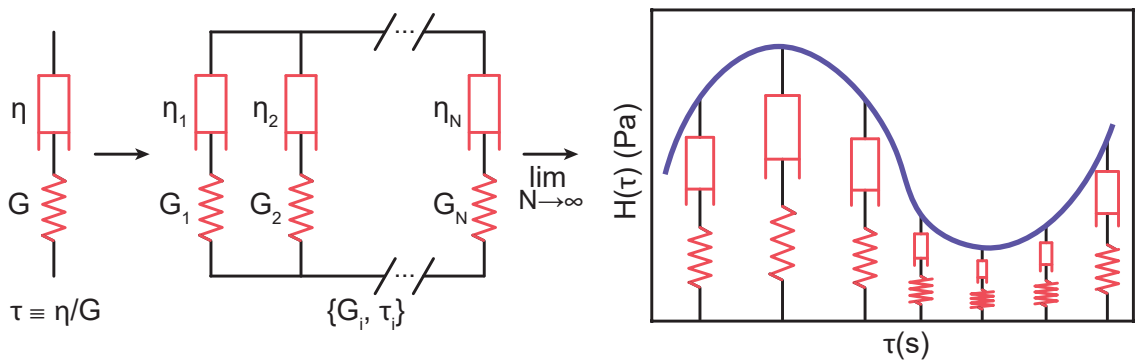

Figure 1.3: Relaxation spectrum of viscoelastic materials. A single Maxwell element, a spring with normalized spring stiffness G (units Pa) in series with a dashpot with normalized damping coefficient η (units Pa·s). The characteristic relaxation time of the Maxwell element is given by the ratio $\tau = \eta/G$; a parallel series of N Maxwell elements can be described by a set of spring stiffnesses and relaxation times $\{G_i, \tau_i\}$. In the limit where $N \to 1$, the discrete set of parallel Maxwell elements becomes a continuous function, the relaxation spectrum $H(\tau)$. Adapted with permission from [55].

We will discuss further in chapter 4 how we can use both the stress relaxation test and the oscillatory strain to understand underlying relaxation mechanisms in the hydrogel network. Furthermore, we will investigate how we can tune the crosslinking of the network to target different relaxation spectra with contrasting rheological properties.

1.5 Design principles

The mechanical properties of a material are quite often the limiting factor when engineering an object. But what if we could create hydrogels that are strong enough to be used as orthopedic implants for example? As discussed in section 1.2, future applications of hydrogels are often limited by the poor mechanical properties of current solutions. And just like in other material classes, a given application might require a specific property

to be especially high. In this section, we will present general principles for the rational design of hydrogels with exceptional mechanical properties, focusing on high strength and high toughness. Engineered applications might require other interesting properties such as high resilience, adhesion, fatigue-resistant adhesion, and fatigue resistance [27], however these are outside the scope of this thesis.

1.5.1 Hydrogels with high toughness

The requirements to achieve high toughness in hydrogels are generally the same as in other engineered materials such as ceramics, metals, composites and polymers. That is to both dissipate mechanical energy and deform without fracturing [58], such that a large dissipative zone develops around the crack tip prior to crack propagation [27]. In brief, the design principle for tough hydrogels is to build dissipation into stretchy polymer networks [59].

Following the pioneering work on double networks [60], interpenetrating, and semi-interpenetrating polymer networks [61, 62] have been widely used for the development of tough hydrogels [63, 64]. In brief, a sacrificial highly crosslinked polymer network dissipates mechanical energy prior to the fracture strain, as shown in Figure 1.4a. We will discuss this implementation strategy in detail in section 1.6.6. Other interpenetrating networks such as triple networks hydrogels [65], or elastomers [66] may further enhance the toughening mechanism, at the expense of increased complexity of their fabrication.

Alternatively, polymer networks with high functionality crosslinks are used to develop tough hydrogels. As opposed to a simple crosslinking site, usually bound to 3-4 polymer chains, high functionality crosslinks bind more than 10 polymers chains together [27]. As the material gets stretched, geometrical constrains will selectively rupture some polymer chains prior to the fracture strain, effectively dissipating mechanical energy, as shown in Figure 1.4b. The high functionality crosslinks may be covalent crosslinks [67], dynamic covalent crosslinks [68, 69], physical crosslinks [70, 71, 72, 73], or a combination thereof [74].

Another approach is the use of fibrous polymer bundles as toughening mechanism. The nano- or micro-fibers can be aligned such that a high stretchability is achieved along the fiber axis, as shown in Figure 1.4c. Combined with a dissipative mechanism, such as the fracture of some of the fibers and the pull-out from the rest of the matrix, fibrous hydrogels may achieve high toughness [75, 76, 77].

More generally, the use of physical crosslinks, and dynamic covalent crosslinks have been added into sparsely covalently crosslinked networks composed of high molecular weight

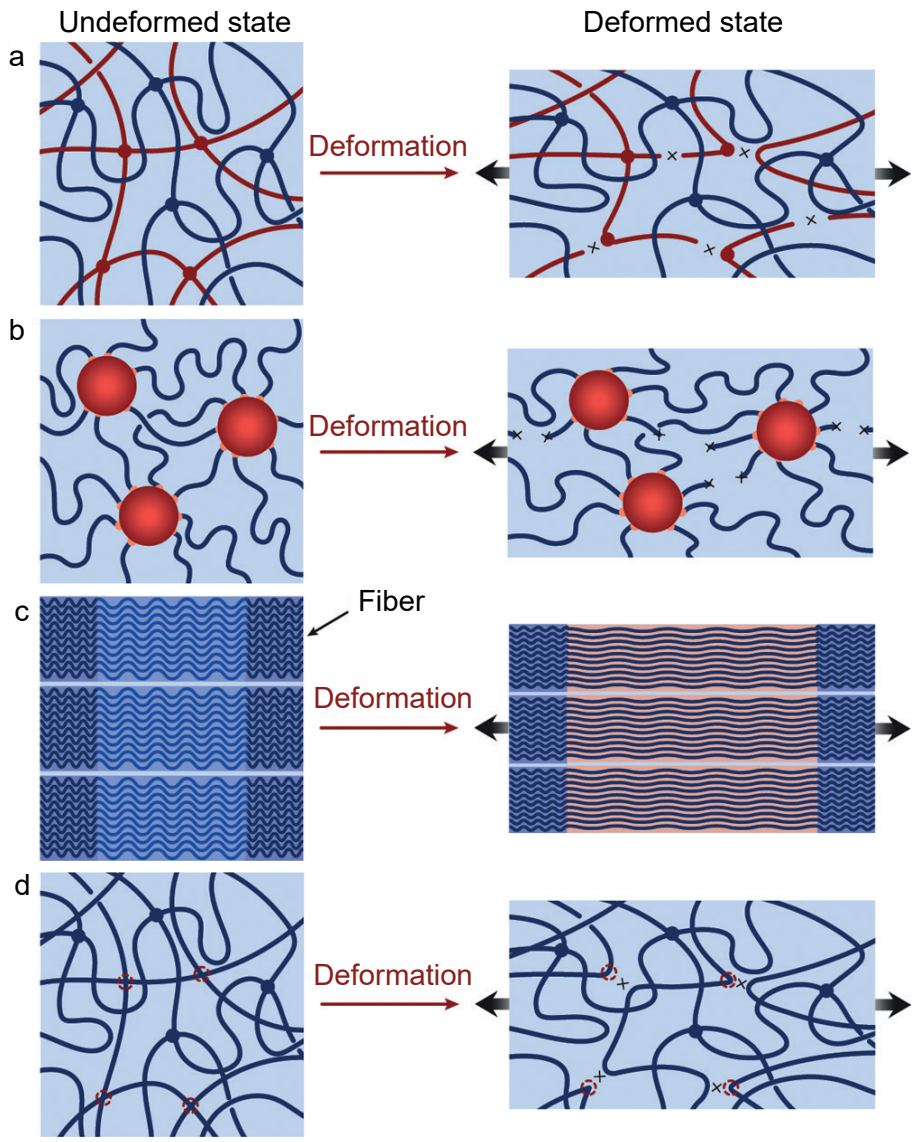

Figure 1.4: Design principles to fabricate tough hydrogels. Schematic representation of (**a**) an interpenetrating network, (**b**) a network with high functionality crosslinks, (**c**) fibrous network, (**d**) a network containing sacrificial crosslinks. Adapted with permission from [27].

polymers, as schematically represented in Figure 1.4d. The sparsely covalently crosslinked network ensures high stretchability of the material, while the reversible crosslinks act as sacrificial and energy dissipating crosslinking sites [78, 79, 80, 81, 82, 83, 84, 85, 86, 33].

1.5.2 Hydrogels with high strength

High strength in hydrogels is achieved by distributing the force over a large number of load-carrying polymer chains up until the failure of the material, at which point they break simultaneously, as sketched in Figure 1.5a. It has been estimated theoretically that a hydrogel with a shear modulus of 100 kPa can have an ideal strength of up to 1 GPa [87]. This value indicates that soft materials can be made to withstand very high strength. The strength of a conventional polymer network is less than 1 MPa [60, 79], several orders of magnitude weaker than the theoretical limit. This discrepancy is attributed to the presence of defects that significantly reduce the strength of the material.

Close-to ideal polymeric networks are shown to greatly increase the strength of hydrogels. For example, two populations of end-functionalized four-armed polymers that bind to each other and assemble into an ideal network can reach high strength [48], as shown in Figure 1.5b. We will discuss this strategy in more detail in section 1.6.5.

Alternatively, high-functionality crosslinks such as nanocrystalline domains are commonly used to strengthen hydrogels. As the network is stretched, polymers are gradually pulled out of the crystalline domain, effectively homogenizing the molecular weight of load-carrying polymer chains, as seen in Figure 1.5c. Therefore, they collectively stiffen the material until its final failure, providing a high strength [88].

The use of fibrous polymer bundles is an effective strategy to form strong hydrogels. The fibers can be designed to stiffen up simultaneously such that they carry load close to the ideal tensile strength [89, 90, 76, 91], as shown in Figure 1.5d. Notably, biological hydrogels commonly make use of nano- and microfibers, often in hierarchical structures, such as in tendons, ligaments, and muscles [92, 93, 94].

1.5.3 Bioinspired materials

The opulence presence of materials with peculiar properties in biological systems has driven the science community to take inspiration from nature for the development of novel materials [95]. State of the art characterization methods shed light on the composition of the biological materials, which are translated into synthetic equivalents for engineered applications. We will focus here on an example where bio-inspiration was used to design hydrogels with unique mechanical properties.

The marine mussel is arguably the most renown organism from which inspiration was taken for the development of hydrogels [96, 97, 98, 99, 100, 101, 102, 55]. Its byssal thread combines several reinforcing strategies discussed earlier in sections 1.5.2 and 1.5.1 such as

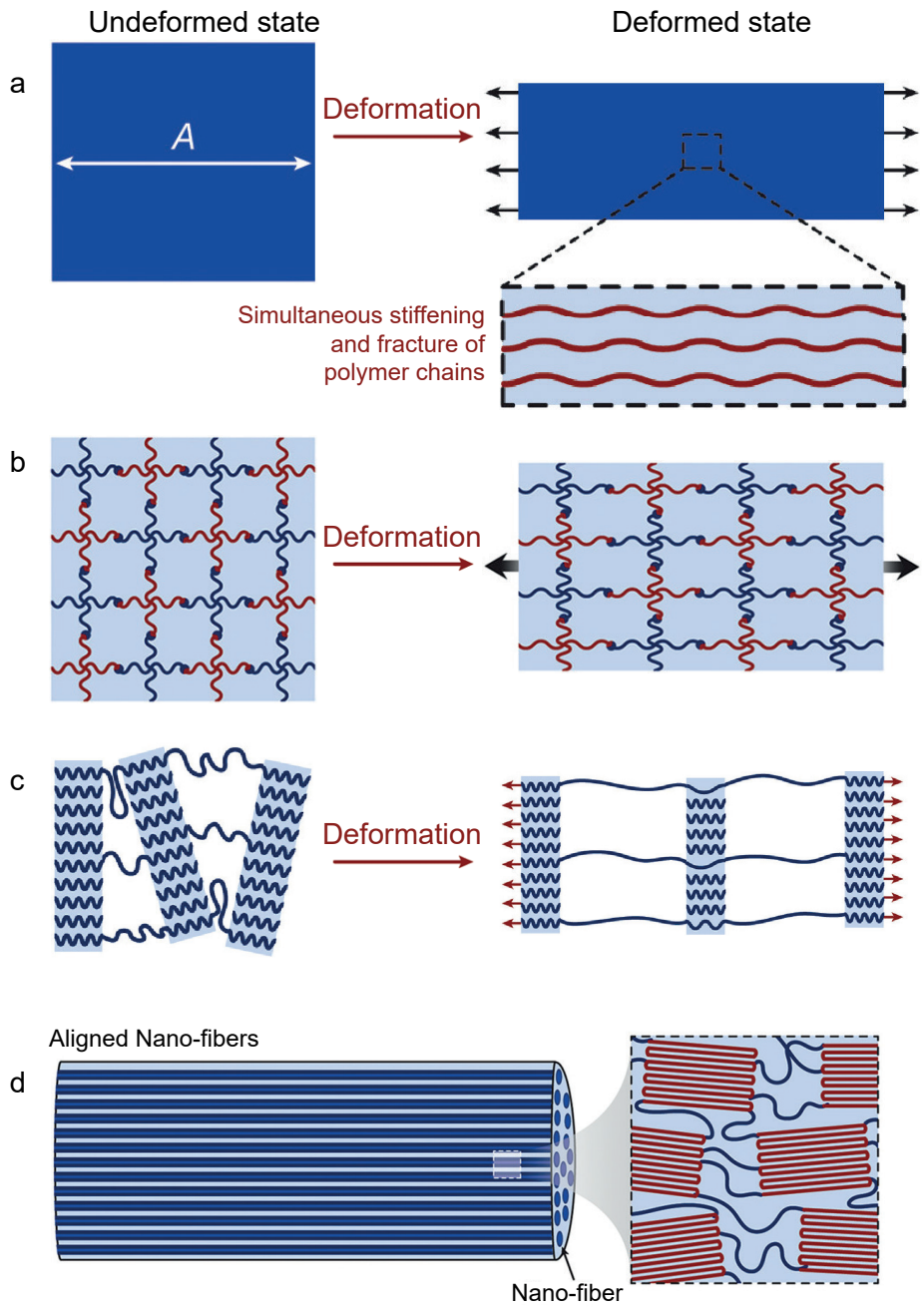

Figure 1.5: Design principles to fabricate strong hydrogels. Schematic representation of (**a**) the general stiffening mechanism of hydrogels. Stiff hydrogels can be fabricated from (**b**) ideal networks, (**c**) hydrogels with nanocrystalline domains, (**d**) fibrous networks. Adapted with permission from [27].

aligned nanofibers and high functionality crosslinks [103]. The thread core is composed of covalent collagen fibrous bundles, that are end-functionalized with ligands that can crosslink through metal-coordination, such that the material is tough and strong [104].

These sacrificial crosslinks provide a hidden length to the collagen polymer to dissipate energy and prevent failure in case of high strain [105]. The shell of the thread contains a large amount of ligands crosslinked into domains that act as high functionality crosslinks, which makes it hard and strong [106, 107, 108].

While the composition of novel materials has been extensively sourced from bio-inspiration, very little has been achieved in regards to how these materials are assembled and manufactured into a well structured hierarchical organization by biological systems [109]. In several well-studied protein-based materials, compartmentalization is used to contain prefabricated reagents which are later assembled into complex materials. For example, the structural complexity of the marine mussel thread is achieved through a supramolecular bottom-up assembly of protein precursors which are contained in dense liquid phases [110]. The proteins and other reagents are stored in coacervates and liquid crystal phases, and quickly assembled into the final fiber when required by the mussel.

The use of controlled microenvironment has been used to develop hydrogels, such as multi-responsive materials, capsules, and drug-carriers [111]. In particular, droplets containing reagents can be used as templates to fabricate hydrogel microparticles that are later assembled into granular materials. We will discuss extensively the assembly and the mechanics of granular hydrogels in section 1.8.

1.6 Implementation strategies

On a global scale, nature is still the largest producer of polymeric materials, and scientist have identified how these materials are assembled using universal inter-atomic interactions. These interactions at the atomic scale, herein referred as bonds, dictate the mechanics of chains, networks, superstructures, and eventually of the macroscopic hydrogel. We will discuss in this section a selection of different bonds found in soft materials, and how they translate to mechanical properties.

1.6.1 Crosslinking strategy: covalent bonds

Covalent bonds are strong electron-sharing interactions with a bonding energy ranging from 220 to 570 kJ·mol^{-1} [27, 113]. Therefore, they form some of the most stable network crosslinks. The most common crosslinker used for synthetic hydrogels is based on the carbon-carbon bonds between acrylates. For example, they can be found in small molecules containing two acrylates such as N,N'-methylenebis(acrylamide) (MBA) [114], or a macromolecule containing a plurality of acrylates such as multi-armed poly(ethylene

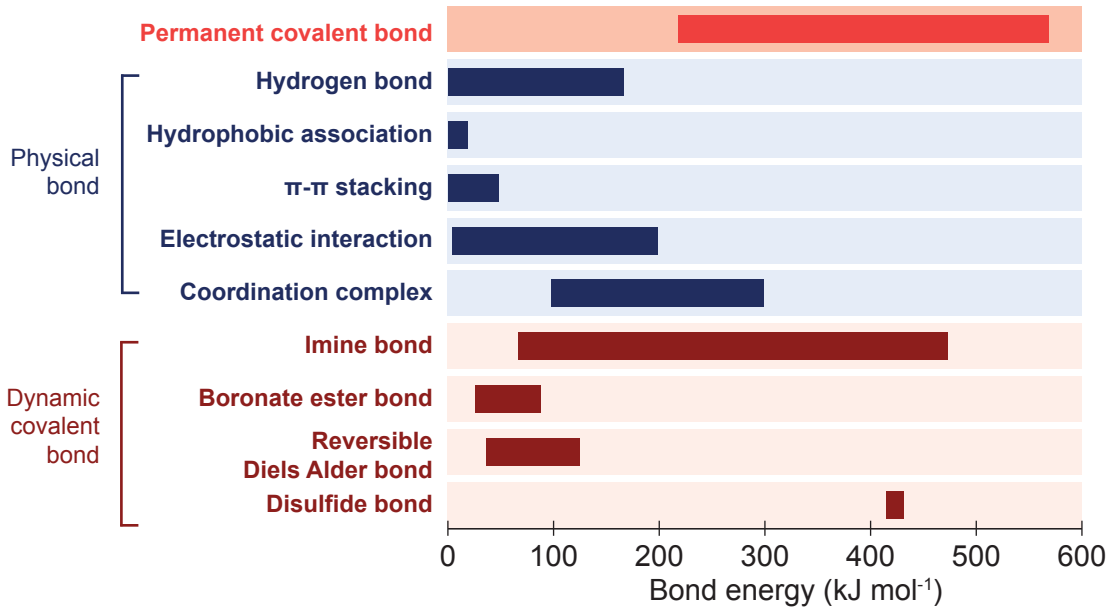

Figure 1.6: Bond energies of various types of permanent covalent crosslinks, physical crosslinks, and dynamic covalent crosslinks, adapted with permission from [27].

glycol)diacrylate (PEGDA) [46, 115]. The photo-activated radical polymerization of the acrylate groups will enable to directly incorporate the crosslinker into the network. Similarly, biopolymers are often functionalized with methacrylate groups that can react to each other, thus promptly forming a covalently crosslinked network [78]. Alternatively, covalent crosslinks can be based on a variety of reactions, including but not exhaustively reactions between amines and carboxylic acids [116], click reactions [117], etc.

1.6.2 Crosslinking strategy: physical bonds

Physical bonds are unshared electron interactions with a bonding energy generally lower than that of covalent bonds, ranging from 0.8 to 200 kJ·mol^{-1} [27]. Owing to this large span of bonding energies, they are commonly used both as reversible transient crosslinks, and collectively as strong interactions between polymeric chains. Commonly used physical bonds include hydrogen bonds, hydrophobic interactions, host-guest interactions, π-π stacking and electrostatic interactions.

Hydrogen bonds are commonly found as crosslinking mechanism of load-bearing hydrogels both in nature, such as in the helical structure of collagen [118], and in the supramolecular polymerization of fibrinogen [119], or in synthetic hydrogels such as crystalline domains of PVA [45]. However, despite the abundance of hydrogen bond groups, the hydrogen bond interaction is difficult to harness as crosslinking mechanism because it is usually screened

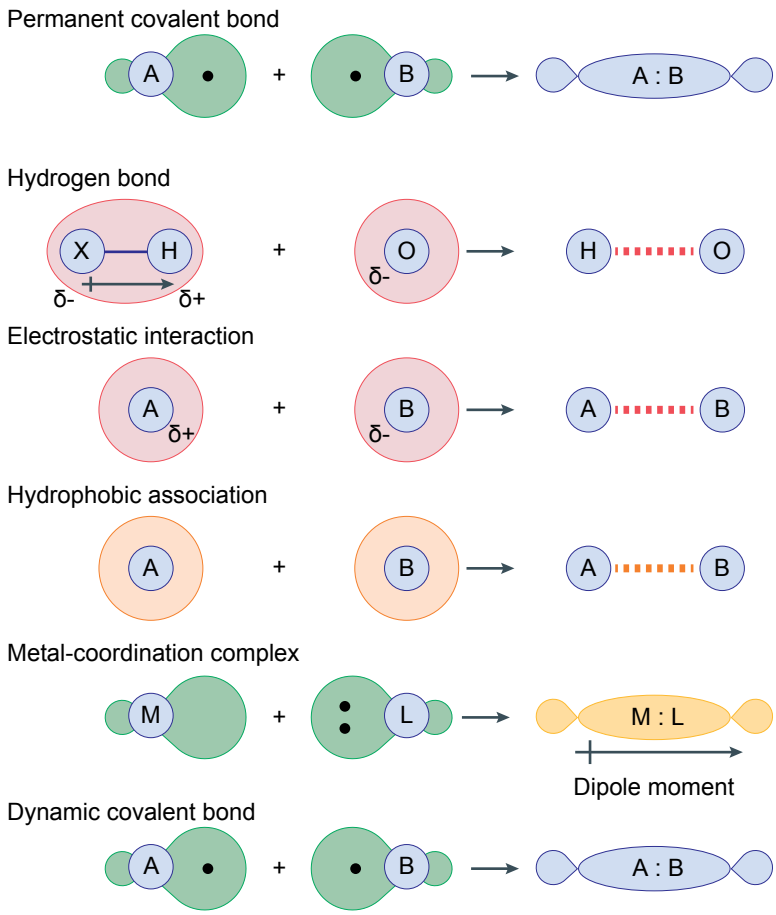

Figure 1.7: Common molecular binding interactions found in hydrogels, adapted with permission from [112].

by water molecules. This limitation can be overcome by locally expelling water molecules, such as in the freeze-thawing cycles used to create PVA micro-crystalline domains [120], or using hydrophobic moieties with several complementary hydrogen bond groups [121, 122].

Host-guest interactions are a type of supramolecular interaction were two or more molecules are held together in a unique structural assembly. As an example, a common host-guest molecule couple is cyclodextrin and curcubit[N]uril [123]. Host-guest crosslinking in hydrogels is achieved by functionalizing polymers such as PEG, PAA or hyaluronic acid with the appropriate molecule, or by copolymerizing monomers containing host / guest molecules [124]. Upon exposure of the reactive molecule, they spontaneously bond into reactive crosslinks [125].

π-π interactions refers specifically to the attractive interactions between π electrons in aromatic groups [126]. As an example, π-π crosslinked networks have been used to selectively release drugs [127, 128].

Hydrophobic interactions rely on the local phase separation of non-hydrophilic molecules from the continuous aqueous phase. When such hydrophobic molecules are copolymerized in a hydrophilic polymer, they phase-separate with other hydrophobic molecules, to reduce the interfacial area of the hydrophobic domains. As a result, the polymers are physically crosslinked into a network [122].

Electrostatic interactions arise from the attraction of oppositely charged molecules, which can be harnessed to crosslink charged polymers. For example, anyonic polymers such as alginate or PAA are crosslinked by the interaction with cations such as Ca^{2+} or Mg^{2+} [129, 130]. Alternatively, oppositely charged polymers can directly interact with each other, such as poly(*p*-styrenesulfonate) and PMPTC [131]. While a single Coulombic interaction might be relatively weak, collectively they can form a strong interactions resulting in hydrogels with high stiffness and strength [132]. In section 1.8, we will discuss further how these interactions may be further utilized to bind hydrogel microparticles together.

1.6.3 Crosslinking strategy: metal-coordination bonds

Metal-coordination bonds are shared electron interactions were several ligands and a single ion form a coordination complex. The ligands act as electron donors and the ion as electron acceptor. Polymers that have been functionalized with ligand molecules can be effectively crosslinked by forming a coordination complex with transition metal ions. As a result, the metal-coordination bonds form reversible crosslinks that have a bonding energy close to the one of covalent bonds, as shown in Figure 1.10. As mentioned in section 1.5.3, metal-coordination bonds provide structural support in the marine mussel byssal thread, but also in several other living tissues, such as sea-worm jaws [133, 134, 135] and insect mandibles [136]. In synthetic hydrogels, a variety of polymers have been functionalized with ligands either grafted along the polymer chains, such as hyaluronic acid [137] or polyallylamine [138], or grafted at the end of polymers such as multi-armed PEG [54, 98]. Catechol [101, 139], histidine [102, 55], bisphophonate [140], thiolate [141], carboxylate [142], pyridine [143], bipyridine [144], nitrocatechol [99], 2-hydroxypyridine-N-oxide [100, 145], and iminodiacetate [146] have been used as ligand molecules. They have been combined with a variety of metal ions, such as Cu^{2+}, Zn^{2+}, Fe^{3+}, Co^{2+}, and Ni^{2+}. The mechanical properties of hydrogels crosslinked by metal-coordination bonds can be tuned by varying the ligand and ion combinations, as extensively studied with functionalized multi-arm PEGs [55, 112].

1.6.4 Crosslinking strategy: dynamic covalent bonds

Unlike permanent covalent bonds, dynamic covalent bonds are cleavable under mild conditions upon exposure to an external stimulus. In the past few decades, they have attracted extensive attention for their use as responsive crosslinks for hydrogel networks [147, 148, 149, 150]. The dynamic nature of dynamic covalent bonds arises from a shift in equilibrium states under mild conditions, that drive the reactive groups either to bond or to break appart. In the bonded state, an equilibrium is reached such that a certain number of covalent bonds are formed to maintain a stable crosslinked network. However, under a mild stimulus a new equilibrium state is reached where most of the bonds are broken, resulting in the destruction of the network [150]. The bonding energy of dynamic covalent bonds is similar or lower than permanent covalent bonds, but higher than weak physical bonds, as shown in Figure 1.10. Common water-compatible dynamic covalent bonds that have been used for the synthesis of hydrogels include imine bonds [151, 152], boronate ester bonds [153], Diels Alder bonds [154, 155, 156], and disulfide bonds [157, 158, 159], as shown in Figure 1.8.

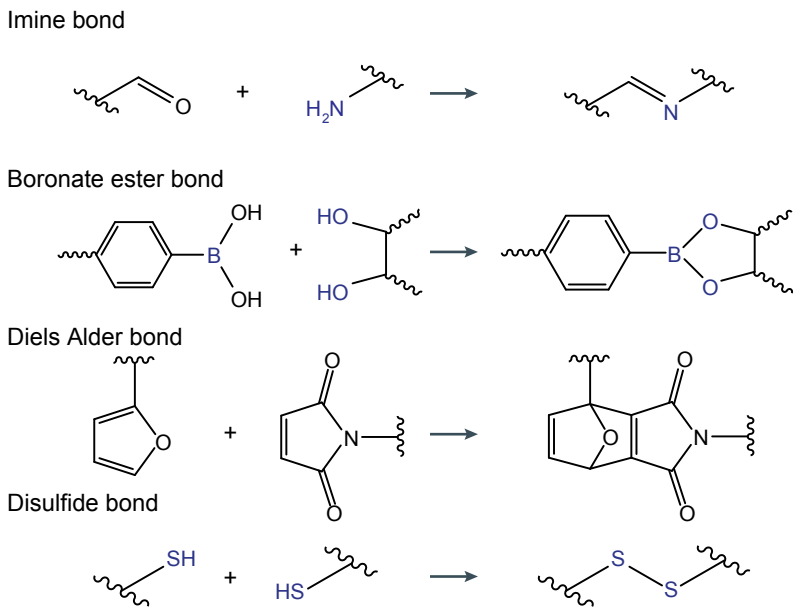

Figure 1.8: Reversible covalent bonds. Chemical crosslinking reactions of commonly used reversible covalent bonds in hydrogels.

In chapter 6, we will incorporate disulfide bonds as a dynamic covalent crosslinks. Disulfide bonds are commonly found in many natural polymers, such as fibrinogen [160] and collagen [161]. Synthetically, disulfide bonds can be introduced in hydrogels using disulfide containing crosslinkers such as 3,3'dithiobis(propanoic dihydrazide) [157, 159] or N'N'-

bis(acryloyl)cystamine (BAC) [158]. They have been used to encapsulate cells [162], or to form strong hydrogels with reversible adhesion [163]. Disulfide bonds can be cleaved under mild conditions by reducing agents such as tris(2-carboxyethyl)phosphine [164], 1,4-dithiothreitol [165], and glutathione [166].

1.6.5 Network architecture: ideal networks

Ideal networks are composed of polymer chains that all have the same molecular weight, the same crosslinking density, and no defects. Close to ideal networks have been fabricated using multi-armed polymers, that are end-functionalized with high efficiency reactive groups. Thanks to the defect-free network, such hydrogels reach extraordinary high stretchability, as was first demonstrated using 4-armed PEG amine and 4-armed PEG NHS-glutarate [48, 51]. The very homogeneous network prevents nucleation of cracks inside the hydrogels, thus explaining the high stretchability. However, more recent work have shown that even in ideal networks, the presence of heterogeneity in the molecular weight of the polymers introduces the presence of sacrificial bonds that delay the final rupture of the hydrogel [167]. We will present in the following section how this strategy can be harnessed to develop strong yet stretchable hydrogels.

1.6.6 Network architecture: double networks

The discovery of the double network (DN) effect [60], is arguably the most important discovery in the field of hydrogel mechanics of the past decades. It enabled the design of hydrogels that are stiff enough for load-bearing applications, yet overcoming the brittleness intrinsically associated with highly crosslinked polymeric networks. Double network hydrogels have a toughness that vastly outperforms any other hydrogels, as shown in Figure 1.9.

In essence, double network hydrogels are composed of a sacrificial highly crosslinked network that is combined with another loosely crosslinked network. The short chains of the highly crosslinked network account for a high stiffness, and break when overloaded. The long chains of the loosely crosslinked network bridge ruptured domains of the first network and help distribute the load, preventing catastrophic failure. Collectively, they form a very tough material, by avoiding local high stress concentrations.

The rigid and brittle polymer network, herein referred as first network, is commonly composed of a polyelectrolyte such as poly(sodium 2-acrylamido-2-methyl-1-propanesulfonate) (PAMPS), and is polymerized first. The network is soaked in a solution of monomers and crosslinkers that will constitute the second network. The use of a super absorbent as the

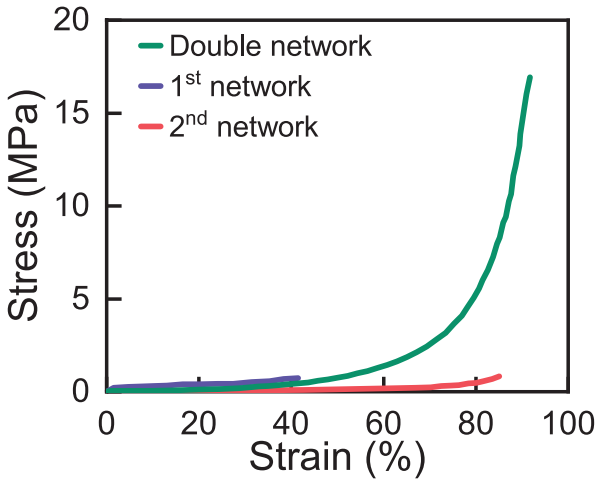

Figure 1.9: Mechanical tests of a double network (**green**), of the first network alone (**blue**), and of the second network alone (**red**), adapted with permission from [63].

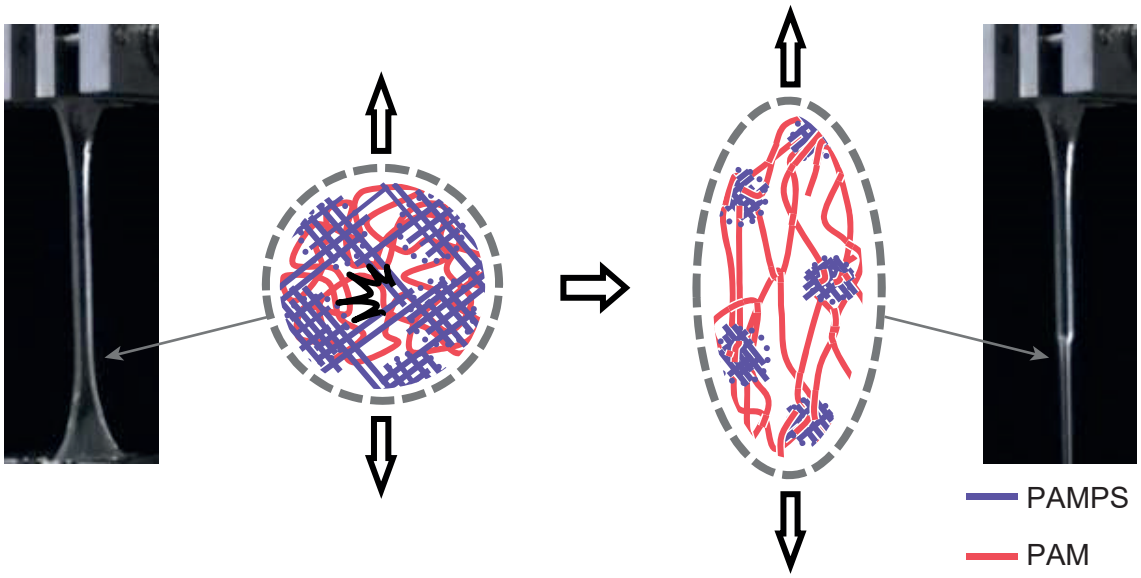

Figure 1.10: Illustration of the double network before (**a**) and after (**b**) necking, adapted with permission from [63].

first network favours the uptake of the monomer solution. The polymerization of the soaking monomer solution constitutes the second network. The swelling of the first network stretches the crosslinked chains, helping to increase its stiffness and brittleness.

In order to understand why the swelling of a network increases the stiffness of the material, we should consider the thermodynamic state of the system before and after swelling. Before swelling, the chains are free to move between crosslinking points. However, as a result of the water uptake during swelling, the individual polymer chains are stretched

which reduces their accessible conformation landscape. The loss of entropy due to chain stretching is balanced by the gain in entropy of mixing with the solvent molecules [168]. When mechanically stretched, the stored entropic elasticity in the chains of the network contributes to the initial elastic properties, resulting in an increased stiffness of the material.

The soft and ductile network, herein referred as second network, is commonly composed of a neutral polymer such as poly(acrylamide) (PAM). It has been established that maximum tensile strength is achieved when the molar concentration of the second network is 20-30 times the first network [63]. The stark contrast between the structures of the two networks enables strong energy dissipation which hinders crack propagation.

When applying cyclic uniaxial tensile and compression tests on DN hydrogels, researchers have observed significant hysteresis, unlike with similar single network hydrogels [169]. When load is applied on a single network, all of the work is stored as elastic energy, which is therefore not dissipated prior to network failure. On the contrary, DNs dissipate energy prior to total network failure, which is attributed to the fracture of covalent bonds in the first network. This internal fracture of bonds explains the difference in loading-unloading cycles, resulting in a hysteresis. In the case of PAMPS-PAM networks, the irreversible breaking of bonds in the covalent networks explains why the hysteresis is only observed during the first cycle. Increasing the strain in subsequent cycles reveals a behavior similar to the Mullins effect, where the $(n+1)$ loading cycle initially follows the (n) unloading stress. At strains higher than the (n) cycle, the $(n+1)$ stress follows the curve of the (n) loading, as schematically represented in Figure 1.11. These observations confirm an irreversible energy dissipation caused by the breaking of covalent bonds. Additionally, it was nicely shown that the heterogeneous structure of the PAMPS/PAM networks leads to very short polymeric strands, that break in significant amounts under load [169].

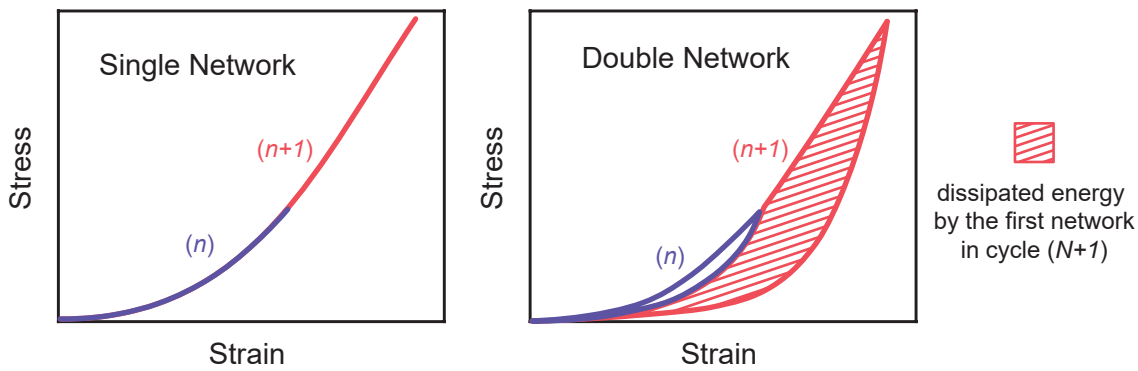

Figure 1.11: Schematic representation of uniaxial cyclic tensile tests of a single network versus a double network.

To better understand the toughening mechanism of DNs, researchers have prepared DNs with boundary ratios of first/second network concentrations. With a dense first network, the DN effect vanishes and is replaced by a brittle fracture. However, with a sparse first network, researchers have observed a necking behavior with a high fracture energy, which differs from the sudden failure of an equivalent single network. The fracture energy of single network hydrogels is relatively low, namely 10^{-1} J·m^{-2} for a PAMPS network, or 10^{0} J·m^{-2} for a PAM network. On the contrary, PAMPS-PAM DN hydrogels have a 100-1000 times larger fracture energy, ranging from 10^{2} to 10^{3} J·m^{-2}. The necking behavior of a DN can be explained by the failure of the first network, which is broken into small clusters, that act as crosslinking anchors of the PAM network. In single networks, the fracture energy is given by the energy cost of breaking bonds along the crack plane. Assuming that the fragmentation of the first network follows the Lake-Thomas model, the fracture of the DN dissipates energy not only along a single plane, but along every small cluster surface. Therefore the fracture energy of DNs scales with bonds broken within a volume, rather than along a single crack plane.

The breaking of bonds within a given volume is regarded as the *damage zone*. Based on characteristic phenomena observed in DNs mentioned above, researchers have proposed a fracture model based on localized necking at the crack tip. In this damage zone, the first network is already fractured into smaller clusters, and the crack tip passes through a softened loosely crosslinked region. Numerical simulations have shown the damaged zone to be in the order of 100 µm, which has been later confirmed experimentally.

It has been established that the widespread fracture of the first network is the key to tough DN hydrogels. Small Angle Neutron Scattering (SANS) has revealed that a widespread periodic feature of 1.5 µm is present in the stretched network [170]. Such a compositional fluctuation on a periodic micrometer length scale is only possible if the deformation process is self-regulating [63]. These observations reveal that the second network is effectively distributing the load over a widespread region of 100 µm in which the first network is broken down into much smaller 1.5 µm domains.

A limitation of the toughening mechanism of double networks composed of covalently crosslinked polymers, is that energy is dissipated irreversibly. Therefore these hydrogels exhibit a high strength and toughness only the first time they are strained, below their fracture strength. Thereafter, the first network is irreversibly broken and the mechanical properties do not match those of the pristine material. To overcome this limitation, researchers have introduced double networks whose first network is crosslinked using reversible bonds. This concept has been nicely demonstrated using alginate crosslinked by Ca^{2+} ions as first network. Combined with a PAM second network, the resulting double network effectively recovers parts of its original mechanical properties over time. This

is attributed to the reversible regeneration of the first network by the dynamic Ca^{2+} crosslinks. As a result, the double network recovers 50 % of its original toughness within a day of storage time after an initial tensile stress [79]. A faster regeneration of the first network would greatly benefit a prompt recovery of the pristine mechanical properties. We will briefly address this limitation in chapter 8.

The double network effect has been observed in various hydrogels compositions, but also in hydrophobic polymer networks, such as elastomers. Nonetheless, among all studied double network hydrogels, the combination of PAMPS as first network, and PAM as second network stands out with exceptional mechanical properties due to the good swelling properties of PAMPS and the good stretchability of the PAM network [63].

1.6.7 Mesoscale structure: granular hydrogels

As mentioned in section 1.1, good mechanical properties of materials are generally achieved if well designed not only at the nanoscale, but also at the microscale. The latter is often overlooked in synthetic hydrogels, which are fabricated from homogeneous solutions. In section 1.5.3, we have seen that well structured biological protein-based materials are sometimes assembled from micro-compartments, such as vesicles. Inspired by this strategy, researchers have used drops as micro-compartments to fabricate the building blocks of larger hydrogel structures, so-called granular hydrogels. They offer a unique strategy to control the structure of hydrogels at the microscale. We will discuss in section 1.8 how granular hydrogels have been used to develop soft materials with peculiar mechanical properties.

1.7 Mechanical reinforcement of metal-coordinated hydrogels

The metal-coordinated hydrogels that were introduced in section 1.6.3 have frequency-dependent mechanical properties that be tuned with unprecedented control. The mechanical properties of these hydrogels is generally reported using oscillatory strain or stress relaxation tests due to the prominence of their viscoelastic behavior. Using oscillatory strain tests, scientists have shown that at a given frequency a metal-coordinated network can be highly dissipative, whereas the same system can be elastically active at the same frequency if another ion is used [101]. Moreover, most reported hydrogels that are entirely crosslinked by metal-coordination bonds have both an elastic regime and a dissipative regime depending on the frequency of the applied strain, or even several dis-

sipative/elastic regimes if a combination of various ions are used [55]. Similarly, stress relaxation measurements demonstrate that metal-coordination hydrogels dissipate stress through network rearrangement over time as a result of the high loss modulus at low frequencies. Effectively, metal-coordination bonds break and reform . As a result, metal-coordinated hydrogels tend to flow, limiting their range of applications.

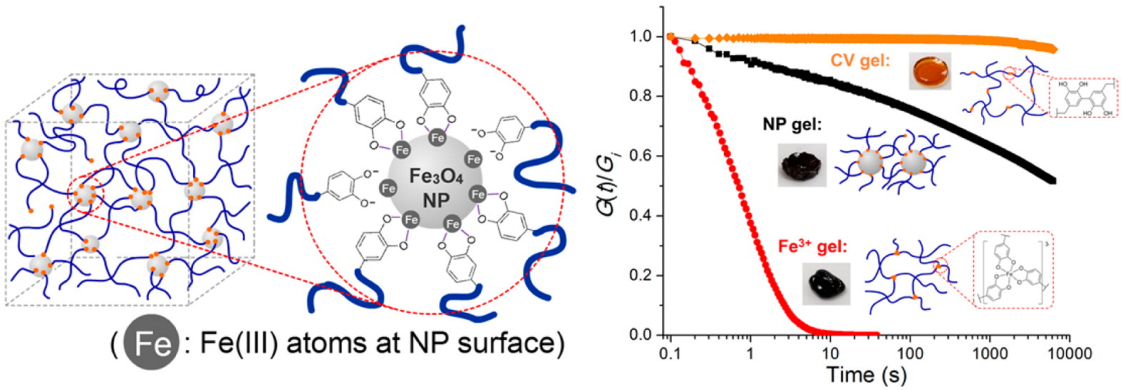

Figure 1.12: Nanoparticles are used as high functionality crosslinks using metal-coordination bonds to interact with the polymer chains, adapted with permission from [171].

Moreover, PEG decorated with ligands have been crosslinked using inorganic nanoparticles instead of single ions. As a result, the nanoparticle which crosslinks several polymers chains acts as a high functionality crosslink [171, 172]. The kinetics of the such crosslinks are slower, resulting in an increased relaxation time. In chapter 4, we will investigate the mechanical properties of pyrogallol decorated PEG that is crosslinked using *in-situ* precipitated nanoparticles.

1.8 Mechanical reinforcement of granular hydrogels

To meet the demanding and versatile requirements that advanced biomedical and material science applications impart on hydrogels, their structure and local composition must be closely controlled. This requires new processes that offer a superior control over the local composition of hydrogels and their structures on the nanometer up to the millimeter lengths scales. A possible route to obtain this superior compositional and structural control is the use of granular hydrogels.

Granular hydrogels are composed of hydrogel-based microparticles, so-called microgels, that are densely packed to form an ink that can be 3D printed or cast into macroscopic structures. They are frequently used as tissue engineering scaffolds because microgels can

be made biocompatible and the porosity of the granular hydrogels enables a fast exchange of reagents, waste products, and if properly designed even the infiltration of cells. Most of these granular hydrogels can be shaped into appropriate macroscopic structures, yet, these structures are mechanically rather weak such that they cannot bear significant loads.

The use of particles to assemble a material offers an additional advantage: It enables control over the microstructure by tuning the size, size distribution, and packing density of the microgels. Moreover, it eases the manufacturing of macroscopic materials possessing well-defined 3D shapes through dip-coating [173] and injection [174, 12, 175, 176]. The use of particles decouples the rheological properties of the precursor solution from those of the ink, unlike commonly used inks for 3D printable hydrogels that are based on a viscous shear thinning behavior [13]. This asset even enables 3D printing of structures possessing intricate shapes that cannot be fabricated with casting methods [177, 178].

1.8.1 Characteristics of microgels based materials

Microgel fabrication

Granular hydrogels are produced in two steps: A precursor solution is initially processed into individually dispersed microgels that are assembled into superstructures in a second step, as was nicely summarized in recent reviews [20, 21]. Microgels are commonly fabricated from emulsion drops that are filled with appropriate reagents. These drops are formed through batch emulsification procedures, electrohydrodynamic spraying, or microfluidics and converted into microgels by solidifying the reagents contained in them, as sketched in Figure 1.13. Alternatively, microgels are fabricated through lithography, or mechanical fragmentation, as shown in Figure 1.13. Typically, microgels are fabricated from biopolymers, monomers, or oligomers. Commonly used biopolymers include alginate, gelatin and hyaluronic acid with molecular weights superior to 20 kDa; these biopolymers are often functionalized with multiple reactive groups for crosslinking, that are covalently connected to their chains. Monomers are most commonly based on acrylates or methacrylates that can be solidified through radical polymerization reactions. The most frequently reported oligomer is PEG, often composed of multi-armed telechelic chains. The intraparticle mechanical properties are determined by the degree of crosslinking of the reagents the particles are made from and can be tuned over a wide range. The resulting microgels are typically washed to remove residues of oil and surfactants before they are swollen to equilibrium in an aqueous solution. They are subsequently jammed using centrifugation or vacuum filtration to form a shear thinning ink that can be further processed into macroscopic materials [179].

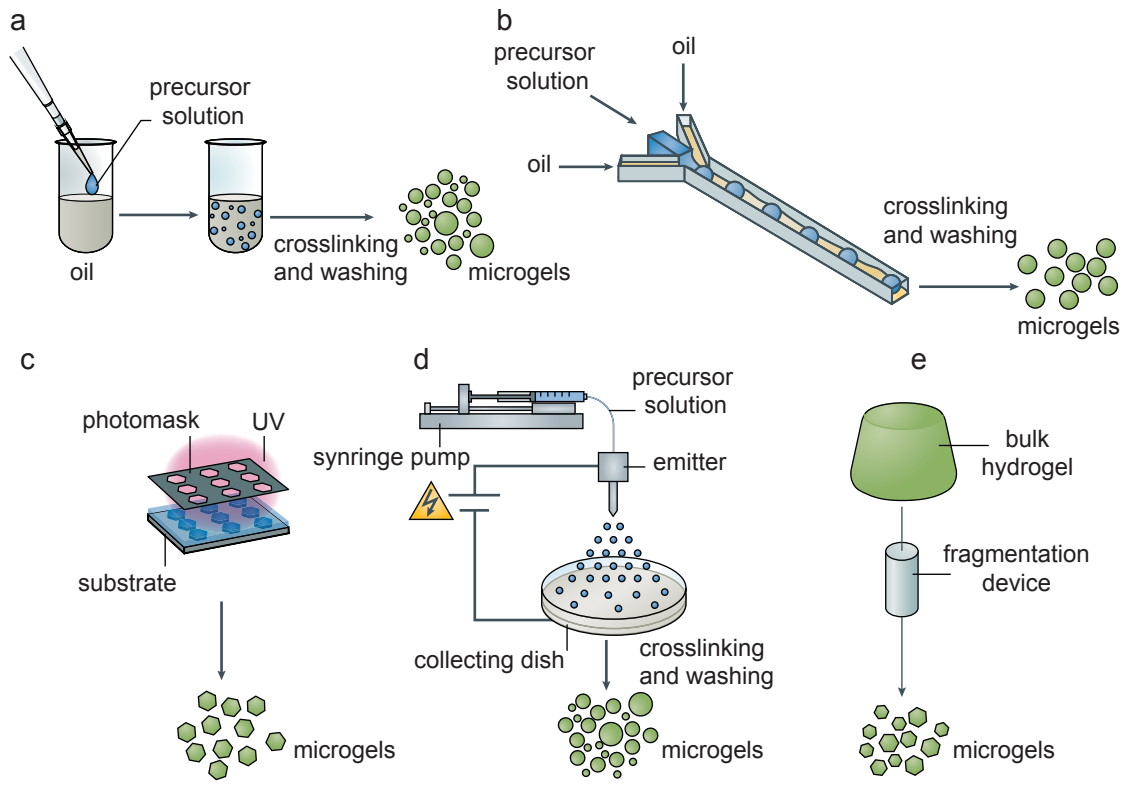

Figure 1.13: Examples of microgel fabrication techniques. (**a**) Batch emulsions are prepared from immiscible liquids, here oil and an aqueous solution, to generate drops that are crosslinked to form microgels. (**b**) Microfluidic emulsions are prepared in a microfluidic device, enabling the formation of monodisperse drops which are crosslinked into microgels. (**c**) Lithography, here sketched as photolithography, can be used as templates for microgel fabrication with precise shapes. (**d**) Electrohydrodynamic sprayed drops are generated by applying electrical forces, and are then crosslinked into microgels. (**e**) Mechanical fragmentation can be used to fragment bulk hydrogels into smaller microgels. Blue shading refers to hydrogel precursor solutions, green shading refers to crosslinked hydrogel or microgels. Adapted with permission from [20]

Jammed microgels as inks

Jammed microgels form a soft viscoelastic material that displays peculiar rheological properties [180]. Unlike microgels that are dispersed in water, jammed microgels are physically constrained by their neighbors limiting their mobility. In the jammed state, individual microgels are held together by weak interparticle forces, that impart elasticity to the media. The weak adhesive forces between soft microgels are associated with interstitial liquid bridges that form between adjacent microgels or frictional forces [181, 182]. Jammed microgels collectively behave as a bingham plastic - they are shear thinning, have a low yield stress, and promptly recover their solid-like behavior after high shear stresses are released,

in stark contrast to hard spheres [183]. These properties are closely correlated to the packing degree, which is higher for soft deformable particles than for hard counterparts.

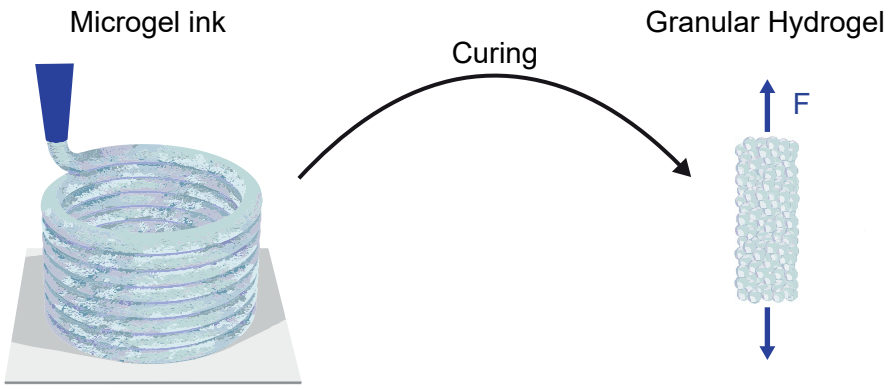

Figure 1.14: Jammed microgels are 3D printed to form complex structures. The microgels are then cured to yield the final solid granular hydrogel.

Jammed microgels are ideal for injection, extrusion, casting and 3D printing applications. The shear thinning behavior and low yield stress enable extrusion through a nozzle under ambient conditions with low pressures (1 – 100 kPa). The fast recovery of the solid properties enables extrusion of shape-retaining stable filaments, as sketched in Figure 1.14, and contributes to the good shape fidelity of 3D printed granular objects.

1.8.2 Reinforcement techniques of granular hydrogels

Jammed microgels typically interact through non-specific physical inter-particle forces, such that they display a low yield stress and easily deform when subjected to mechanical strain. These properties are desirable if used for tissue engineering applications. However, they prevent the use of these materials for load-bearing applications. The mechanical properties of granular hydrogels can be improved by strengthening inter-particle interactions, for example by crosslinking adjacent particles through strong physical or chemical links, herein referred as curing. This curing step imparts elasticity to the granular hydrogels beyond the yield stress of the original jammed microgels, as sketched in Figure 1.14. More generally, the mechanical properties of granular hydrogels can be tuned with the inter-particle crosslinking strategy. Indeed, by exploiting the vast range of bond types in organic polymeric networks, the viscoelastic properties of granular hydrogels can be tuned over a considerable range. Here, we will classify the strategies used to connect adjacent microgels into binding mechanism groups, namely covalent crosslinking of adjacent microgels, the use of binders and additives, supramolecular interactions, and interpenetrating networks, as summarized in Figure 1.15d-i. We will discuss the impact of the inter-particle

binding strategy on the elastic properties of granular hydrogels, such as the oscillatory storage modulus, the compressive modulus, and the tensile Young's modulus.

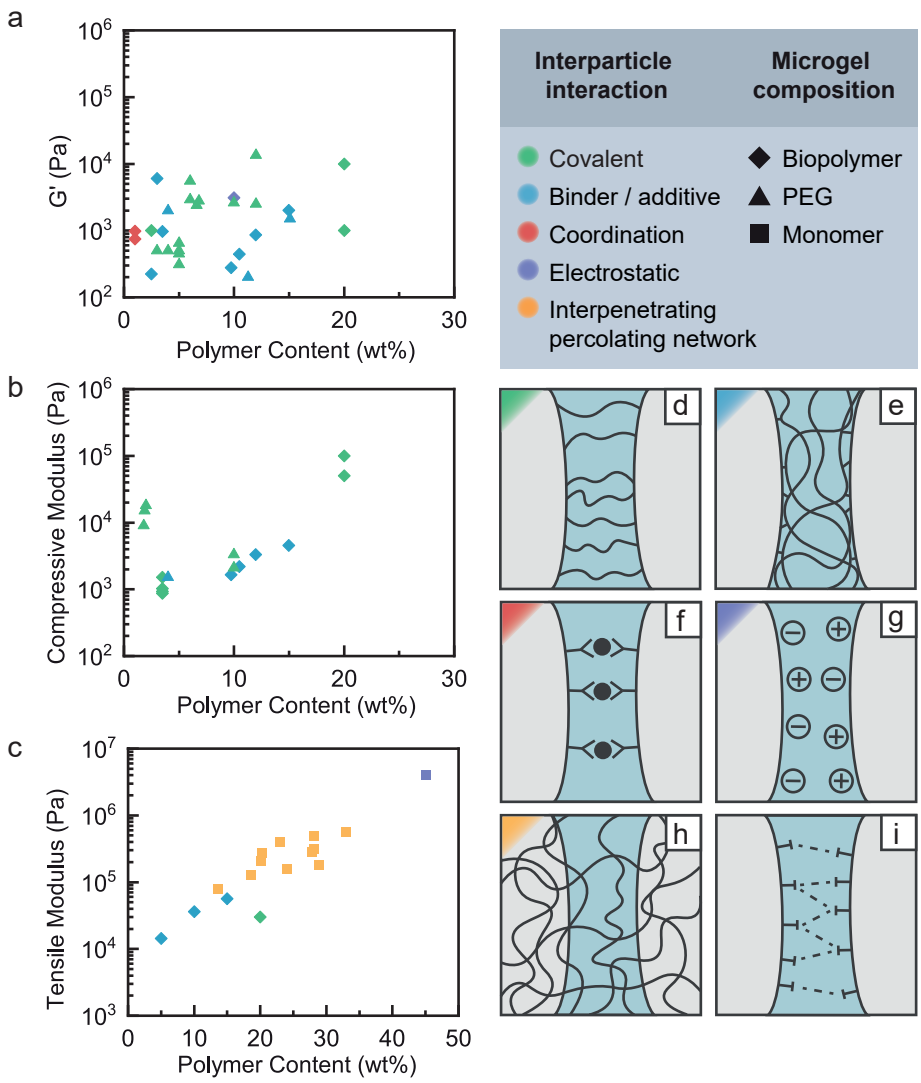

Figure 1.15: Elastic mechanical properties of granular hydrogels cured through various interparticle binding strategies. Ashby plots of the storage (**a**), compressive (**b**), and tensile (**c**) modulus as a function of polymer content. Schematic representation of the interparticle interaction mechanisms: covalent interaction (**d**), binder and additives (**e**), coordination interactions (**f**), charge interactions (**g**), interpenetrating percolating network (**h**) and other supramolecular interactions (**i**).

Radical methacrylate polymerization

Microgels can by synthesized to present chemically active sites at their surfaces such that they can form covalent inter-particle bonds. A common chain-growth mechanism used to form microgels and to covalently link them is the free-radical polymerization of acrylates and methacrylates. This solidification and connection strategy is attractive because of the large range of commercially available monomers, their ease of use, and the good mechanical properties of the resulting polymerized materials. Methacrylates are particularly suited for biomedical applications because they are biocompatible [184] and react under ambient wet conditions [185].

Covalent crosslinking of microgels composed of physically crosslinked networks requires a chemical modification of the polymers prior to their conversion into microgels. This is commonly done for naturally occurring biopolymers, such as gelatin or alginate that are functionalized with acrylates or methacrylates [178, 186, 187]. For example, microgels composed of thermally gelled gelatin, or ionically crosslinked alginate, expose dangling methacrylate groups. A simple UV-triggered polymerization enables the formation of strong permanent bonds between adjacent microgels. The resulting granular hydrogels possess storage moduli ranging from a few kPa [178, 187, 188, 189] to 10 kPa [190]. Within 60 s of moderate UV exposure (10 $mW \cdot cm^{-2}$), jammed microgels are converted into granular hydrogels with a compressive modulus of 100 kPa and a tensile modulus of 30 kPa [190]; these mechanical properties are similar to those of a human muscle. However, radical polymerization is prone to oxygen quenching, which can compromise the crosslinking efficiency and lead to inferior mechanical properties of granular hydrogels [185]. Furthermore, despite the increased biocompatibility of methacrylate radical reactions compared to those of acrylates, free-radical reactions are incompatible with certain biologically active tissues. Residual free radicals can induce oxidative stress on human tissues, which is associated to serious chronic diseases such as cancer and osteoporosis [191].

Table 1.1: List of reported granular hydrogels as a function of their interaction type.

Interaction type		Microgel composition		Microgel size (µm)	Polymer content (wt%)	G' (kPa)	Ec (kPa)	Et (kPa)	ref
Covalent	Rad. Pol.	Biop.	Ox. Alg-MA	300	2.5	1	-	-	[178]
			Gel-MA	140	20	1	100	30	[187]
			Gel-MA	90	20	10	50	-	[190]
		PEG	4-PEG-MAL-MA (20 kDa)	75	6.6	2.4	-	-	[188]
	Click	Biop.	HA-Acryl.+di-SH	74	3.5	-	1.0	-	[189]
		PEG	4-PEG-Azide (10 kDa)+8-PEG-Alkyne (20 kDa)	10-100	10	-	2.1-3.3	-	[192]
	Enzym.	Biop.	HA-Acryl.+di-SH	74	3.5	-	0.9	-	[189]
			HA-Acryl.+di-SH	45	3.5	-	1.5	-	[193]
		PEG	4-PEG-VS (20 kDa) + di-SH	30-150	5	0.3	-	-	[194]
			4-PEG-VS (20 kDa) + di-SH	100	4-12	0.5-2.6	-	-	[195]
			8-PEG-VS (20 kDa) + di-SH	100-107	3-12	0.5-13.5	-	-	[196]
			4-PEG-VS (20 kDa) + di-SH	100	5	0.65	-	-	[6]
			4-PEG-VS (20 kDa) + di-SH	100	5	0.5	-	-	[197]
			4-PEG-MAL (10kDa)+4-PEG-SH(10 kDa)	38	1.8-2	-	9-18	-	[198]
Binder / Additives	Click	Biop.	HA-AdNB+di-SH. Binder: HA-CD/AdNB	45	3	6	-	-	[12]
			HA-NB+di-SH. Binder: 4-PEG-tetrazine (20 kDa)	86	2.5	0.2	-	-	[199]
			HA-NB+di-SH. Binder: 4-PEG-tetrazine (20 kDa)	86	3.5	1.0	-	-	[200]
			HA-NB+di-SH. Binder: 4-PEG-tetrazine (20 kDa)	126	9.7-15.0	0.3-2.0	1.6-4.5	-	[201]
			HA-NB+di-SH. Binder: di-SH	100	2	-	5	-	[177]

Table 1.1: List of reported granular hydrogels as a function of their interaction type (continued).

Interaction type		Microgel composition		Microgel size (µm)	Polymer content (wt%)	G' (kPa)	Ec (kPa)	Et (kPa)	ref
Binder	Click	PEG	2-PEG-NB(5-20kDa)+2-PEG-SH(3.4 kDa).Binder:2-PEG-SH(3.4 kDa)	200	11.3-15.1	0.2-1.5	-	-	[202]
			2-PEG-NB(5-20kDa)+2-PEG-SH(3.4 kDa).Binder:2-PEG-SH(3.4 kDa)	200-500	10-15	1	-	-	[203]
	NHS coupling	Biop.	Gel-NB+2-PEG-SH(2 kDa).Binder:4-PEG-NHS(20 kDa)	600	4	2	1.5	-	[204]
	Matrix	Biop.	Gel-TG.Binder: Gel-TG	120-300	5-15	-	-	14.4-56.8	[205]
Coord. bonds	-	Biop.	Carboxy-Cellul. Nanofibrils	10	1	0.7-1.0	-	-	[206]
			HA-MA-gallol. Binder:Gallol $+Ag^{+}$	-	-	0.13	-	-	[176]
Electro. inter.	-	Biop.	Gel-MA+ Chito-MA	170	10	3.1	-	-	[186]
		Mon.	PNaSS + MPTC	-	58	-	-	4'000	[131]
Inter. network	-	Mon.	PAMPS +PAM	10-200	-	-	-	250	[173]
			PAMPS +PAM	65	13.6-45.7	-	-	20-570	[207]

Click chemistry reactions

Click chemistry reactions occur between two well-defined chemical moieties that covalently bind to each other when they approach each other. These reactions overcome some of the limitations of free-radical acrylate-based reactions because they are efficient, selective, less sensitive to the presence of oxygen, have high yields and can be performed under ambient conditions without producing biologically harmful byproducts [208, 209]. In particular, two types of thiol-ene reactions have gained attraction. The first is a photo-mediated radical crosslinking method between molecules containing thiols and those containing -enes. This method is particularly widely used by the biomaterial community owing to

the vast range of available starting materials [210]. The second heavily used reaction, is a base-catalyzed Michael-type conjugate addition of thiols to electron deficient alkenes such as acrylates, vinyl sulfones and maleimides [211, 212, 213]. This reaction can be performed under mild conditions in the absence of free-radicals, which makes it ideal for *in situ* gelation of hydrogels intended for *in vivo* applications [214, 215]. While both these crosslinking strategies have been used to synthesize microgels [6, 12, 177, 188, 189, 194, 193, 202, 199, 195, 196, 200, 201, 197, 216, 198, 203], they are much more rarely used to cure granular hydrogels. This shortcoming is most probably related to the limited availability and mobility of reactive groups at the surfaces of microgels. An azide alkyne click reaction has been reported to cure granular hydrogels by mixing two populations of microgels, one containing excess azides, and the other excess alkyne groups. The resulting granular hydrogels displayed compressive moduli of 2-3 kPa [217]. This approach requires a very high control over stoichiometric ratios of the reagents, and is synthetically more involved than radical polymerization reactions, due to the limited commercial availability of reactants. Furthermore, microgels composed of end-functionalized crosslinked polymers tend to have limited numbers of reactive groups on their surface. The limited number of reactive groups available at the microgel surface inhibits the formation of a sufficient number of load-transferring inter-particle bonds. As a result, granular hydrogels that were cured through this approach typically display poor mechanical properties [217].

Enzymatic coupling reactions

Enzymes drive reactions with product selectivity and yields beyond what is achieved by engineered catalysts. One of the most prominent examples of enzymatically driven mechano-morphing events is the formation of blood clots during hemostasis [192, 218]. This fast sol-gel transition is triggered by the covalent crosslinking of the supramolecular assembly of fibrin chains into macroscopic fibers. The covalent crosslinking occurs between amine groups present in glutamines and lysine peptides and is initiated by enzyme XIIIa. This fast and selective process inspired the use of enzyme XIIIa as the curing agent of synthetic granular hydrogels [6, 174, 189, 193, 195, 196, 197, 216, 198]. These granular hydrogels were composed of microgels with dangling lysine- and glutamine-containing peptides; these sites were used to cure the granular hydrogels after the microgels have been shaped into the desired macroscopic granular materials. The resulting materials have a compressive modulus of $1 - 20$ kPa and a storage modulus of $0.5 - 15$ kPa, which are in the order of soft biological tissues such as the skin or muscles. Their softness can be attributed to the low density of binding sites at the microgel interfaces that results in a low inter-particle crosslink density and hampers the use of such granular hydrogels for load-bearing applications. Enzymes have also been used to increase the stiffness and toughness of bulk

hydrogels by inducing the mineralization of amorphous calcium phosphate [219]. Taking advantage of these insights, the vast range of available enzymatically driven reactions could be harnessed to crosslink microgels. However, to take full advantage of the insights gained in bulk hydrogels, the microgel formation and curing mechanism would have to be tailored to ensure a high density of reactive groups present at the microgel surface and that their mobility is sufficiently high. These assets would enable the formation of a high density of inter-particle links that ensure an efficient load transfer between adjacent microgels, which would translate into an increased stiffness of the granular hydrogels.

Binder and additives

An alternative approach to firmly connect microgels is to embed them in a matrix. A recurrent limitation of the previously described cases is the low mobility of reactive groups on the microgel's surface, that prevents an efficient formation of inter-particle connections. This limitation can be overcome if binders are used to connect adjacent particles because they are typically dissolved in a liquid surrounding the microgels, such that they possess a high mobility. This feature has been demonstrated on microgels that were synthesized using a click chemistry reaction, here norbornene-thiol. The molar ratio of the reagents contained within the drop template was not stoichiometric such that some norbornene groups remained active even after the microgels have been formed. These reactive sites could be used to form inter-particle connections by exposing them to a solution containing linear PEG that was end-functionalized with thiol groups [202]. Another study reports the use of a curing solution containing a short di-thiol molecule and norbornene-functionalized hyaluronic acid, which efficiently cured microgels presenting the same reactive groups at their surfaces to covalently crosslink them at a high density. The high crosslinking density can be assigned to the deformation of soft microgels that increases the contact area between adjacent microgels and hence, the density of inter-particle crosslinks when the bridging molecule is very short. As a result, these granular hydrogels displayed a compressive modulus of 5 kPa [177]. This result hints at the importance of the inter-particle contact area and the associated inter-particle crosslink density for the mechanical properties of granular materials.

Binders can be composed of low molecular weight polymers that possess a high mobility. Even if di-functional binders with a molecular weight as low as 3400 Da are used to connect adjacent microgels, the storage moduli of the resulting granular hydrogels can reach values between 0.2 – 1.5 kPa [202, 203]. This result demonstrates that even low molecular weight crosslinkers can efficiently form covalent bonds between adjacent microgels. We again attribute this feature to the softness of the microgels that allows them to deform, thereby

maximizing the contact area between adjacent microgels. Alternatively, microgels can be connected through higher molecular weight binders that possess multiple functionalities, such as 4-armed PEG (20 kDa). The resulting granular hydrogels display storage moduli between 0.2 – 2 kDa and compressive moduli in the range of 1 – 5 kPa [199, 200, 201, 204]. The storage modulus can be increased up to 6 kPa if higher molecular weight multi-functionalized biopolymers are used, such as hyaluronic acid (HA) [12]. This result indicates that the inter-particle crosslinking efficiency increases with increasing molecular weight of the crosslinker, most likely because of the higher flexibility of these molecules. A general limitation of this approach is the poor control over the exact concentration of binding polymers at the microgel interfaces. This parameter is directly related to the packing degree of jammed microgels, and the local binding affinity of binders to the microgel surface and is hence difficult to systematically vary. As a result of this limitation, the mechanical properties of the resulting granular hydrogels cannot be deliberately tuned over a wide range. Microgels can also be dispersed in a matrix without being covalently linked to it. For example, a gelatin matrix has been reinforced with microgels composed of gelatin with a higher concentration than the matrix. The composite has a Young's modulus under tension of 40 kPa, 8-times that of the matrix alone, because gelatin chains physically interact with the microgels [205]. However, the control over the microstructure of the resulting composites is very limited because the microgels are not jammed and randomly distributed within the matrix material.

Physical and coordination bonds

Previously discussed granular hydrogels are mostly composed of microgels that are irreversibly bonded to each other through covalent bonds. Irreversible inter-particle connections typically result in rather brittle granular hydrogel, because microgels cannot re-arrange if subjected to stress, and the mechanisms that dissipate energy and thereby prevent a catastrophic failure are very limited. This shortcoming can be overcome if microgels are reversibly crosslinked through physical interactions, coordination bonds or dynamic covalent bonds. For example, microgels composed of carboxylated cellulose have been cured by exposing them to a Ca^{2+}-containing solution. The resulting granular hydrogels whose microgels are physically connected to each other possess storage moduli between 0.5 – 1 kPa, similar to those of microgels that have been connected with covalent binders [206]. Stronger inter-particle bonds can be formed if metal-ligand coordination chemistry is used, whose binding strength is close to the one of covalent bonds [220]. Extensive research has been done on harnessing coordination chemistries to design dynamic, viscoelastic, self-healing bulk hydrogels whose mechanical properties can be tuned with the choice of the type of chelator and metal ion [112]. A similar strategy has been

employed to link adjacent microgels that have been functionalized with pyrogallols. Pyrogallols possess a high affinity to certain metal ions, such as Fe^{3+}. Moreover, they can catalyze the reduction of certain ions, such as Ag^{+}, resulting in the formation of silver nanoparticles. The latter strategy was used to fabricate granular hydrogels whose grain boundaries were reinforced with silver nanoparticles. However the mechanical properties of the resulting granular hydrogel were poor, with a storage modulus reaching only 0.13 kPa [176]. The poor contribution of the pyrogallol nanoparticle complexes to the elasticity of the granular hydrogels suggests that the pyrogallols have limited mobility and cannot significantly contribute to interparticle bonding. Hence, while metal-ligand coordination chemistries have been successfully used to design advanced bulk hydrogels, their use as efficient inter-particle crosslinkers remains to be shown.

Electrostatic interactions

The marine sandcastle worm uses a variety of supramolecular interactions to form strong granular media. These fascinating mechanical properties are a result of strong adhesive coacervates that link adjacent grains. Inspired by the marine sandcastle worm, hydrogels have been reinforced with oppositely charged polymers. For example, a single percolating polyelectrolyte network was swollen with oppositely charged monomers to form a secondary network. Importantly, the second network was formed in a saline solution to speed up the swelling of the first network that ensures a homogeneous distribution of the second type of monomers also within the microgels [131]. The resulting swollen microgels were subsequently dialyzed to cancel ion screening, resulting in a poly-ion complex between positively and negatively charged strands located within and between microgels. The strong electrostatic interactions between microgels resulting from a high density of charges resulted in fracture strengths of the resulting granular hydrogels that are as high as 1.5 MPa, and a Young's modulus of 4 MPa, orders of magnitude superior to the same sample under saline conditions [131]. Interestingly, the use of saline solution to screen ionic bonding, as a reversible on/off switch of electrostatic interactions, yields promising use for additive manufacturing applications under mild conditions.

Positive and negative charges can also be separated in space by using a mixture of cationic and anionic polyelectrolyte microgels to form granular hydrogels [186]. This concept was nicely demonstrated on granular hydrogels composed of a mixture of chitosan-based and gelatin-based microgels. At neutral pH, chitosan is a cationic polyelectrolyte, whereas gelatin is an anionic one. The resulting granular hydrogel has a storage modulus of 3 kPa. This value is significantly lower than that of granular hydrogels whose microgels are connected through polyionic complexes, due to a lower Coulombic attraction between

charged microgel surfaces, and the limited contact areas between adjacent microgels.

Secondary percolating network

The vast majority of granular hydrogels are cured by linking adjacent microgels through their interfaces. This crosslinking strategy requires a high degree of control over the availability and mobility of chemical groups to ensure an efficient load transfer between microgels, a requirement that is synthetically demanding. An alternative approach is to embed the microgels within a percolating network, that transfers load from microgel to microgel over a larger volume, reducing locally high strains that typically lead to catastrophic failure of the material. Using this approach, the curing of the granular hydrogel is not only based on local adhesion between microgels, but on the cohesion of the percolating network. Microgels dispersed in a hydrogel matrix can act as reinforcing fillers [221] because they contribute sacrificial bonds to the microgels. Hence, their effect on the mechanical properties of the composite hydrogels is similar to that of the sacrificial network in double network hydrogels. To increase the density of microgels within the hydrogel matrix and thereby the control over the microstructure of the material, dried grinded microgels can be directly soaked in solution containing monomers that are used for the assembly of the secondary network. Upon polymerization of the secondary percolating network, a granular hydrogel with a 250 kPa Young's modulus can be achieved [173]. We will further investigate this strategy in chapters 5 and 6 to fabricate strong and tough granular hydrogels.

CHAPTER 2

Scope of the thesis

Hydrogels have the potential to revolutionize how we think about soft materials in various applications such as the biomedical field or soft robotics. A key limitation is often related to the inadequate mechanical properties of hydrogels, which lack a combination of high strength and toughness. As a result of intensive research in the field, various strategies have emerged to mechanically reinforce hydrogels. However, an important challenge remains to combine these reinforcing strategies with a good manufacturability. In this thesis, I aim at investigating reinforcement strategies, such as metal-coordination and double networks, and combine them with state of the art manufacturing techniques, such as 3D printing. With this work, I hope to contribute to the field of soft materials, by presenting novel methods for processable load-bearing hydrogels.

Structure of thesis

This thesis is organized in five following chapters. First, we will present the materials and methods in chapter 3, used to establish our discoveries. The following chapters 4, 5 and 6, are based on published work, in which I personally contributed as first author or co-first author. In each of these chapters, we investigate a strategy to reinforce hydrogels, and in the last two chapters we present a combination of reinforced hydrogels and improved manufacturability. Finally, chapter 8 contains the conclusions and an outlook towards the open problems along the different directions explored in the thesis.

CHAPTER 3

Materials and methods

3.1 Materials

All reagents are used as received: Acrylamido-2-methylpropane sulfonic acid (AMPS) (Sigma-Aldrich, 282731), acrylamide (AM) (Sigma-Aldrich, A4058), N,N'-methylene bis-acrylamide (MBA) (Carl Roth, 7867.1), 2-hydroxy-2-methylpropiophenone (PI) (Sigma-Aldrich, 405655), mineral oil light (Sigma-Aldrich, 330779), Span80 (TCI Chemicals, S0060), sulforhodamine B sodium salt (Sigma-Aldrich, S1402), fluorescein disodium salt (Carl Roth, 5283.1), ethanol (Sigma-Aldrich, 459844). We used deionized water with a resistivity of 18.2 MOhm·cm^{-1}.

3.2 Metal-coordinated hydrogels

3.2.1 Synthesis of PEG-COOH

PEG-OH is functionalized with carboxylic groups, using protocols previously established [55] and shown in Figure 3.1. In short, we add 30 g of OH-terminated linear PEG (6 kDa) and 600 mL H_2O to a 1 L round bottom flask and stir the solution. Once the PEG has dissolved, 200 mg (2,2,6,6-tetramethylpiperidin-1-yl)oxyl (TEMPO) and 200 mg sodium bromide (NaBr) are added. After a homogeneous solution is formed, 110 mL of aqueous sodium hypochlorite (NaClO) (10 - 20 % available chlorine) is added. The solution is stirred for 30 min while continuously monitoring the pH. The pH is maintained between 10 and 11 with 1 M NaOH. To halt the reaction, 50 mL of ethanol is added, and the pH is decreased to 2 by adding 12.1 M HCl. The aqueous mixture is extracted with four portions of 150 – 200 mL dichloromethane (DCM). The combined organic layers are extracted with 700 mL Milli-Q H_2O and dried with $MgSO_4$. After filtering, the DCM is

removed by rotary evaporation. The crude PEG-COOH is purified by precipitating in -20 °C methanol and freeze dried for 24 h. Any PEG-COOH not immediately used is stored at -20 °C.

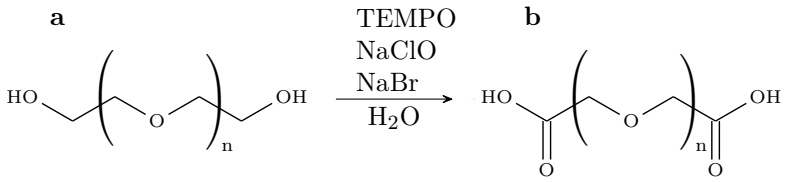

Figure 3.1: Conversion of poly(ethylene glycol) (PEG) (**a**) to poly(ethylene glycol) dicarboxy (PEG-COOH) (**b**). Primary alcohol endgroups are converted to aldehyde and then carboxy groups following a selective oxidation reaction using oxoammonium salt as catalyst [222].

3.2.2 Synthesis of 2gPEG

PEG-COOH is converted to 2gPEG, using protocols previously established [55] and shown in Figure 3.2. In brief, 1.39 g PEG-COOH, 50 mL DMF, and 25 mL CH_2Cl_2 are added to a 250 mL round bottom flask and mixed until the PEG-COOH is completely dissolved. 5-hydroxydopamine hydrochloride (1.05x mol eq. relative to -COOH) and (benzotriazol-1-yloxytripyrrolidinophosphonium hexafluorophosphate) (PyBOP) (1.05x mol eq. relative to -COOH) are sequentially added and mixed until completely dissolved. N,N-Diisopropylethylamine (DIPEA) (1.05x mol eq. relative to -COOH) is added to start the reaction, which proceeds at room temperature for 2 h. The reaction solution is reduced via rotary evaporation to remove the DCM. The crude 2gPEG (di-hydroxydopamine PEG) is purified by precipitation in acidified diethyl ether, and dried using rotary evaporation. The product is dissolved in Milli-Q water (pH = 5) in a falcon tube (50 mL). The tube is centrifuged for 10 min at 4000 rpm, and filtered using filter paper. The clear solution is extracted in DCM and dried with MgSO4. The organic phase is dried using rotary evaporation. The crude 2gPEG is purified by precipitation in diethyl ether.

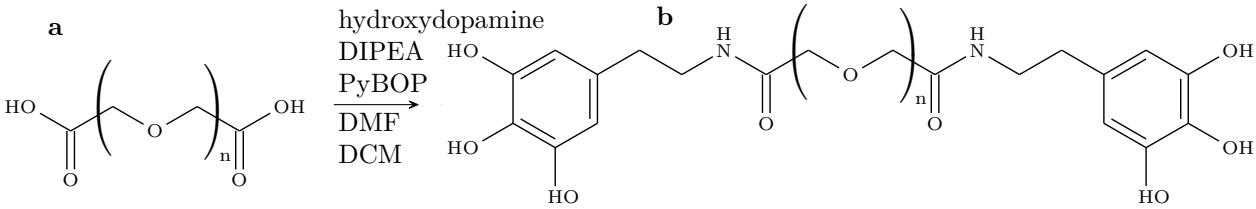

Figure 3.2: Conversion of di-carboxy (PEG-COOH) (**a**) to poly(ethylene glycol) di-pyrogallol (2gPEG) (**b**) by coupling the amine group of 5-hydroxydopamine to the carboxy group of PEG-COOH.

3.2.3 Synthesis of 2cPEG

2cPEG is prepared similarly to 2gPEG, by replacing 5-hydroxydopamine chloride with dopamine hydrochloride, as shown in Figure 3.3.

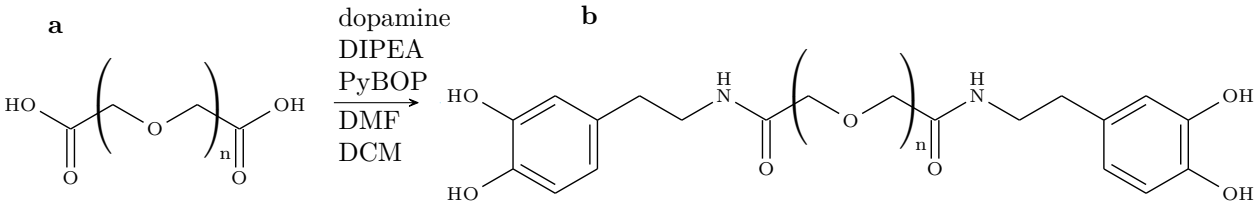

Figure 3.3: Conversion of di-carboxy (PEG-COOH) (**a**) to poly(ethylene glycol) di-catechol (2cPEG) (**b**) by coupling the amine group of dopamine to the carboxy group of PEG-COOH.

3.2.4 Spectroscopy of synthesis products

To investigate the coupling of 5-hydroxydopamine and PEG, we perform FTIR spectroscopy on dry PEG, PEG-di-COOH and 2gPEG using a 6700 Nicolet (Thermo Fischer Scientific) spectrometer. We confirm the successful 2-step synthesis by the observation of the vibrational stretch of the carboxylic C=O bond at 1750 cm^{-1} in PEG-di-COOH and the observation of the amide I and II stretches at 1650 and 1550 cm^{-1} respectively of 2gPEG, as shown in Figure 3.4. To further confirm the presence of catechol and pyrogallol coupled onto PEG, we dissolve 2cPEG and 2gPEG in D_2O, and ^1H spectra are taken on a Bruker AVANCE III 400 MHz spectrometer and processed using the MestReNova software (www.mestrelab.com). Chemical shifts are reported in ppm relative to tetramethylsilane. The presence of the catechol and pyrogallol are confirmed with NMR spectra for 2cPEG and 2gPEG respectively, as shown in Figure 3.5. Spectrum of 2cPEG: ^1H NMR (400

MHz, Deuterium Oxide) δ 6.78 (d, J = 8.1 Hz, 1H), 6.72 (s, 1H), 6.64 (dd, J = 8.1, 2.1 Hz, 1H). Spectrum of 2gPEG: ^{1}H NMR (400 MHz, Deuterium Oxide) δ 6.32 (s, 2H).

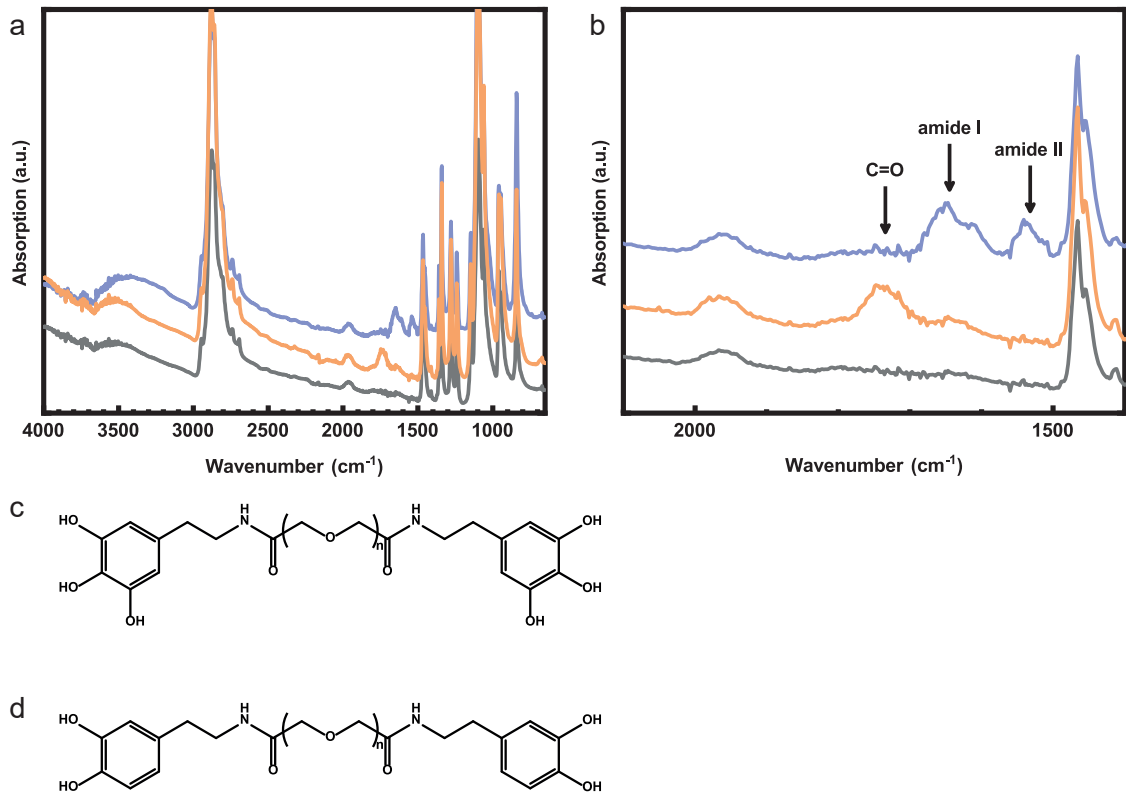

Figure 3.4: (**a,b**) FTIR spectra of 2gPEG (**top, blue**), PEG-di-COOH (**middle, orange**), and PEG (**bottom, grey**). The carboxylic end-group functionalization of PEG is validated by the C=O stretch at 1760 cm^{-1}. The further coupling of the carboxylic group with the amine of 5-hydroxydopamine is validated by the presence of the amide I and II stretches at 1650 and 1550 cm^{-1} respectively. (**c**) Chemical structure of the 2gPEG molecule. (**d**) Chemical structure of the 2cPEG molecule.

3.2.5 Preparation of 2gPEG hydrogels

For a 100 µL hydrogel sample, 10 mg of 2gPEG is dissolved in milli-Q water, in V_{water} = 100 µL - V_{ion} - V_{base}. A solution containing 1 M of the appropriate ion chloride solution is prepared separately, and diluted in the water solution. The resulting solution is deposited on a piece of parafilm. The adequate volume of 1 M NaOH is added, and manually mixed with the solution by folding the parafilm onto itself until the hydrogel appears homogeneous.

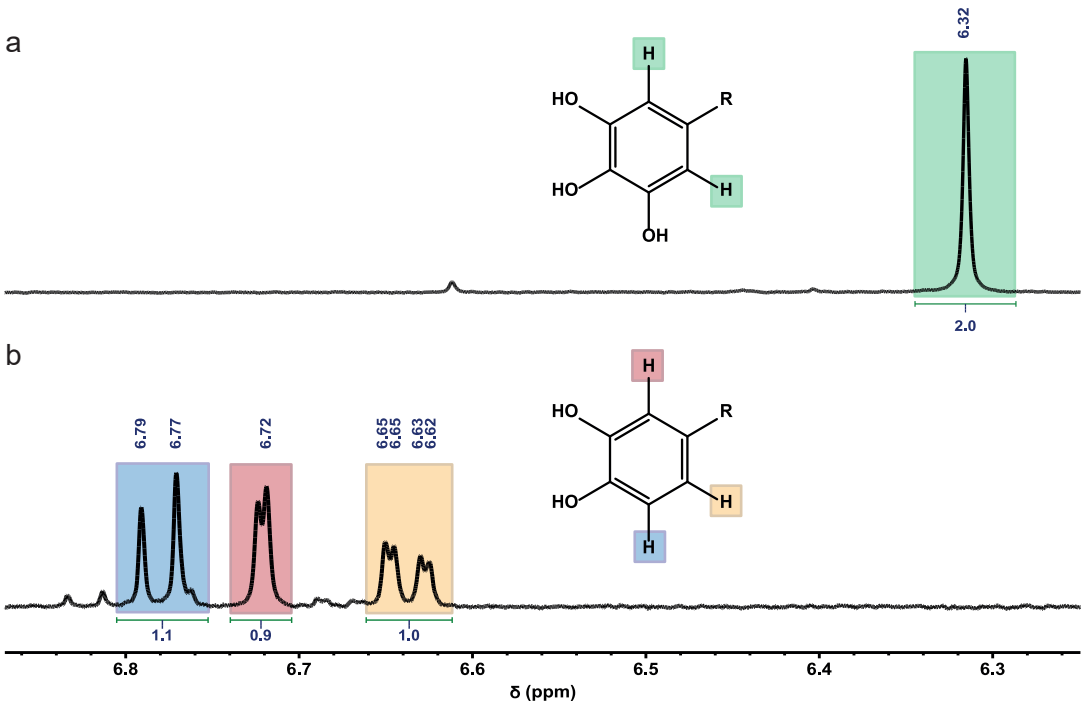

Figure 3.5: ^{1}H NMR spectra of 2gPEG (**top**) and 2cPEG (**bottom**) in D_2O. Spectrum of 2gPEG: ^{1}H NMR (400 MHz, Deuterium Oxide) δ 6.32 (s, 2H). Spectrum of 2cPEG: ^{1}H NMR (400 MHz, Deuterium Oxide) δ 6.78 (d, J = 8.1 Hz, 1H), 6.72 (s, 1H), 6.64 (dd, J = 8.1, 2.1 Hz, 1H).

3.2.6 Rheological characterization

Rheometry is performed using a DHR-3 TA Instruments rheometer, with an 8 mm diameter plate-plate steel geometry. The gap is set to 1000 µm. Stress relaxation measurements are made using an initial 10% step strain, followed by a continued monitoring of the modulus as a function of time over 1000 s. The sample is allowed to relax for 600 s at the set temperature before starting a measurement. Frequency sweeps are made at 25°C, using a 1% strain; the sample is allowed to initially relax for 600 s.

3.2.7 Stress relaxation model

The recorded modulus (G(t)) is fitted using a Kohlrausch stretched exponential relaxation model, G(t)=G_0 exp$[-(t/\tau)^\alpha]$ where $0 < \alpha < 1$ and τ(T)= τ_0 exp$[E_a/kT]$; here G_0 is the plateau modulus, τ the characteristic relaxation time, α the Kohlrausch exponent, and E_a the dissociation energy of the metal-ion complex. The characteristic relaxation time is temperature-dependent (Figure 3b for Ca^{2+}). We use this dependence to extract the

dissociation energy by fitting the data to the model. The final Kohlrausch exponent is averaged over the measured temperature.

3.2.8 Rheometric data analysis

Data is exported using the TA Instrument TRIOS software (www.tainstruments.com), and extracted using a python script into DAT files (www.python.org). The fitting is done using the Anaconda library (docs.anaconda.com), using the `curve_fit` function.

3.2.9 SAXS method and data analysis

The following SAXS data analysis was performed by our collaborator Viviane Lutz-Bueno. The particle size is estimated from transmission electron microscopy (TEM) images that were taken by Lucas Güniat, shown in Figure 4.5b. The correlation lengths are deducted from small-angle scattering (SAXS) of the hydrogels in capillaries. We use a Kratky system (Bruker). The low pH 2gPEG solution is used as the background for the solutions at low pH. Only the empty sample holder is used as the background correction for the gels. All curves are corrected by sample transmission and exposure time. All measurements are performed at room temperature. The intensity I is radially integrated as a function of the scattering vector q. The scattering intensity I(q) is fitted non-linearly by [223]:

$$I(q) = I_L(0)\left(1 + q^2\xi^2\right)^{-1} + I_G(0)exp\left(-\frac{q^2\psi^2}{2}\right) \tag{3.1}$$

Where I_L (0) is the linear coefficient of the Lorentzian and I_G (0) of the Gaussian. ξ and φ are varied iteratively to minimize the variance between the data and Equation 1. The first term arises from the solution-like, “free” polymer chains. The second term arises from the polymer chains fixed at the junction points. At the measured q-range, no contribution from the ions/particles are observed. For the fitting, we use the SasView software (www.sasview.org) and the `gel_lorenz_gaussian` model [224].

3.2.10 Resonance Raman characterization

A Renishaw Raman spectrometer, equipped with a confocal microscope, a 785 nm laser line, a 1200 l/mm grating and a Renishaw camera is used. For each spectrum the average

of 60 exposures of 1 s each is taken. The peaks at 806 and 1140 cm^{-1} can be assigned to PEG [225]. The peaks at 1251-1270, 1312-1322, 1416-1423, 1468-1476 cm^{-1} can be assigned to the catechol ring vibration [107]. The Raman spectrum of synthesized dry 2gPEG is shown in Figure 3.6.

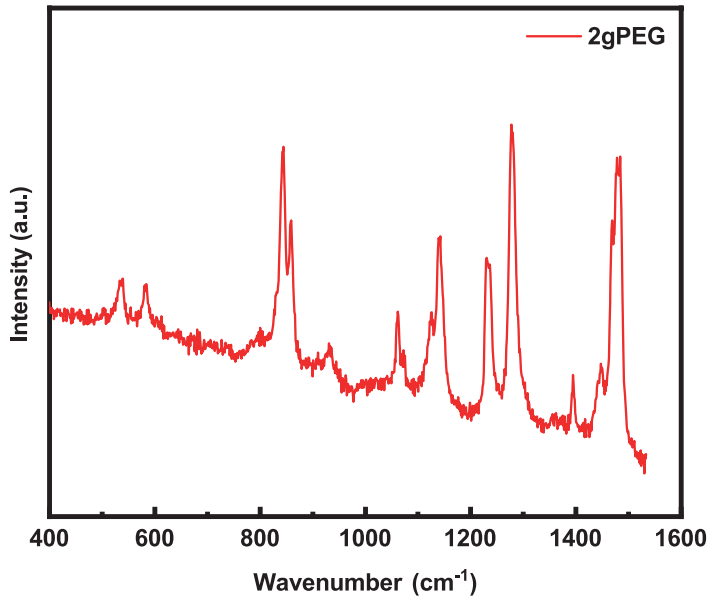

Figure 3.6: Raman shift spectrum of 2gPEG in the dry state.

3.2.11 XRD characterization

Measurements are made on an Empyrean system (Theta-Theta, 240 mm) equipped with a PIXcel-1D detector, Bragg-Brentano beam optics (including hybrid monochromator) and parallel beam optics. A reflection transmission spinner is used.

3.3 Double network granular hydrogels

3.3.1 Preparation of PAMPS microgels

An aqueous solution containing 30 wt% AMPS, 3.5 mol% MBA, and 3.5 mol% PI is prepared, unless specified differently. The aqueous phase is emulsified with a mineral oil solution containing 2 wt% Span80. The volume fraction of water is set to 25%. The water-in-oil emulsion is stirred while being illuminated with UV light (OmniCure S1000, Lumen Dynamics, 320-390 nm, 60 mW/cm^2) for 5 min to convert drops into microgels.

The resulting PAMPS microgels are transferred into ethanol and centrifuged at 4700 rpm for 15 minutes (Mega Star 1.6R, VWR) to remove the oil. The supernatant is discarded, and the process is repeated three times with ethanol and three times with water. Clean PAMPS microgels are resuspended in water for storage. To render microgels fluorescent, we add 0.05 mg of sulforhodamine B sodium salt or fluorescein disodium salt per mL of microgel solution.

3.3.2 Preparation of jammed PAMPS microgel ink

The solution containing dispersed PAMPS microgels is centrifuged and the supernatant is exchanged with excess aqueous solution containing 20 wt% AM, 0.2 mol% MBA, and 1.5 mol% PI. Microgels are soaked overnight. The solution containing PAMPS microgels is vacuum filtrated (Steriflip 50 mL tube, 0.22 µm, Millipore) to yield a jammed microgel ink.

3.3.3 Preparation of molded DNGHs

The granular ink is casted into Teflon molds of cylindrical (d = 8 mm, h = 2 mm) or rectangular (15 x 5 x 2 mm^3) shape, for compression and tensile measurements respectively. The samples are crosslinked for 5 min under UV light (UVP CL-1000, Analytik Jena, 365 nm, 2 mW/cm^2).

3.3.4 Preparation of bulk double network hydrogels

An aqueous solution containing 30 wt% AMPS, 3.5 mol% MBA, and 3.5 mol% PI is prepared. The AMPS solution is casted into Teflon molds for tensile measurements. The samples are crosslinked for 5 min under UV light (UVP CL-1000, Analytik Jena, 365 nm, 2 mW/cm^2). PAMPS hydrogels are immersed overnight in an aqueous solution containing 20 wt% AM, 0.2 mol% MBA, and 1.5 mol% PI. Soaked samples are then exposed to UV illumination for 5 minutes to trigger the PAM second network percolation.

3.3.5 3D printing of DNGHs

The jammed microgel ink is loaded in a 3 mL Luer lock syringe. To remove trapped air, the syringe is sealed and centrifuged at 4700 rpm for 1 min. Additive manufacturing of jammed microgels is performed with a commercial 3D bioprinter (Inkredible+, Cellink). The granular ink is extruded from a conical nozzle (410 µm) through a pressure driven

piston (30 kPa). Printing is controlled through G-code commands that are generated by a built-in machine software (Cellink HeartWare). Printing is performed on a glass substrate with a starting gap of 0.1 mm. Printed structures are crosslinked by exposing them to UV light (UVP CL-1000, Analytik Jena, 365 nm, 2 mW/cm^2) for 5 min.

3.3.6 Rheology of jammed PAMPS microgels

Rheology is performed on a DHR-3 TA Instrument with an 8 mm diameter parallel plate steel geometry. All measurements are performed at 25°C, with an 800 µm gap. Frequency dependent viscosity measurements are made at 0.5% strain. Amplitude sweep is performed at 1.0 rad/s oscillation. Self-healing measurements are performed at 1.0 rad/s, alternating 200 s at 1% strain, with 200 s at 30% strain. Samples are allowed to relax for 200 s at the set temperature before a measurement starts. Stress relaxation measurements are made for crosslinked and uncrosslinked microgels with an initial step strain of 10% and measured for 10 s. The gelation measurement is done at 1% strain and 10 rad/s frequency for 250 s. The liquid sample is loaded on the rheometer, and the UV lamp is switched on at t = 25 s to initiate the polymerization reaction.

3.3.7 Mechanical characterization of DNGHs

Tensile measurements are performed with a commercial machine (zwickiLine 5 kN, 100 N load cell, Zwick Roell). Rectangular DNGH are mounted and stretched at a constant velocity of 100 mm/min. The Young's modulus is calculated as the slope of the initial linear region (from 5% to 15% strain). The toughness is calculated as the area below the stress-strain curve of an un-notched sample until fracture. The quantity is expressed as the energy absorbed until fracture per unit volume (J/m^3). Compression measurements are performed on a rheometer equipped with a parallel plate geometry (DHR-3, 50 N load cell, TA Instrument). Cylindrical DNGH are compressed at a constant velocity of 1.2 mm/min until 60% strain is reached.

3.3.8 Dry polymer content and EWC

Dry Polymer Content and EWC. The dry polymer content of AMPS microgels and DNGHs is calculated as the ratio of dry sample weight over as-prepared weight ($W_d/W_{ap}\cdot 100$). The equilibrium water content (EWC) is calculated as the ratio of dry sample weight over fully swollen sample weight ($W_d/W_s\cdot 100$).

3.4 Recyclable double network granular hydrogels

3.4.1 Materials

Acrylamido-2-methylpropane sulfonic acid (AMPS) (Sigma-Aldrich, 282731), N,N'-methylene bisacrylamide (MBA) (Carl Roth, 7867.1), 2-hydroxy-2-methylpropiophenone (PI) (Sigma-Aldrich, 405655), mineral oil light (Sigma-Aldrich, 330779), Span80 (TCI Chemicals, S0060), ethanol (Sigma-Aldrich, 459844), acrylamide (AM) (Sigma-Aldrich, A4058), N,N'-Bis(acryloyl)cystamine (BAC) (Alfa Aesar, J66893), Tris(2-carboxyethyl)phosphine HCl (TCEP) (Combi-Blocks, OR-5119), methylene blue hydrate (Acros Organics, 229801000) are all used as received.

3.4.2 Preparation of PAMPS microgels

PAMPS microgels were prepared following the protocol described in section 3.3.1. Briefly, an aqueous solution containing 25 wt% AMPS, 3.5 mol% MBA, and 3.5 mol% PI is prepared, unless specified differently. The aqueous phase is emulsified with a mineral oil solution containing 2 wt% Span80. The volume fraction of water is set to 25%. The water-in-oil emulsion is stirred while being illuminated with UV light (OmniCure S1000, Lumen Dynamics, 320-390 nm, 60 mW/cm^2) for 5 min to convert drops into microgels. The resulting PAMPS microgels are transferred into ethanol and centrifuged at 4700 rpm for 15 min (Mega Star 1.6R, VWR) to remove the oil. The supernatant is discarded, and the process is repeated three times with ethanol and three times with water. Clean PAMPS microgels are resuspended in water for storage.

3.4.3 Preparation of rDNGHs

The solution containing dispersed PAMPS microgels is centrifuged at 4500 rpm for 10 min and the supernatant is exchanged with excess aqueous solution containing 30 wt% AM, 0.1 mol% BAC, and 1.5 mol% PI. The solution containing PAMPS microgels is centrifuged at 4700 rpm for 15 minutes and further jammed over filter paper. The granular paste is casted into dog-bone shaped Teflon molds and crosslinked under UV irradiation (UVP CL-1000, Analytik Jena, 365 nm, 2 mW/cm^2) for 5 min.

3.4.4 3D printing of rDNGHs

The jammed microgel ink is loaded in a 3 mL Luer lock syringe. To remove trapped air, the syringe is sealed and centrifuged at 4700 rpm for 1 min. 3D printing of jammed microgels is performed with a commercial 3D bioprinter (BIO X, Cellink). The granular ink is extruded from a conical nozzle (410 µm) through a pressure driven piston (30 kPa). Microgels are dyed with 0.001 mg/mL methylene blue for visualization.

3.4.5 Degradation and recycling of rDNGHs

Crosslinked rDNGH samples are immersed in 50 mM TCEP aqueous solution at pH 9, unless specified differently. The solution is left to stir at 300 rpm until complete rDNGH dissolution is observed. Degradation kinetics is monitored through gravimetric analysis. Dispersed microgels are recovered through centrifugation at 4700 rpm for 15 min. Recovered particles are washed in excess water and centrifuged. The process is repeated three times. Recovery yield is calculated as the weight of recovered microgels with respect to the initial microgel weight. Cleaned microgels are reused as pristine ones for the preparation of new rDNGH samples.

3.4.6 Resonance Raman characterization

Samples are characterized using a Renishaw Raman spectrometer, equipped with a confocal microscope, a 785 nm laser line, a 1200 l/mm grating and a Renishaw camera. Each spectrum is taken as the average of 500 exposures of 1 s at 125 mW laser power.

3.4.7 Rheology of pristine and recycled PAMPS microgels

Rheology is performed on a DHR-3 TA Instrument with an 8 mm diameter parallel plate steel geometry. All measurements are performed at 25 °C, with an 800 µm gap. Amplitude sweeps are performed at 1.0 rad·s^{-1} oscillation.

3.4.8 Mechanical characterization of rDNGHs

Tensile measurements are performed with a commercial machine (AllroundLine Z005, 50 N load cell, Zwick Roell). Dog-bone shaped rDNGHs are mounted and stretched at a constant velocity of 100 mm/min. The Young's modulus is calculated as the slope of the initial linear region (from 5% to 15% strain). Three-point bending measurements are

performed on rectangular beams (20.0 x 10.2 x 1.4 mm^3). The load is applied by a central roller (d = 3 mm) at a displacement rate of 1 mm/min. The sample is placed on two cylindrical rollers (d = 3 mm) spaced 16 mm apart. The flexural modulus is calculated as the slope of the initial linear region (from 0.1% to 0.3% strain).

CHAPTER 4

Shape retaining self-healing metal-coordinated hydrogels

In this chapter, I present a metal-coordinated hydrogel based on pyrogallol functionalized PEG. I observe that the ionically crosslinked network has shape retaining yet self-healing properties. I investigate the use of precipiated inorganic nanoparticles, that act as high functionality crosslinks. As a result, this hydrogel displays exceptional solid-like mechanical properties as compared to other metal-coordinated hydrogels.

This chapter is adapted from the paper entitled "Shape retaining self-healing metal-coordinated hydrogels" authored by Alvaro Charlet, Viviane Lutz-Bueno, Raffaele Mezzenga and Esther Amstad. A. Charlet and E. Amstad designed the experiments. V. Lutz-Bueno and A. Charlet performed the SAXS measurements. V. Lutz-Bueno analyzed the SAXS data. A. Charlet performed all other experiments. A. Charlet and E. Amstad analyzed the data and wrote the manuscript.

Contents

4.1 Abstract

Metal-coordinated hydrogels are physical hydrogels entirely crosslinked by complexes between ligand decorated polymers and metal ions. The mechanical properties of these hydrogels strongly depend on the density and dynamics of the metal-coordinated interactions. Most commonly, telechelic metal-coordinated hydrogels contain catechol or histidine ligands although hydrogels containing a stronger complexation agent, nitrocatechol, have been reported. Here, we introduce a pyrogallol end-functionalized polymer that can be crosslinked with di- and trivalent ions, in contrast to previously reported metal-coordinated hydrogels. We can tune the mechanical properties of the hydrogels with the type of ions and the density of crosslinking sites. Ions form nm-sized precipitates that bind to pyrogallols and impart distinct properties to the hydrogels: Strong ion-pyrogallol interactions, that form in the presence of Al^{3+}, V^{3+}, Mn^{2+}, Fe^{3+}, Co^{2+}, Ni^{2+}, Cu^{2+}, result in long relaxation times. The resulting hydrogels display solid-like yet reversible mechanical properties such that they can be processed into macroscopic 3D structures that retain their shapes. Weak ion-pyrogallol interactions, that form in the presence of Ca^{2+} or Zn^{2+} result in short relaxation times. The resulting hydrogels display a fast self-healing behavior, suited for underwater glues, for example. The flexibility of tuning the mechanical properties of hydrogels simply by selecting the adequate ion-pyrogallol pair broadens the mechanical properties of metal-coordinated hydrogels to suit a wide range of applications that require them to retain their shape for a given time yet to act as dampers.

4.2 Introduction

Inspired by nature, metal-coordinated telechelic hydrogels, composed of polymer chains end-functionalized by ligands and crosslinked by metal complexes, have potential to generate mechanically active, reversible networks [96, 54, 98, 99, 100, 101, 102, 55, 226]. The dynamic properties of these hydrogels can be conveniently tuned with the choice of the cationic crosslinker, its relative concentration, and the solution pH [55, 138, 227]. The reversible nature of their constituting crosslinks gives them self-healing properties, such that a damaged network can heal defects. To obtain this self-healing behavior, the ions must complex the ligand sufficiently strongly to result in an integral hydrogel. Unfortunately, the selection of ions that fulfil this criterion is very limited, narrowing the range of mechanical properties of metal-coordinated hydrogels.

Hydrogels with long relaxation times have solid-like behaviors and are capable of retaining their shape, yet are able to self-heal [171]. As mentioned in section 1.6.3, the relaxation time of metal-ion coordination sites increases if ions are replaced by their corresponding nanoparticles [171], which must have adequate surface chemistry to interact with the surrounding ligands. Polysaccharides functionalized with a high density of ligands can also increase the relaxation time [228, 229, 230]. These ligands improve the adhesion of the polysaccharides towards surfaces [231], which reinforce the mechanical strength [228, 231], and impart self-healing properties to the hydrogels [232, 233]. However, these systems can often only be used in a very limited pH range mainly because the most commonly used ligands, catechols, and some of its derivatives have a high propensity to oxidize. The oxidation of catechols can lead to inter-catechol covalent bonds, which may result in hydrogels possessing a mixture of covalent and ionic bonds [98]. The combination of transient ion-ligand interactions and the oxidation of the ligand complicates their characterization, limiting their applications to non-oxidizing environments.

Several natural organisms, some of which live in quite harsh environments, employ metal complexes for mechanical reinforcement, hard coatings or energy dissipation [107, 234, 108, 235]. A prominent example is a class of marine water-filtering invertebrates, ascidians, which employ pyrogallol groups complexed by vanadium ions to heal their cellulosic tunic [236, 237, 238]. Pyrogallols are catechol derivatives possessing an additional alcohol group on the carbon ring. This electronegative group reduces their propensity to oxidize when compared to catechols. They are known to complex a broad range of ions of d-block elements [239]. This feature has been exploited, for example, by using tannic acid, which contains several pyrogallols, to form coatings [240, 241, 242, 243], metallogels [227, 244, 245], and capsules [240, 246]. Pyrogallols have also been employed in synthetic hydrogels, however in the absence of ionic crosslinks: they were oxidized to crosslink

polysaccharides [228, 229, 176, 247]. The contribution of pyrogallols to the dynamic and reversible mechanical properties of polysaccharide-based hydrogels remains unclear [229]. The formulation of ionically crosslinked hydrogels whose mechanical properties can be tuned over a much wider range than what is currently possible requires a better understanding of the influence of chelators, such as pyrogallols that can bind to a wide range of ions, on the mechanical properties of the resulting hydrogels.

Here, we introduce shape retaining self-healing metal-coordinated telechelic hydrogels with well-defined, solid-like and tunable mechanical properties. To achieve this goal, we end-functionalize linear PEG with pyrogallols (2gPEG). We investigate the influence of the type and concentration of ions used as crosslinkers on the macroscopic properties and structure of the hydrogel. The mechanical properties of these metal-coordinated hydrogels, such as their storage modulus at low frequencies, vary over an order of magnitude if adequate ions are selected. Remarkably, these telechelic PEGs can be crosslinked with di- and trivalent ions, thereby broadening the selection of ions and the range of accessible mechanical properties. During the ion-2gPEG interaction, the ions preferentially form small particles that act as high functionality crosslinks, thereby facilitating the formation of a percolating network and increasing the effective crosslink density. We demonstrate the formation of viscoelastic macroscopic freestanding 3D structures, which can be applied as underwater adhesives that can bear load even under tension. Additionally, these hydrogels can be functionalized with inorganic particles to respond to external stimuli, such as external magnetic fields.

4.3 Experimental section

Details about the experimental procedure are presented in chapter 3 from section 3.2.1 on page 39 to section 3.2.11 on page 45.

4.4 Results and discussion

To ensure scalability, we end-functionalize commercially available hydroxy-terminated linear PEGs, analogous to nitrocatechol-functionalized linear PEGs [248]. We produce the hydrogels by dissolving 10 wt% 2gPEG in water and adding iron chloride ($FeCl_3$), selected because of the high affinity between pyrogallol and iron(III) (Fe^{3+}). For each pyrogallol end-group, we add twice the molar concentration of Fe^{3+} to achieve gelation, a ratio higher than the stoichiometric ratio of 3 ligands per ion, known for catechol hydrogels [98, 101], resulting in a solution pH of 1.5. The complex formation is triggered by increasing the pH

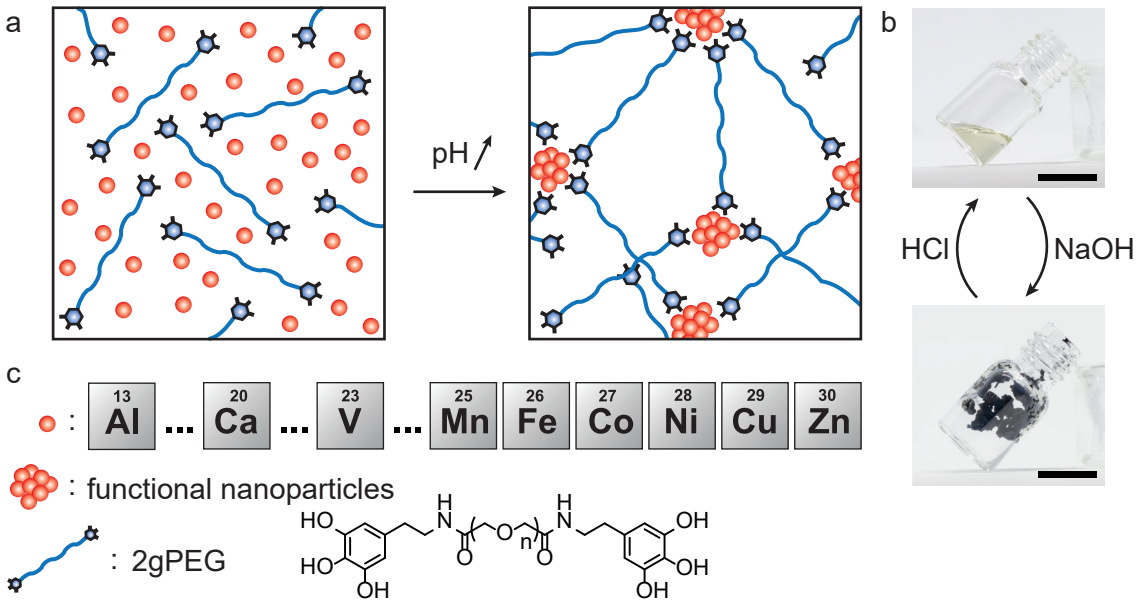

Figure 4.1: Gelation mechanism of 2gPEG hydrogels. (**a**) Schematic illustration of the hydrogel formation. The blue line terminated by blue hexagons represents the 2gPEG polymer, end-functionalized by the pyrogallol molecule. The ions are sketched as red circles. The increase in pH causes the precipitation of the ions into nanoparticles and the deprotonation of the pyrogallol groups that bind to the precipitates. The nanoparticles act as multivalent crosslinking sites of the hydrogel network. (**b**) Photographs of the solution of 2gPEG and iron ions before (**top**) and after gelation (**bottom**) induced through the addition of NaOH. The coordination bond between pyrogallols and iron ions has strong absorption in the visible range, which results in a dark purple hydrogel. After adding HCl, the hydrogel liquefies to a light-yellow solution, indicating that some pyrogallol groups oxidized. The scale bar is 1 cm. (**c**) Schematic illustration of the selection of bivalent and trivalent ions that can crosslink 2gPEG, the nano- particles, and the 2gPEG molecule. Adapted with permission from [249].

to deprotonate pyrogallols. When the pH is increased to 4.8 by adding sodium hydroxide (NaOH), the system instantaneously gels, as shown in Figure 4.1a and 4.1b. Importantly, the system remains gelled even if the pH is increased to physiological values, such that these hydrogels can be used for biomedical applications, in stark contrast to catechol-functionalized counterparts. The hydrogel remains stable in deionized water for 24 h, before it starts to dissociate.

4.4.1 Impact of ion valency

To expand the selection of ions that can be used to crosslink telechelic molecules, we crosslink 2gPEG with a divalent ion, calcium(II) (Ca^{2+}). If the same stoichiometry is

maintained as for Fe^{3+}, no gelation is observed. However, if we increase the Ca^{2+} concentration 5-fold and increase the pH to 12, we observe the gelation of the hydrogel. A similar behavior occurs if 2gPEG is crosslinked with other divalent d-block elements such as manganese(II) (Mn^{2+}), cobalt(II) (Co^{2+}), nickel(II) (Ni^{2+}), copper(II) (Cu^{2+}), and zinc(II) (Zn^{2+}). This is a remarkable property of these hydrogels, because metal-coordinated telechelic hydrogels have not been shown to crosslink with both trivalent and divalent ions. Typically, 4-armed catechol-functionalized PEG molecules are crosslinked only by trivalent ions such as Fe^{3+}, vanadium(III) (V^{3+}), and aluminum(III) (Al^{3+}) [98, 101]. In contrast, histidine-functionalized PEG molecules can only be crosslinked with divalent ions [102, 55], but not with trivalent ones. The fact that 2gPEG gels in the presence of divalent and trivalent ions opens up new possibilities to tune the mechanical properties of such metal-coordinated hydrogels over a much wider range.

Our results suggest that the ion-pyrogallol interactions are key in the hydrogel formation. To investigate the implications of these ionic interactions on the mechanical properties of the hydrogels, we systematically measure their rheological behaviors following the method in section 3.2.6 and the tests presented in section 1.4.4. The dynamic mechanical properties of ionically crosslinked telechelic hydrogels depend on the average lifetime of the crosslinks, and hence, the ion-ligand affinity. We use frequency sweeps to quantify the lifetime of these crosslinks by determining the frequency where the storage modulus (G') equals the loss modulus (G'') [98]. 2gPEG hydrogels crosslinked with Fe^{3+} display a solid-like behavior: their G' is higher than G'' over the entire measured frequency range, as shown in Figure 4.2a. As a reference, we end-functionalize linear PEG molecules possessing the same molecular weight as the 2gPEGs with catechols (2cPEG). 2cPEG hydrogels crosslinked with Fe^{3+} that have been prepared with the same protocol as the 2gPEG counterparts, only display a solid-like behavior for frequencies higher than 10 $rad \cdot s^{-1}$, as shown in Figure 4.2a. Hence, 2cPEG hydrogels are unable to retain their shape over time. This behavior reveals that 2gPEG hydrogels have much longer relaxation times than their 2cPEG analogues at a given pH. Furthermore, the observed G' of 2gPEG is an order of magnitude above the one of 2cPEG, confirming that pyrogallol-Fe^{3+} crosslinks are significantly stronger or more numerous than their catechol-Fe^{3+} counterparts.

We explore the range of accessible mechanical properties by crosslinking 2gPEG with other trivalent and divalent ions. Al^{3+}-, V^{3+}-, and Fe^{3+}-functionalized hydrogels have similar mechanical properties, as shown in Figure 4.2b. In contrast, the mechanical properties at low frequencies of 2gPEG hydrogels crosslinked with divalent ions vary over an order of magnitude, as shown in Figure 4.2c. Note that this trend does not significantly affect the plateau modulus, since it is a static network property, unaffected by crosslink kinetics. We decided to report here the value of the modulus at an arbitrarily low frequency of

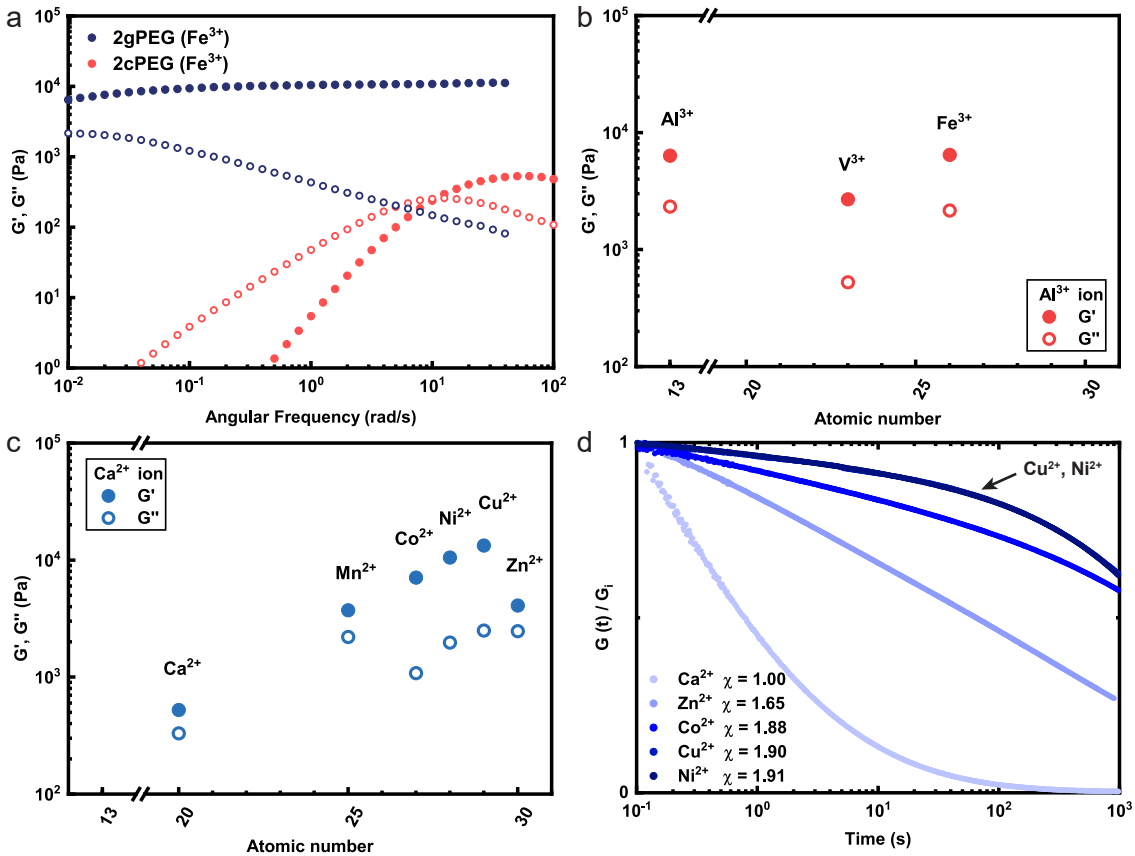

Figure 4.2: Rheology of 2gPEG hydrogels. (**a**) Frequency sweep of 2cPEG and 2gPEG crosslinked with Fe^{3+}, where we keep the molar ratio of pyrogallols to Fe^{3+} constant at 2. Both hydrogels contain the same concentration of ligand-functionalized polymer, the same concentration of ions, and pH. The different mechanical properties are attributed to different ion-ligand binding affinities. (**b,c**) The storage and loss moduli at 10^{-2} rad/s of 2gPEG crosslinked with different (**b**) trivalent and (**c**) divalent ions. (**d**) Stress relaxation measurements of 2gPEG hydrogels at 25 °C. The modulus is normalized to the initial modulus measured at 0.1 s. The different binding affinities lead to different relaxation behaviors. Filled symbols represent G' and empty symbols represent G''. Adapted with permission from [249].

10 rad·s^{-1} to represent the relaxation of the network over long time scales. In rubber elasticity theory, the modulus is defined by G=nRT, where n is the concentration of load-bearing network chains. This theory predicts that the modulus is not a function of the bonding energy. As a result, the plateau modulus is not affected by the kinetics of the metal coordination complex. Using the same reasoning, we do not observe significant differences for the trivalent ions, as the reported value at a frequency of 10^{-2} rad/s is already close to the plateau modulus, as seen in Figure 4.2a for 2gPEG crosslinked by Fe^{3+}. In order to better elucidate the role of the crosslink kinetics on the relaxation behavior of the network, we continue with stress relaxation measurements.

The solid-like mechanical properties displayed by 2gPEG hydrogels, combined with a decaying G′ at low frequencies, suggest that ion-pyrogallol crosslinks have longer relaxation times than ion-catechols. Despite these longer lifetimes, the ion-2gPEG crosslinks remain dynamic, and the network can rearrange to dissipate stresses. The rate of relaxation can be described based on the relaxation time, which for divalent ions is longest for pyrogallols complexed with Ni^{2+} and shortest for those complexed with Ca^{2+}, as measured by stress relaxation and summarized in Figure 4.2d. We assign this decrease in relaxation times to the decreasing electronegativity (χ) of the complexing ions, from Ni^{2+} ($\chi = 1.91$) to Ca^{2+} ($\chi = 1.00$), suggesting a decreased binding affinity of the cations to pyrogallols.

Why do we need so much more divalent ions than trivalent ones to gel the 2gPEG network? This significant difference in stoichiometry hints towards a particle based crosslinking mechanism. To explore this hint, we measure the energy barrier of bond dissociation and the spread in relaxation times; both these parameters are significantly larger if nanoparticles act as crosslinkers [171]. We select two divalent ions, of a low (Ca^{2+}) and high (Zn^{2+}) atomic number, and Fe^{3+} to represent the trivalent ions. We perform temperature-dependent strain relaxation measurements with a step strain of 10% [171], as exemplified in Figure 4.3a for Ca^{2+} and extrapolate the dissociation energy of the crosslink, as shown in Figure 4.3b for Ca^{2+}. The dissociation energy for 2gPEG-Fe^{3+} hydrogels is similar to that of 2cPEG-Fe^{3+} hydrogels (Figure 4.3c), and in good agreement with literature [171], confirming that our hydrogels are mainly ionically crosslinked. Note that the dissociation energy is related to the dynamics of the hydrogel and not its elastic behavior. The comparison molecule, 2cPEG, cannot be crosslinked by divalent ions such as Ca^{2+} and Zn^{2+}, such that the dissociation energies are considered to be below k_BT. For the crosslinked samples, we extrapolate the Kohlrausch exponent of our model that can be understood as the spreading of relaxation times [250], as shown in Figure 4.3d and e and described in the method in section 3.2.7. At Kohlrausch exponent values close to 1, the stress relaxation is fitted to a single relaxation time that is typical for ion-catechol tris complexes. At low Kohlrausch exponent values, the relaxation time spectrum $H(\tau)$

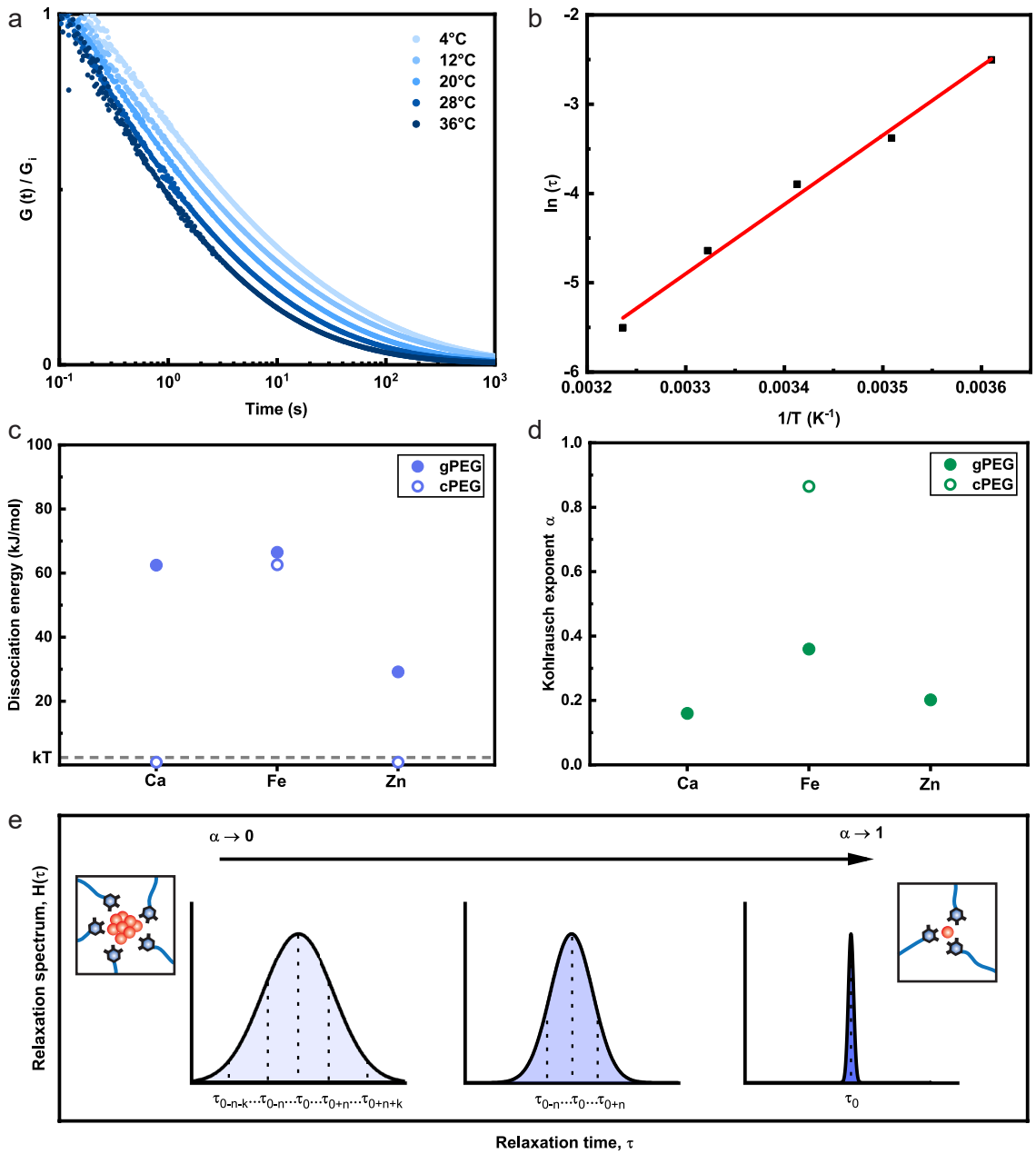

Figure 4.3: Ionic bond relaxation. (**a**) Temperature-dependent stress relaxation of 2gPEG crosslinked with Ca^{2+}. Higher temperatures lead to faster stress relaxation. (**b**) The curves in (**a**) are fitted using a stretched exponential decay function, and the natural logarithm of the average relaxation time coefficient is plotted against the inverse temperature. The Arrhenius plot is fitted using a linear function to extract the dissociation energy of the network. (**c**) Calculated dissociation energies of 2gPEG crosslinked with Ca^{2+}, Fe^{3+} and Zn^{2+} ions and 2cPEG crosslinked with Fe^{3+}. 2cPEG does not gel with Ca^{2+} and Zn^{2+}, indicating that their dissociation energy is below k_BT at room temperature. (**d**) The calculated average Kohlrausch exponent of the stretched exponential decay. (**e**) Schematic illustration of the relaxation spectrum as a function of the Kohlrausch exponent α. Larger Kohlrausch values lead to a narrower distribution of relaxation times, corresponding to a narrower distribution of relaxation mechanisms in the hydrogel network. Adapted with permission from [249].

(introduced in section 1.4.4) broadens, as observed in the 2gPEG hydrogels. A broadening of the relaxation time spectrum hints at different relaxation mechanisms, which are present in these hydrogels. A single ion in a tris complex leads to a single relaxation time. By contrast, nanoparticles result in different binding affinities with ligands, and hence, different relaxation times, because their size distribution varies. The observed lower values for the Kohlrausch exponents therefore suggest that divalent ions precipitate at the crosslinking sites to form nanoparticles. Following the same argument, we postulate that nanoparticles also form in the case of trivalent ions. Note that even though our hydrogels are primarily crosslinked by nanoparticles, we call them metal-coordinated hydrogels as the chelator-nanoparticle interactions are based on coordination chemistries. The smaller concentration of trivalent ions and the lower pH required to form the hydrogel are likely related to their stronger affinity to pyrogallols, their poorer solubility that results in the formation of precipitates at lower pH values, or a combination of the two aspects.

4.4.2 Structure of ion - 2gPEG hydrogels

To assess the effect of crosslinking chemistry on the network structure, we perform small-angle X-ray scattering (SAXS) on selected samples and analyze the data following the method described in section 3.2.9. The scattering of the network of telechelic crosslinked polymers, such as 2gPEG, reveals structures within 1 - 33 nm. To determine the contribution of ions and polymers to the scattering signal, we measure a solution of ions and 2gPEG under acidic conditions. To determine the scattering signal of the ions in solution, we subtract the signal of pure 2gPEG in solution. There is no structuring for ions under acidic conditions even in the presence of 2gPEG, indicating that they remain in solution and do not form precipitates or structures in the size range of 1 - 33 nm that can be detected by SAXS (Figure 4.4a). With increasing pH, the ion-2gPEG systems start to gel, and clear differences appear in the plot of the scattering intensity (I) as a function of the scattering vector (q) (Figure 4.4 and 4.5a). The strong increase in the scattering intensity measured at low q-values indicates that larger scattering objects are formed within the network's structure. At the length scale covered by SAXS, two characteristic dimensions are observed in the crosslinked hydrogel networks: (i) a short correlation length (ξ) describes rapid fluctuations of the position of the polymer chains in solution, represented by a single Lorentzian curve at high q-values; and (ii) a long correlation length (φ) describes the static distance between the crosslinking points, and is estimated by a Gaussian that shows the formation of a network with stationary crosslinking points at low q-values [223].

With increasing volume fraction of the polymer, ξ and φ tend to decrease because the polymer network becomes denser such that the crosslinking density increases, thereby reducing

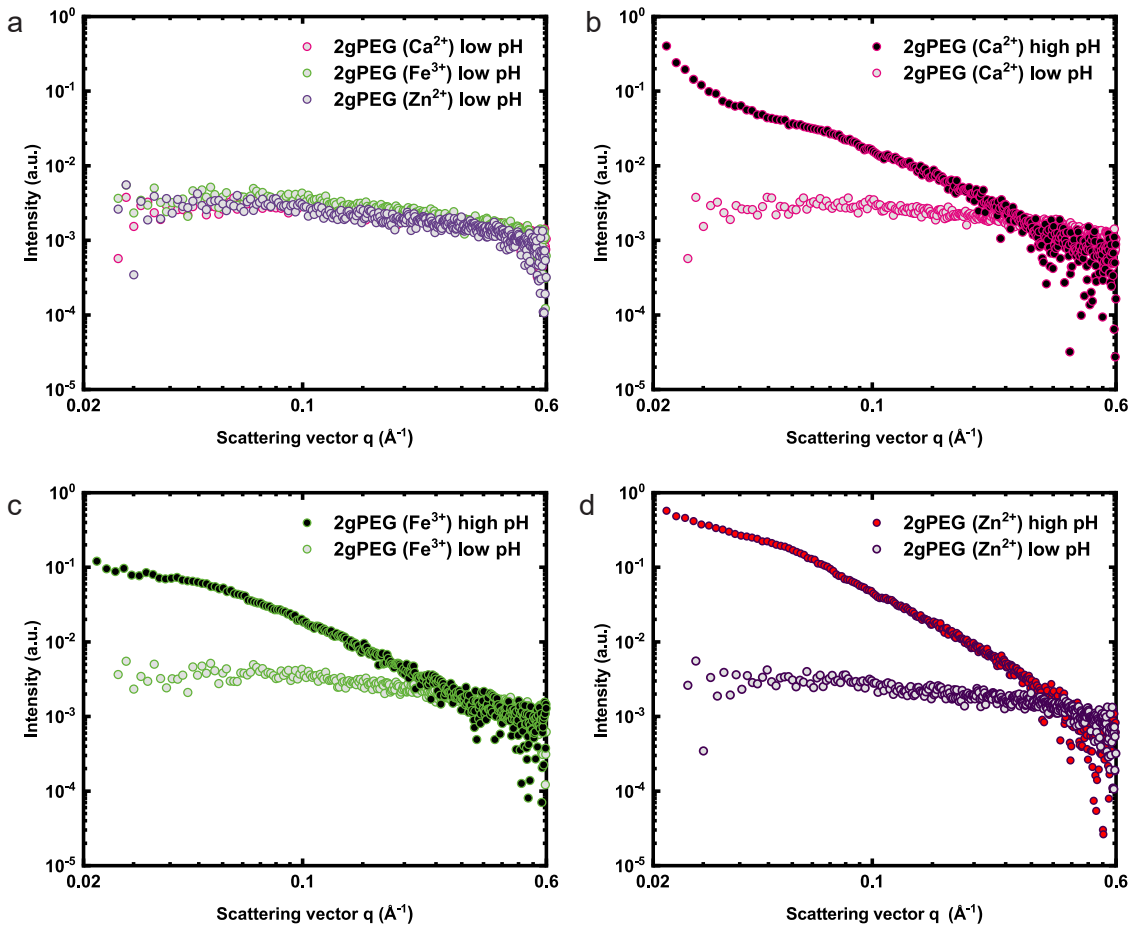

Figure 4.4: SAXS measurements of ions and 2gPEG molecules in solution and in the crosslinked state. (**a**) Scattering of the 2gPEG solutions containing Ca^{2+}, Fe^{3+} and Zn^{2+} ions at low pH. (**b-d**) Scattering of the low pH solutions of 2gPEG containing (**b**) Ca^{2+}, (**c**) Fe^{3+}, and (**d**) Zn^{2+} respectively (**light grey fill**); and of the high pH Ca^{2+}, Fe^{3+}, and Zn^{2+} hydrogels (**black fill**). Adapted with permission from [249].

the mobility of the polymer chains [223]. The type of ions used to crosslink 2gPEG gels does not significantly influence the short correlation length ξ. This result indicates that the mobility of the individual polymer segments is independent of the ionic crosslinker, as can be expected for linear telechelic polymers. By contrast, the type of ions used to crosslink 2gPEG influences the long correlation length φ attributed to the crosslinking sites: Fe^{3+} ions result in the smallest values of φ, indicating that these ions result in the highest crosslinking density. This finding is in good agreement with our rheology results. It hints at the fact that Fe^{3+} crosslinked samples have the least dangling bonds, which could be a result of the long dissipation times of Fe^{3+}-2gPEG hydrogels. This finding could also indicate that the valency of Fe^{3+}-containing crosslinking sites is the highest, which could be the case if ions are transformed into nanoparticles at the crosslinking sites

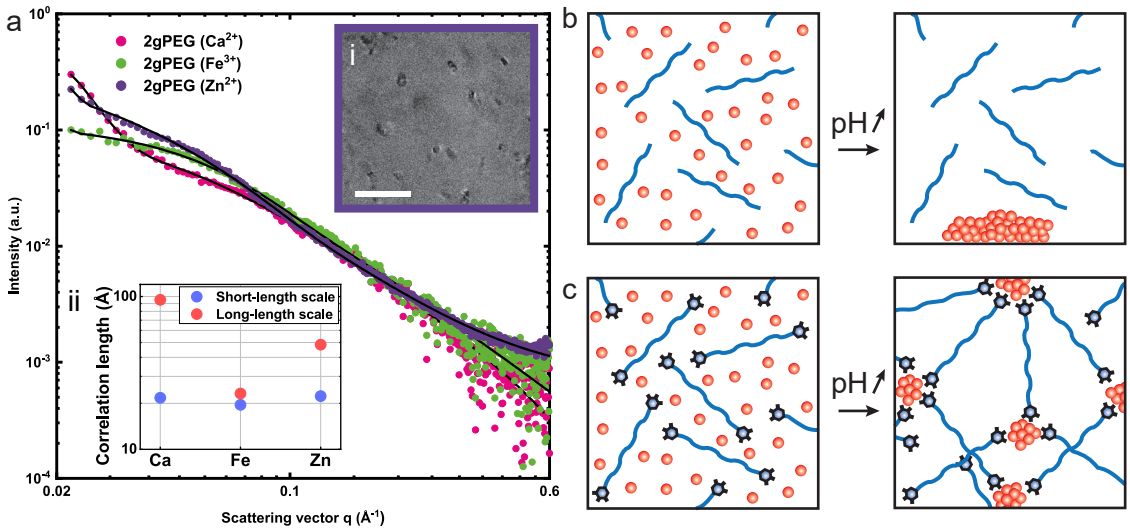

Figure 4.5: Characterization of the crosslinking mechanism in 2gPEG networks. (**a**) SAXS measurements of 2gPEG hydrogels crosslinked with Ca^{2+}, Fe^{3+}, and Zn^{2+}. The spectra are fitted using a Lorentzian-Gaussian model (**black line**). TEM of freeze-dried 2gPEG hydrogels crosslinked with Zn^{2+} is shown in inset (**i**). Polydisperse nanoparticles are observed; the scale bar is 100 nm. The fitting parameters of the short-length scale and long-length scale scattering are shown in inset (**ii**). All samples have a similar short-length scale parameter ξ because they are composed of the same polymer. In contrast, the long-length scale parameter φ, which is attributed to the average distance between crosslinks, differs significantly. (**b**) Schematic illustration of the formation of macroscopic inorganic precipitates upon pH increase in the absence of ligands on the polymer chains. The ions precipitate and agglomerate, without interacting with the polymer such that the solution remains liquid. (**c**) Schematic illustration of the hydrogel gelation when the polymer chains are functionalized with pyrogallol groups that act as nanoparticle stabilizers and metal coordinating sites. Adapted with permission from [249].

and the density of pyrogallols that bind to each nanoparticle is comparably high. The lack of structure and form factor peaks in these SAXS curves suggest that nanoparticles, if present, are polydisperse. We confirm the presence of polydisperse nanoparticles in the size range of 20 nm by TEM, as shown in the inset of Figure 4.5a. To test if smaller or crystalline nanoparticles form at the crosslinking sites, we perform XRD on dried samples. We only obtain diffraction peaks from PEG and NaCl, both formed during the drying process of the XRD samples, as shown in Figure 4.6. The lack of additional peaks indicates that the nanoparticles formed at the cross-link sites do not possess crystalline domains or that they are not sufficiently large or numerous to be detected by XRD.

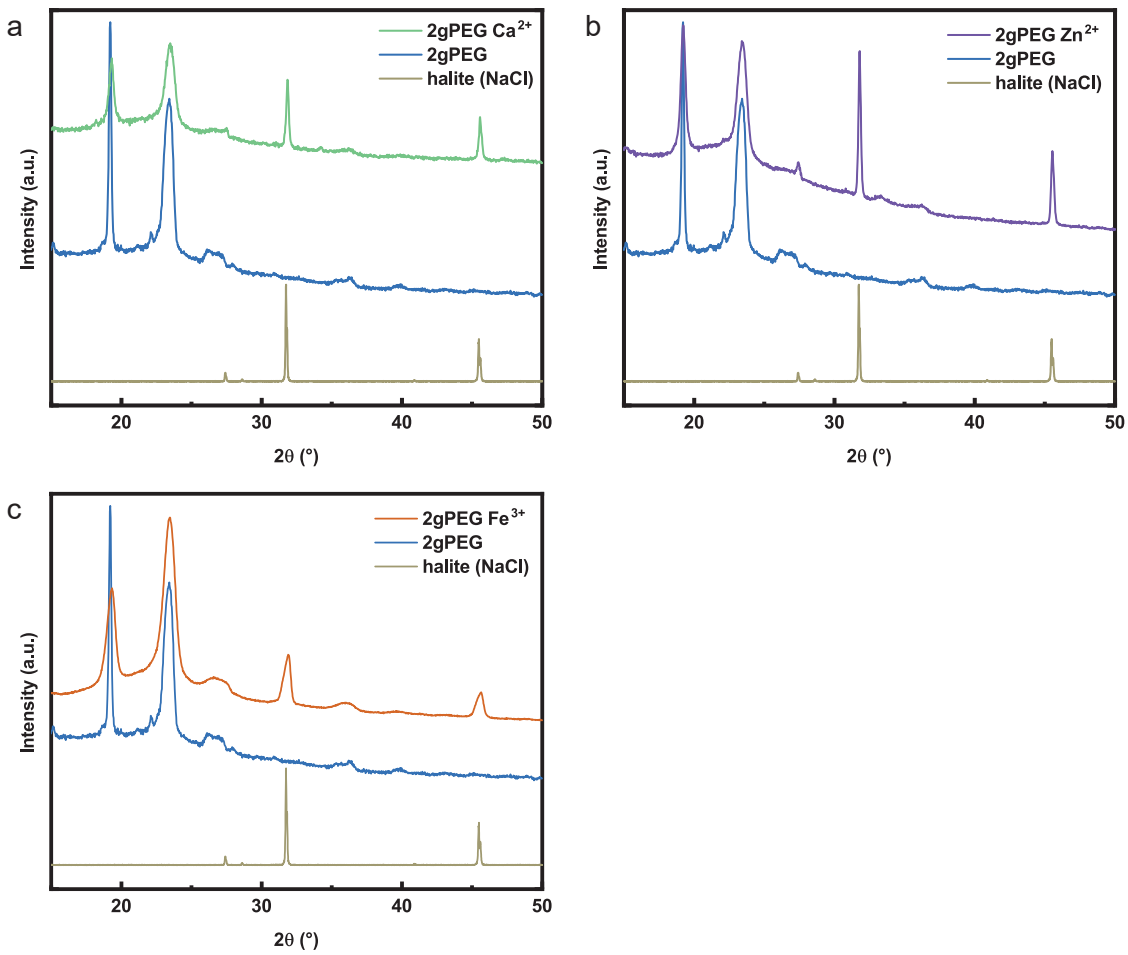

Figure 4.6: XRD diffraction spectra of dried 2gPEG hydrogels that have been crosslinked with (**a**) Ca^{2+}, (**b**) Zn^{2+}, and (**c**) Fe^{3+} are compared to the bare dry 2gPEG and the diffraction pattern of NaCl (RRUFF database). A comparison between the spectra reveals that the observed diffraction peaks are due to the crystalline domains of PEG and NaCl crystals. No other diffractions can be identified. Adapted with permission from [249].

4.4.3 Crosslinking mechanism

To understand the mechanism of formation of these nanoparticles, we prepare a solution containing unfunctionalized PEG and ions and increase the pH, as we did to gel 2gPEG samples. If unfunctionalized PEG is used, we observe the precipitation of macroscopic particles (Figure 4.5a and 4.7). This result suggests that the pyrogallol groups strongly bind to the surfaces of the forming particles, thereby slowing down or even arresting their growth, as schematically shown in Figure 4.5c. This observation is well in agreement with previous reports on pyrogallol-functionalized individually dispersed particles [176, 251, 252]. We measure resonance Raman spectroscopy on Fe^{3+} crosslinked 2gPEG hydrogels

to assess the ligand-ion interactions, as shown in Figure 4.8. Three signature peaks are known for catechols if excited with a 785 nm laser source [107, 98, 253]. They are assigned to the charge transfer (533 cm^{-1}) and the bidentate chelation of Fe^{3+} by oxygens on the catechol ring (590, 633 cm^{-1}). Due to the chemical similarity of pyrogallols and catechols, we observe similar resonance peaks in our 2gPEG hydrogels. The Fe^{3+} complexed 2gPEG hydrogel displays a strong charge transfer peak at 537 cm^{-1} and the bidentate chelation peaks at 588 and 620 cm^{-1} (Figure 4.8). Remarkably, the two latter resonance peaks are broader than those of catechol-functionalized hydrogels, suggesting that pyrogallol-iron complexes possess a range of different binding affinities [98, 171]. This result is in good agreement with the observed small values of the Kohlrausch exponent. The Raman peaks are weaker and broader if 2gPEG is crosslinked with V^{3+}, in stark contrast to catechol-functionalized hydrogels crosslinked with V^{3+} that result in stronger Raman signals [101]. We cannot excite any phonon resonance in the 500-680 cm^{-1} region with a 785 nm laser if 2gPEG is crosslinked with Zn^{2+} and Ca^{2+}, as shown in Figure 4.9. This result hints at clear differences in the metal-pyrogallol interactions that are likely responsible for the observed differences in mechanical properties.

4.4.4 Application as underwater adhesives

Ligands present in functionalized hydrogels can bind to the surface ions of bulk materials, making them interesting candidates for underwater adhesives. Catechols, commonly found in the marine mussel foot plaque, which holds onto rocks under harsh conditions, are the text book example of underwater adhesion. Synthetic catechol-functionalized telechelic PEGs have already been applied as medical sealing for the amniotic sac after fetal surgery [254]. The adhesion of catechols and pyrogallols to wet surfaces is increasingly reversible if ions are added [229, 255, 256]. Here we demonstrate that our 2gPEG hydrogels can be employed as self-healing underwater adhesives. We crosslink 2gPEG with a weak crosslinker, Ca^{2+}, such that it displays a fast relaxation and can adapt its shape quickly to the roughness of the solid surface. We deposit the hydrogel onto an inox steel surface, immerse it in water, and place it in contact with the surface of a 500 g brass weight. After the two metal surfaces are hand-pressed against each other for 10 s, the weight can be lifted out of the water, as shown in Figure 4.10a. This result demonstrates that the thin hydrogel layer sustains a pressure of 50 kPa. Note that the tested hydrogel is one of the weaker ones we introduced such that it shows a fast self-healing behavior. Nevertheless, its mechanical properties are similar to recently reported underwater adhesives and superior to the state-of-the-art cyanoacrylates [257]. This is only possible if the adhesion between the hydrogel and the solid surfaces is strong such that the load can efficiently be transferred, and the cohesion within this rather dynamic hydrogel is still sufficiently high.

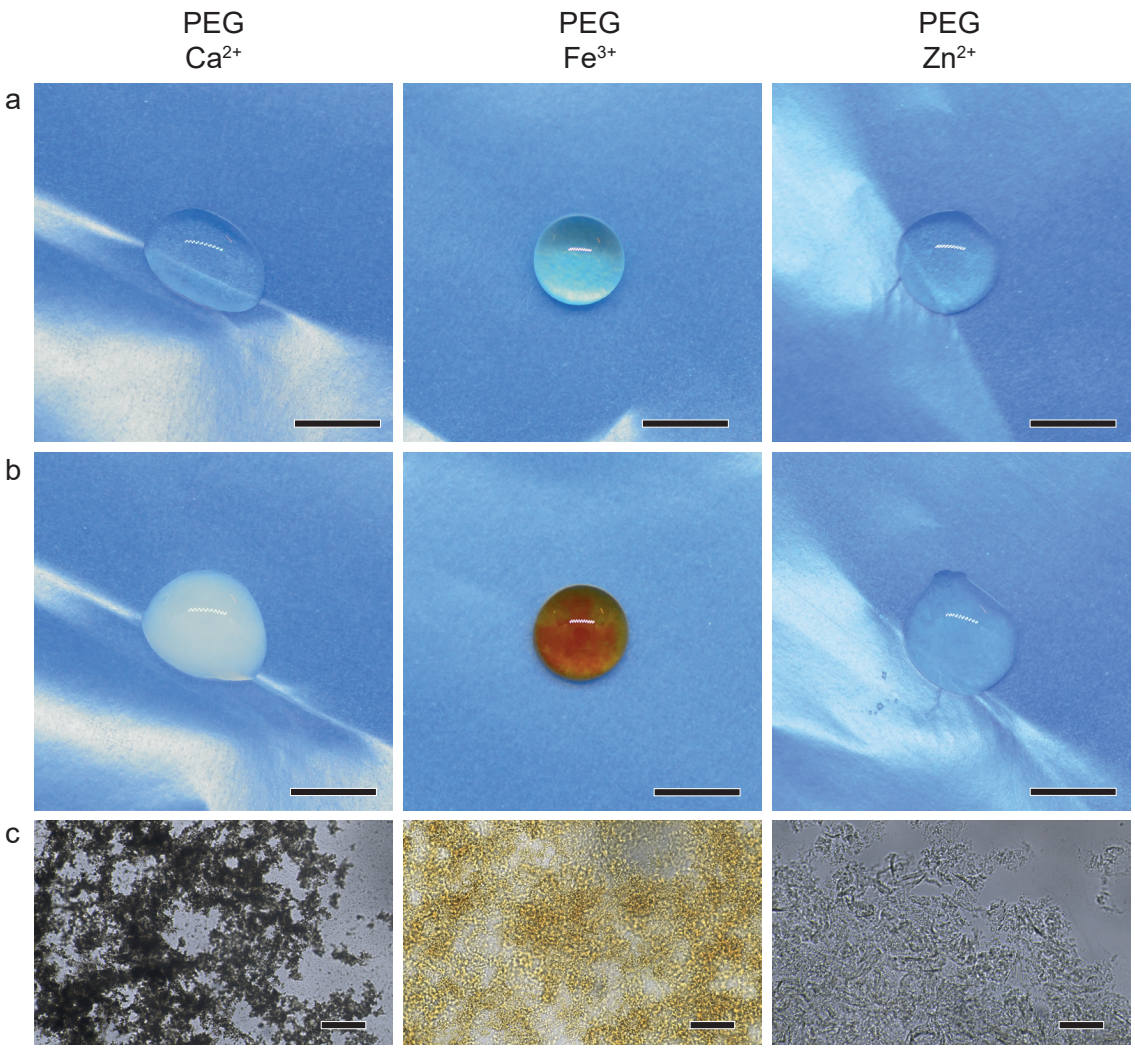

Figure 4.7: Photographs of PEG solutions, containing Ca^{2+}, Fe^{3+}, and Zn^{2+} ions. (**a**) The concentrations of PEG and the ions are the same as in the solutions used to prepare 2gPEG hydrogels (scale bar is 5 mm). (**b**) The pH shift induced through the addition of NaOH triggers the precipitation of microparticles, visible to the naked eye (scale bar in 5 mm). (**c**) Micrographs of the microparticles in suspension (scale bar is 200 μm). Adapted with permission from [249].

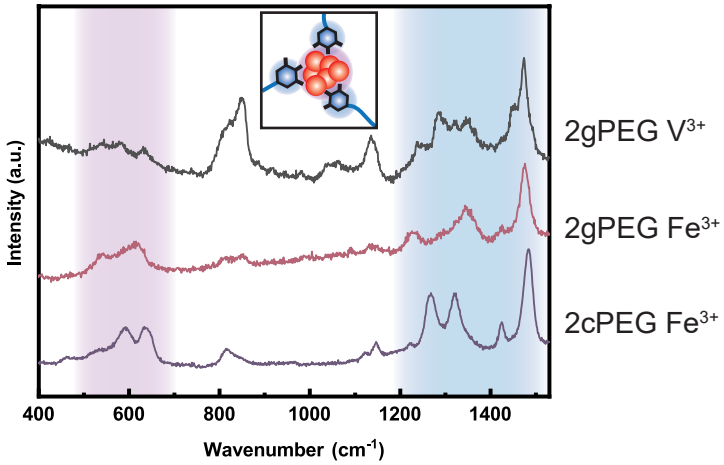

Figure 4.8: Raman characterization of 2gPEG hydrogels. Resonance Raman spectra of 2gPEG crosslinked with V^{3+} and Fe^{3+}, and 2cPEG crosslinked with Fe^{3+}. The peaks between 500 and 680 cm^{-1} are attributed to the catechol-Fe^{3+} coordination or pyrogallol-Fe^{3+} coordination, while the peaks between 1230 and 1500 cm^{-1} are due to the carbon ring vibration. Adapted with permission from [249].

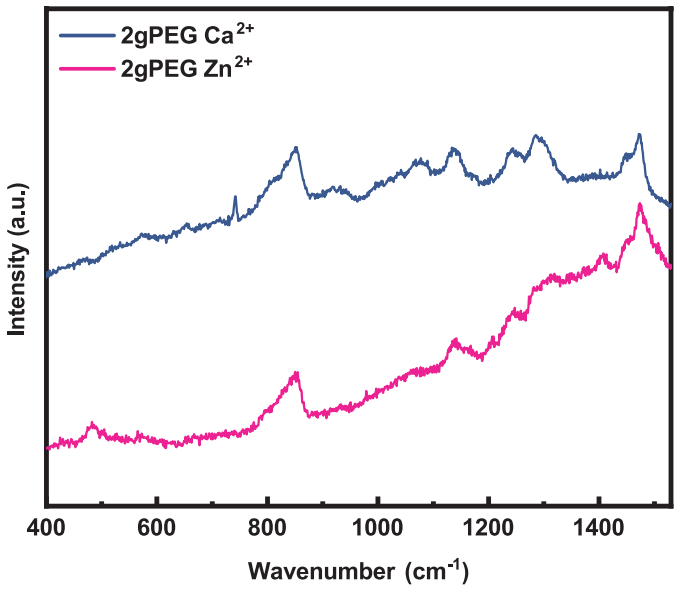

Figure 4.9: Raman shift spectrum of 2gPEG crosslinked with Ca^{2+} and Zn^{2+}. No peaks are observed in the range of 500 - 680 cm^{-1}. Adapted with permission from [249].

4.4.5 Self-healing properties

A key feature of our ion-2gPEG hydrogels is the possibility to tune the relaxation times and hence the time scales over which they self-heal and start to flow over a much wider range than currently known. To demonstrate this feature, we cut the hydrogels that have been crosslinked with different ions, and monitor their self-healing as a function of time. Hydrogels that are crosslinked with the most commonly employed metal coordination motif, catechol-Fe^{3+}, start to lose their shape within seconds. By contrast, 2gPEG that is crosslinked with the same ion, Fe^{3+}, retains its shape for at least 20 min, which is the duration of our experiment, as shown in Figure 4.10b. We attribute the much higher shape stability of 2gPEG-Fe^{3+} hydrogels to the longer dissipation times of pyrogallol-Fe^{3+} complexes compared to their catechol-Fe^{3+} counterparts. However, the good shape stability comes at the expense of the self-healing properties: these hydrogels only self-heal within an hour when placed in contact. If faster self-healing is required, 2gPEG can be crosslinked with weaker complexation agents, such as divalent ions. For example, if 2gPEG is crosslinked with Zn^{2+}, the hydrogel self-heals within 15 minutes, whereas those crosslinked with Ca^{2+} self-heal within a minute, as shown in Figure 4.10b. Note that, despite the relatively weak interactions of pyrogallol and Ca^{2+}, the time scale over which this sample loses its shape is much longer than that of the much more commonly used catechol-Fe^{3+} crosslinked counterpart. These results illustrate the potential of 2gPEG-based hydrogels to adjust their dynamic mechanical properties to the needs of the specific application.

4.4.6 Functionalization with nanoparticles

The wide range of ions that can be used to crosslink 2gPEG hydrogels opens up new possibilities to functionalize them with nanoparticles. To demonstrate this feature, we crosslink 2gPEG hydrogels with iron oxide nanoparticles. To achieve this goal, we mix 2gPEG with an aqueous solution of Fe^{3+} and Fe^{2+} ions where we fix the molar ratio of Fe^{3+}:Fe^{2+} to 2:1. Upon exposure to ammonia, the cations precipitate to form iron oxide nanoparticles. The resulting hydrogel is brittle and forms pieces when mechanically mixed. If densely packed using centrifugation, these pieces can be casted, resulting in an integral part within a minute that retains its shape upon demolding for more than 24 h. Furthermore, the resulting nanoparticles impart the hydrogels with magnetic properties, as illustrated by the movement of the hydrogel towards the externally applied magnetic field, shown in Figure 4.10c, 4.10d. This result demonstrates the possibility to introduce functionalities into these hydrogels without sacrificing their mechanical properties.

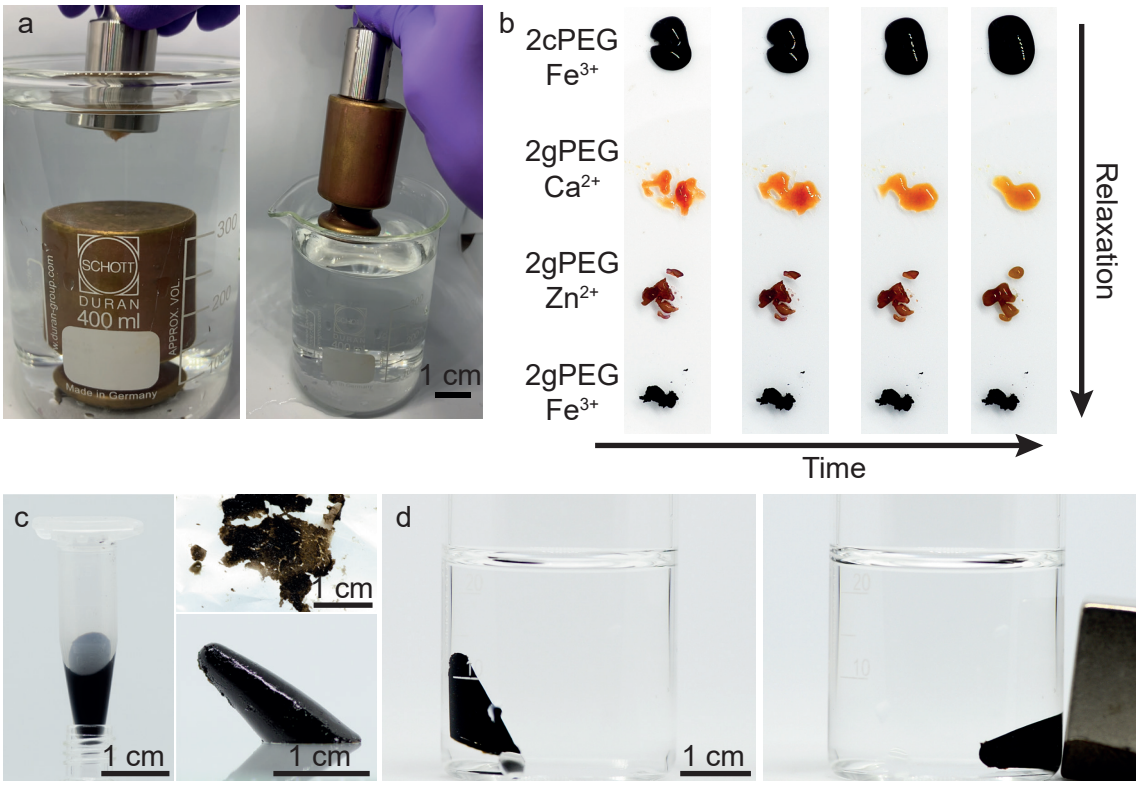

Figure 4.10: Applications of 2gPEG hydrogels. (**a**) Photographs of 2gPEG crosslinked with Ca^{2+}, acting as an underwater glue. The hydrogel glue is able to lift a 500 g copper weight outside of the water, corresponding to a 50 kPa pressure. (**b**) Time-lapse photographs of the self-healing behavior of hydrogels possessing various relaxation times. The left image is taken 10 s after cutting through the hydrogels, and the right image 20 min thereafter. (**c**) Photograph of 2gPEG crosslinked by iron oxide precipitates formed by exposing the 2gPEG solution containing an excess of Fe^{2+} and Fe^{3+} ions to ammonia. The hydrogel forms macroscopic particles when mechanically mixed on Parafilm. The particles are casted in an Eppendorf tube using centrifugation (**left**) and merged to yield a single integral solid hydrogel piece. Upon removal from the mold, the hydrogel retains its shape (**right**). (**d**) The iron oxide precipitates impart magnetic properties to this hydrogel: if immersed in water (**left**), it can be displaced by an external magnetic field (**right**). Adapted with permission from [249].

4.5 Conclusion

We introduce a metal-coordinated hydrogel whose mechanical properties can be tuned over a wide range by selecting appropriate ions. The broadening in the dynamic mechanical properties of the hydrogel is achieved using telechelic linear PEGs that are end-functionalized with pyrogallols. Pyrogallol-ion complexes have longer dissipation times than the more commonly used catechol-ion or histidine-ion counterparts, and consequently they can retain their shapes much longer. This asset opens up new possibilities to construct truly 3D self-healing materials from metal-coordinated hydrogels. We attribute the long dissipation times of the metal-coordination sites to the precipitation of nanoparticles at the crosslinking sites. The pyrogallols slow down or even prevent the growth of precipitates, resulting in multivalent crosslinking sites that impart excellent mechanical properties to the dynamic networks. Importantly, the mechanical properties of these networks can be tuned with the choice of divalent and trivalent ions used to create the crosslinking sites. The tunable mechanical properties promise to advance the design of multifunctional mechanically robust dynamic hydrogels and might find applications in biomedicine, for example if antibacterial nanoparticles are included, or in optics, if high refractive index nanoparticles are employed. Finally, the inherent adhesion of pyrogallols to wet surfaces allows the creation of medical seals with well-defined mesh structures, which offer a tight control over the diffusion of essential small molecules.

CHAPTER 5

3D printing of strong and tough double network granular hydrogels

In this chapter, I present a double network granular hydrogel, made from hydrogel microparticles that are connected by a second percolating network. The rheological behavior of the precursor loaded jammed microparticles imparts them optimal extrusion properties for additive manufacturing. The subsequent polymerization of the secondary network forms a percolating phase, effectively solidifying the printed hydrogel. This approach is in stark contrast with standard homogeneous double network hydrogels, enabling 3D printing while maintaining good mechanical properties.

This chapter is adapted from the paper entitled "3D Printing of Strong and Tough Double Network Granular Hydrogels" authored by Matteo Hirsch, Alvaro Charlet and Esther Amstad. M. Hirsch and A. Charlet are equally contributing co-first authors. M. Hirsch, A. Charlet and E. Amstad designed the experiments. M.Hirsch designed the tensile test studies and A.Charlet designed the rheological test studies. M. Hirsch, A. Charlet performed all experiments collectively. M. Hirsch, A. Charlet and E. Amstad analyzed the data and wrote the manuscript.

Contents

5.1 Abstract

Many soft natural tissues display a fascinating set of mechanical properties that remains unmatched by manmade counterparts. These unprecedented mechanical properties are achieved through an intricate interplay between the structure and locally varying composition of these natural tissues. This level of control cannot be achieved in soft synthetic materials. To address this shortcoming, we introduce a novel 3D printing approach to fabricate strong and tough soft materials, namely double network granular hydrogels (DNGHs) from compartmentalized reagents. This is achieved with an ink composed of microgels that are swollen in a monomer-containing solution; after the ink is 3D printed, these monomers are converted into a percolating network, resulting in a DNGH. These DNGHs are sufficiently stiff to repetitively support tensile loads up to 1.3 MPa. Moreover, they are more than an order of magnitude tougher than each of the pure polymeric networks they are made from. We demonstrate that this ink enables printing macroscopic strong and tough objects that can optionally be rendered responsive with a high shape fidelity. The modular and robust fabrication of DNGHs opens up new possibilities to design adaptive strong and tough hydrogels that have the potential to advance, for example, soft robotic applications.

5.2 Introduction

Most hydrogels that must retain their 3D structure and bear some load are covalently crosslinked and hence, if swollen, they are inherently brittle. As discussed in section

1.5.1, their toughness can be strongly increased, if reversible crosslinks that rely on non-covalent interactions [258, 102], slide-ring structures [259], host-guest interactions [124], nanoparticle fillers [252], or a combination of them [171] are introduced. Indeed, this strategy enables the design of extremely tough hydrogels that can be stretched up to 50 times [260, 261, 262]. However, these tough hydrogels are typically rather soft such that they cannot bear significant loads under tension. To overcome this shortcoming, double network (DN) hydrogels composed of two interpenetrating polymeric networks have been introduced, as introduced in section 1.6.6. These DN hydrogels are composed of a highly crosslinked network, the filler, that imparts stiffness to the hydrogel and a second loosely crosslinked one, the matrix, that imparts toughness to it [60]. This advance enabled engineering the mechanical properties of DN hydrogels to be similar to those of certain natural tissues such as cartilage [263, 58].

Despite the great improvement in mechanics, manmade hydrogels are typically inert and hence, cannot adapt their properties in response to external stimuli, in stark contrast to many natural counterparts. An important difference between these two types of materials is their structure and local composition. Soft natural materials possess locally varying compositions and structures that are well-defined over many length scales. By contrast, synthetic hydrogels typically have ill-defined microstructures and their composition is most often homogeneous. Variations in the composition can be introduced using magnetic nanoparticle gradients [264], UV patterning [265], micro-molding [266], photo-triggered chemical crosslinkers [262], or micro-phase separation [267]. However, these methods are often labor intense such that they cannot fabricate soft materials with structures that are similar to those of natural models. A contributing reason for the discrepancy in the structure and local composition of soft natural versus synthetic materials is the difference in their processing. Nature produces many of its strong and tough materials from compartmentalized reagents. For example, most marine mussels fabricate their byssus from precursor-containing vesicles that are released on demand and self-assemble into well-defined structures [103, 105]. By contrast, synthetic hydrogels are typically fabricated by mixing reagents in bulk. This technique offers an excellent control over the overall composition of the hydrogels. However, it lacks control over the local composition and microstructure. Complex 3D structures can be achieved through patterned droplet networks [111] or jammed microgels for example using additive manufacturing techniques [12, 177, 187, 196]. However, as mentioned in section 1.8, monodisperse spherical microgels have a small contact area such that the resulting superstructures are weak [268]. The mechanical properties of these granular materials can be improved if the surfaces of the microgels are modified with thiols [203] or metal-coordinating groups [176], through covalent crosslinking of adjacent microgels [269], or by means of a percolating second network

[270, 173]. However, the increased adhesion between microgels compromises the stretchability of the materials, thereby reducing their toughness. Methods to fabricate strong and tough complex 3D hydrogels that have the potential to be used, for example, as load bearing parts of soft robots, remain to be established.

Here, we introduce a new ink that can be additive manufactured into strong and tough DNGHs with locally varying compositions. The ink is composed of polyelectrolyte-based microgels that are swollen in a monomer-loaded solution. This monomer-loaded solution can be converted into a percolating network after the ink has been processed into macroscopic materials. The new two-step approach separates the fabrication of microgels and their annealing. Thereby, it combines the advantages of jammed granular solutions such as injectability and printability with the excellent mechanical properties of DN hydrogels. Importantly, the mechanical properties of the additive manufactured materials can be tuned with the composition of the ink and are independent of the printing parameters such as the printing direction. Because this new technology employs a microgel-based ink, it significantly extends the choice of materials that can be additive manufactured such that the range of mechanical properties that can be accessed with 3D printed hydrogels is much wider. Our new DNGH promise to bridge the gap between structural complexity and mechanical performance that is key in the advancement of soft materials for load-bearing applications. These features will likely enable the design of new, functional, responsive hydrogels that can be used for soft robots and actuators, and membranes for wastewater treatment.

5.3 Experimental section

Details about the experimental procedure are presented in chapter 3 from section 3.3.1 on page 45 to section 3.3.8 on page 47.

5.4 Results and discussion

5.4.1 Microgel ink design and fabrication

To maximize the contact area between adjacent microgels and minimize interstitial spaces, we synthesize microgels possessing a high swelling capacity. Polyelectrolyte-based microgels have been shown to fulfil these requirements. Hence, we select AMPS as a model system and fabricate PAMPS microgels from reagent-loaded water in oil emulsion drops,

as sketched in Figure 5.2a and detailed in section 3.3.1. To test if the size of the microgels we produce scales with that of the emulsion drops, we quantify this parameter from optical microscopy images. Drops and crosslinked microgels are nearly identical in size, as shown in Figure 5.1. After having been crosslinked, microgels are washed several times in ethanol and deionized water to remove unreacted molecules, as sketched in Figure 5.2b. To ensure good inter-particle adhesion, which is key for obtaining good mechanical properties, we swell the microgels in a solution containing reagents that can be converted into a percolating network after the microgels have been 3D printed. Here, we swell the microgels in an aqueous solution containing AM monomers, as sketched in Figure 5.2c. To avoid any dilution effects from the water exchange, we soak microgels in the monomer solution for 24h in large excess of the second network precursor solution. The degree of swelling of the microgels strongly depends on the crosslinker concentration of the microgels: microgels containing 14 mol% crosslinker have an average diameter of 40 µm whereas those containing 3.5 mol% crosslinker have a diameter of 120 µm, as shown in Figure 5.1.

An important feature of our technique is the processing of individually dispersed microgels into macroscopic materials with structures that are well-defined over the millimeter up to the centimeter-length scales. This structural control is achieved through 3D printing. To enable 3D printing of the dispersed microgels, we jam them using vacuum filtration, as shown in Figure 5.2d. The resulting ink is 3D printed into complex structures, as schematically presented in Figure 5.2e. The printed construct is post-cured by exposing it to UV light to allow the formation of a percolating second network, as exemplified on Figure 5.2f.

5.4.2 Rheological characterization of microgel inks

A prerequisite for inks to be 3D printed into macroscopic complex structures is their shear thinning behavior, which is a common property of bioinks [272, 273] and jammed microgels [181]. To ensure a reproducible jamming of the microgels, we measure the solid polymer content of samples swollen in deionized water, as reported in Table 5.1. The results suggest a good reproducibility of our jamming process, where the AMPS polymer content accounts for 4.83 wt% of the resulting ink. The standard deviation of the solid fraction is as low as 0.22 wt%.

As expected, our jammed microgels are shear thinning, as demonstrated by oscillatory rheology in Figure 5.3a. The viscosity of the jammed PAMPS microgels can be tailored with the crosslinker concentration; it increases from 100 to 1000 Pa·s at a shear rate of 10 s^{-1}, if the crosslinker concentration is increased from 3.5 to 14 mol%. To enable precise dosing, the solid granular ink should possess a low flow point. This requirement is fulfilled

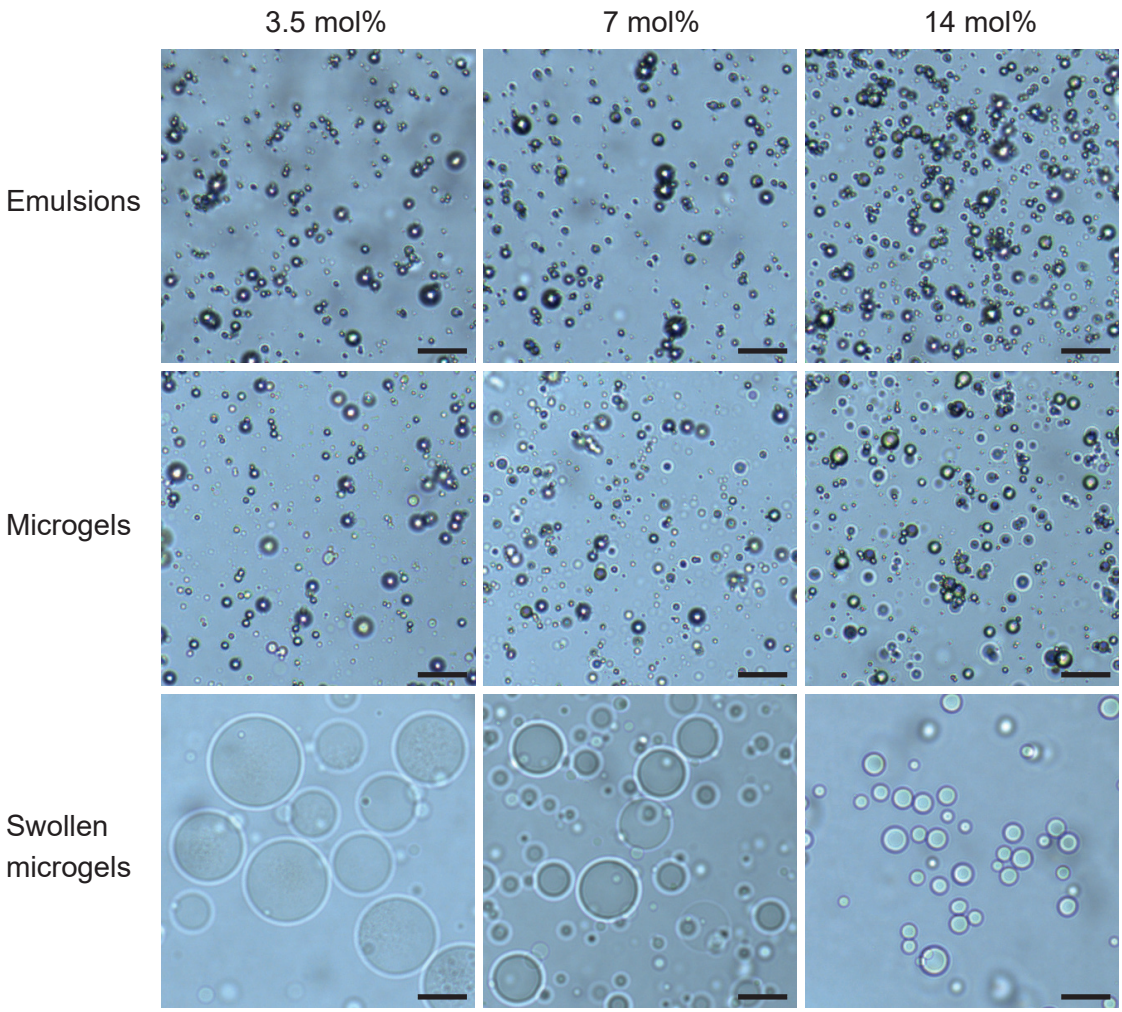

Figure 5.1: Influence of crosslinker concentration on the swelling of microgels. Optical micrographs of (**top**) emulsions (**middle**) after the reagents have been crosslinked to form microgels, and (**bottom**) microgels swollen in an AM-containing solution. Microgels contain (**left**) 3.5 mol%, (**middle**) 7 mol%, and (**right**) 14 mol% crosslinker. The average diameter of emulsion drops is 20 µm, that of swollen microgels containing 3.5 mol% crosslinker 120 µm, those containing 7 mol% crosslinker have an average diameter of 65 µm, and those containing 14 mol% crosslinker have a diameter of 40 µm. Scale bars are 100 µm. Adapted with permission from [271].

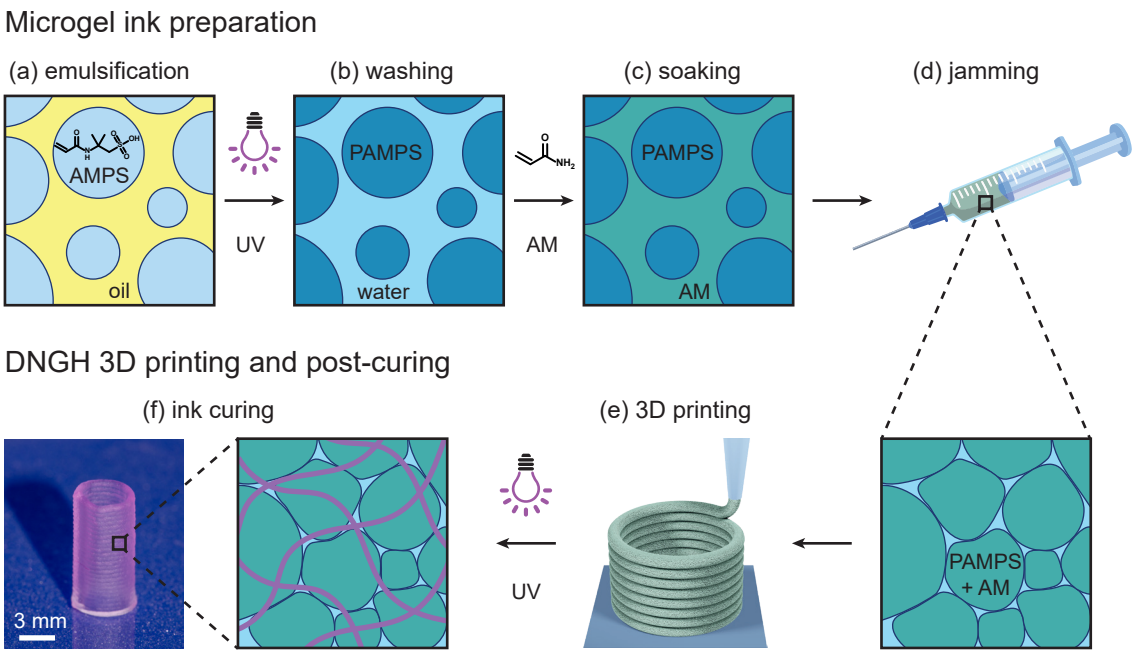

Figure 5.2: Additive manufacturing of DNGHs. Schematic representation of microgel fabrication. (**a**) A monomer-containing aqueous solution is processed into a water-in-oil emulsion. (**b**) AMPS-loaded drops are converted to PAMPS microgels through an UV-induced polymerization. (**c**) Microgels are soaked in an AM monomer-containing solution. (**d**) Monomer-loaded microgels are jammed to yield a printable ink. (**e**) Jammed microgels are extruded as a continuous filament that displays fast shear recovery, enabling the printing of granular hydrogels possessing high aspect ratios with a high shape fidelity. (**f**) The 3D printed objects are post-cured through an exposure to UV light that initiates the polymerization of the AM monomers to form a percolating network, as exemplified by the 3D printed cylinder. Adapted with permission from [271].

by our jammed PAMPS microgels, as shown in Figure 5.3b. Indeed, the flow point is in the range of 10% for all the different formulations. Furthermore, we observe no influence of the monomer loading on the flow point of our granular ink, as shown in Figure 5.4.

To obtain a good printing resolution, the ink must rapidly solidify after it has been extruded, which is the case if it displays fast stress healing properties. Indeed, our jammed PAMPS solution recovers almost immediately and repetitively, from a liquid-like state at high strains, to a solid-like state at low strains, as shown in Figure 5.3c. To test if this behavior is temperature-dependent, we perform step strain relaxation measurements at temperatures varying between 5°C and 45°C. The relaxation time of our jammed microgels remains the same between 5°C and 45°C, as shown in Figure 5.5a, indicating that these microgels can be easily processed within this temperature range. This behavior is inherent to jammed microgels that behave as solid-like materials because their linear elasticity is governed by the microgel composition [181]. Hence, our results indicate that the jammed

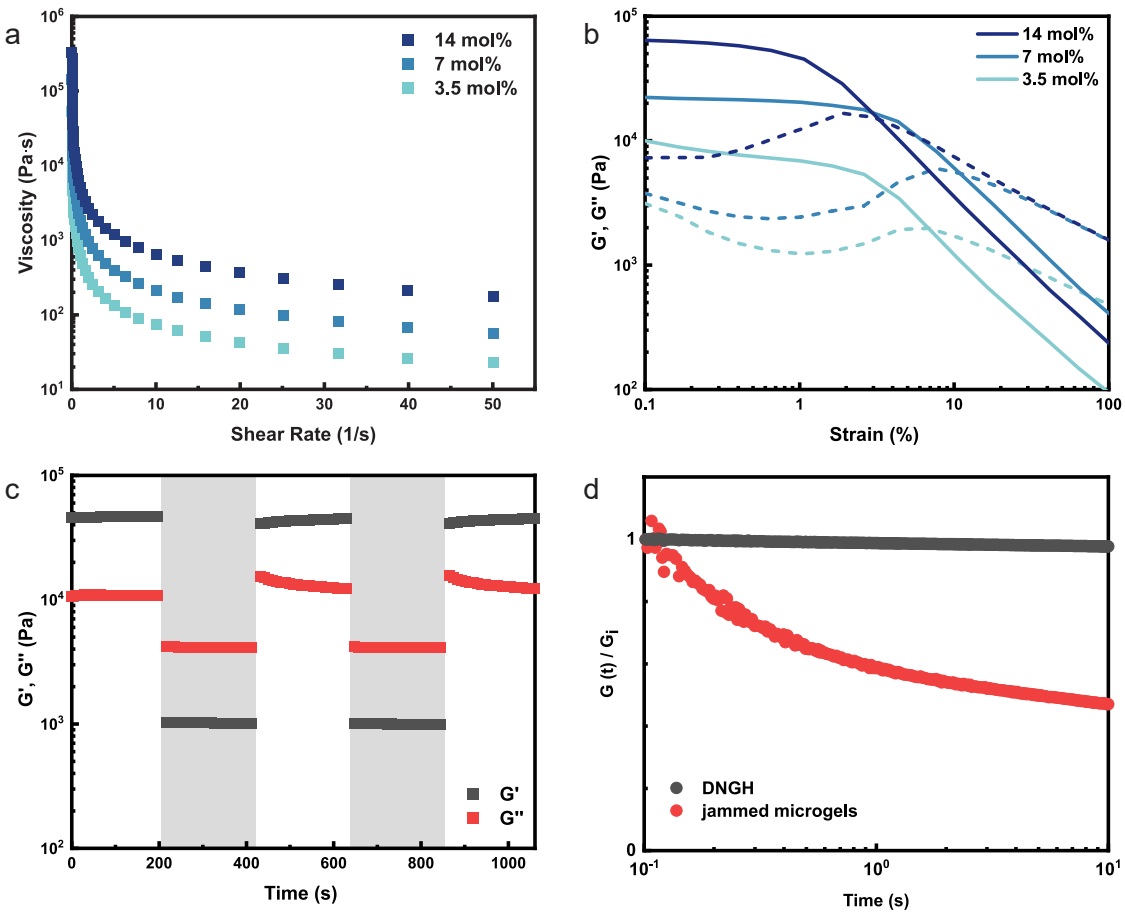

Figure 5.3: Rheology of jammed microgels. (**a,b**) Frequency dependent viscosity (**a**) and amplitude sweep (**b**) of jammed microgels containing different cross-linker concentrations. All three samples display a characteristic shear-thinning behavior and a low yield strain. (**c**) Self-healing behavior of jammed microgels containing 3.5 mol% cross-linker. The material transitions from a solid-like to a liquid-like state when subjected to high shear ($\gamma = 30\%$). The jammed solution recovers rapidly to its initial condition at low shear ($\gamma = 1\%$). The process can be repeated cyclically without deterioration of the ink performance. (**d**) Step strain relaxation of a DNGH and jammed microgel ink. The difference in relaxation time is due to the presence of the second percolating network in DNGH. Adapted with permission from [271].

Table 5.1: Dry polymer content of jammed microgels. Solid polymer content of water swollen and jammed microgels prepared from a 30 wt% AMPS solution. The standard deviation of the weight fraction of jammed microgels calculated from nine independent measurements is 0.22 wt%, indicating that this procedure is reproducible.

30wt% PAMPS microgel sample	Solid Content (wt%)
#1	4.45
#2	4.78
#3	4.49
#4	4.78
#5	4.85
#6	5.02
#7	4.97
#8	5.04
#9	5.06
Average	4.83
+/- SD	0.22

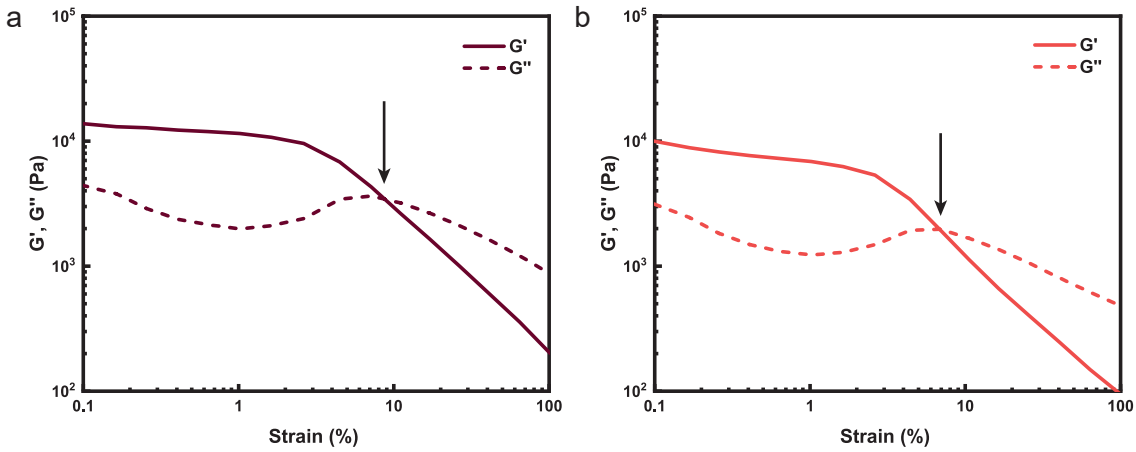

Figure 5.4: Rheological behavior of jammed microgels. Amplitude sweep of microgels swollen (**a**) directly in a monomer containing solution and (**b**) in water before they were swollen again in a monomer containing solution. The flow point, represented by an arrow, is within experimental error the same for the two samples. Therefore, the two samples can be extruded with similar printing parameters. Adapted with permission from [271].

microgels possess rheological properties that are well-suited for additive manufacturing.

Jammed microgels can form macroscopic, porous materials that retain their structure [12, 196, 269]. However, the lack of covalent adhesion between particles makes them mechanically weak such that they cannot bear significant loads. To overcome this shortcoming, we transform jammed microgels into a mechanically robust material by forming a second percolating network within the jammed microgels. This is achieved by exposing

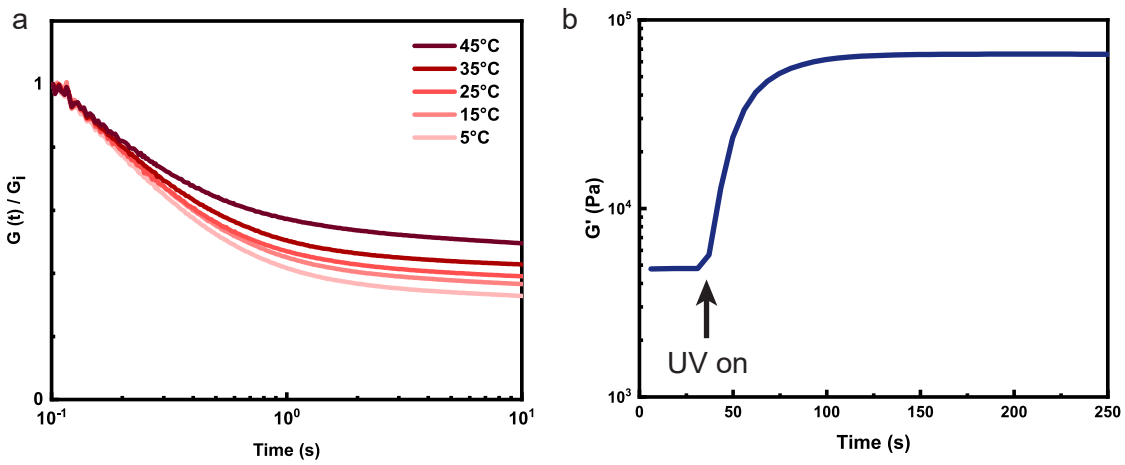

Figure 5.5: Temperature-dependent rheology of jammed microgel ink and its gelation kinetics. (**a**) Step strain relaxation of the jammed microgel ink at 5, 15, 25, 35, and 45 °C. The relaxation time of all measurements is almost independent of temperature. (**b**) Gelation kinetics of the DNGH. The jammed microgel ink is subjected to an oscillatory strain of 1% at constant frequency of 10 rad/s. Starting from t = 25 s, the sample is continuously illuminated with UV light. The increase in storage modulus is attributed to the polymerization of the percolating second network (PAM). Adapted with permission from [271].

the granular construct to UV light to initiate the polymerization of the AM monomers. To follow the gelation kinetics of the percolating second network, we perform time-dependent oscillatory rheology measurements. Results suggest that gelation plateaus around 150 s, as shown in Figure 5.5b. As a result of the formed percolating PAM network, the DNGH retains its integrity, in stark contrast to jammed microgels that relax stress over time, as shown in Figure 5.3d.

5.4.3 Mechanical characterization of DNGHs

The mechanical properties of hydrogels are strongly influenced by the weight fraction of the polymers. To characterize the polymer fraction of our DNGHs, we compare the weight of DNGHs as prepared and that of dried DNGHs as a function of their composition. Depending on the composition of our DNGHs, their dry polymer content ranges from 13.6 wt% to 45.7 wt%, as summarized in Figure 5.6a. To predict their swelling behavior, we compare the dry polymer content with the equilibrium water content (EWC) of our DNGHs. EWCs range from 81.5 wt% to 98.0 wt% depending on DNGH composition, as summarized in Figure 5.6b.

Granular hydrogels inherently possess locally varying compositions. In our case, grains are

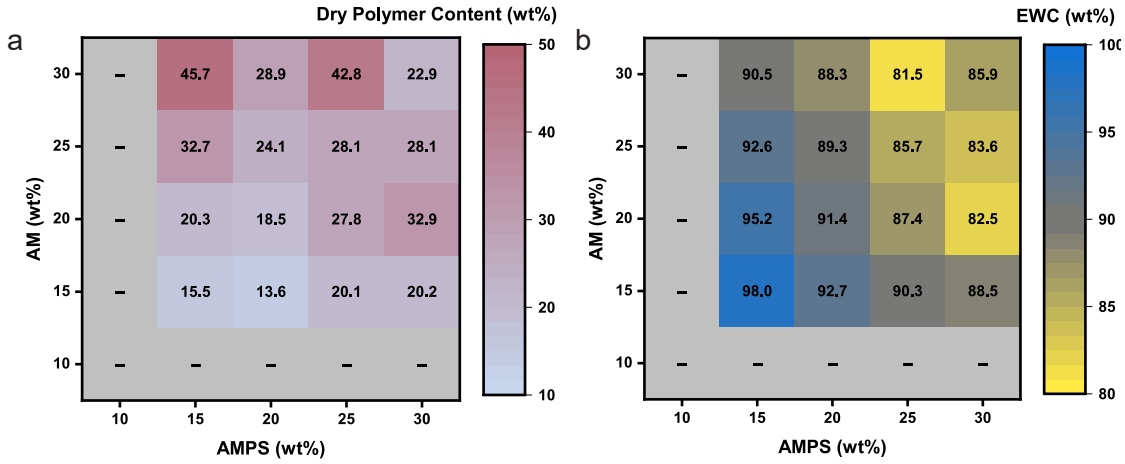

Figure 5.6: Dry polymer content and EWC measurements. (**a**) Dry polymer content of DNGHs with varying network concentrations. The values are calculated as the dried sample weight divided by the as prepared sample. The dry polymer content increases with increasing secondary network concentration. (**b**) EWC of the same DNGHs concentration combinations. Adapted with permission from [271].

composed of PAMPS that are reinforced by PAM and hence, they constitute DN hydrogels. By contrast, the grain boundaries are composed of PAM only. To test the influence of the composition of our hydrogels on their mechanical properties under tension, we perform tensile tests on as-prepared DNGHs composed of PAMPS microgels fabricated from a 30 wt% monomer solution and a second network made from a solution containing 20 wt% AM. The granular hydrogel is significantly stiffer and tougher than bulk hydrogels composed of either PAMPS or PAM. The Young's modulus of the DNGH is 5-fold higher than that of PAMPS and 3-fold higher than that of PAM. We attribute the high stiffness of DNGH to the chain entanglements that are topologically constrained between PAM chains and the microgel network, such that they cannot be easily displaced [221]. However, our DNGHs are two-fold softer than unstructured DN counterparts, as summarized in Figure 5.8a. We assign this difference to the PAMPS network that is not percolating the entire DNGHs but is only present within the microgels, in stark contrast to the bulk unstructured DNs presented in section 1.6.6.

A key requirement for the use of hydrogels for load bearing applications is that they are tough such that they do not fail catastrophically if deformed within a well-defined range. To assess the toughness of our DNGHs, we quantify their fracture strength. The fracture strength of the DNGH is more than 10-fold higher than that of bulk PAMPS and PAM. Remarkably, the fracture strength of DNGHs is even three-fold higher than that of the unstructured DN counterparts, despite of its lower Young's modulus, as shown in Figure 5.8a. We attribute the corresponding increase in toughness to a stress concentration at the

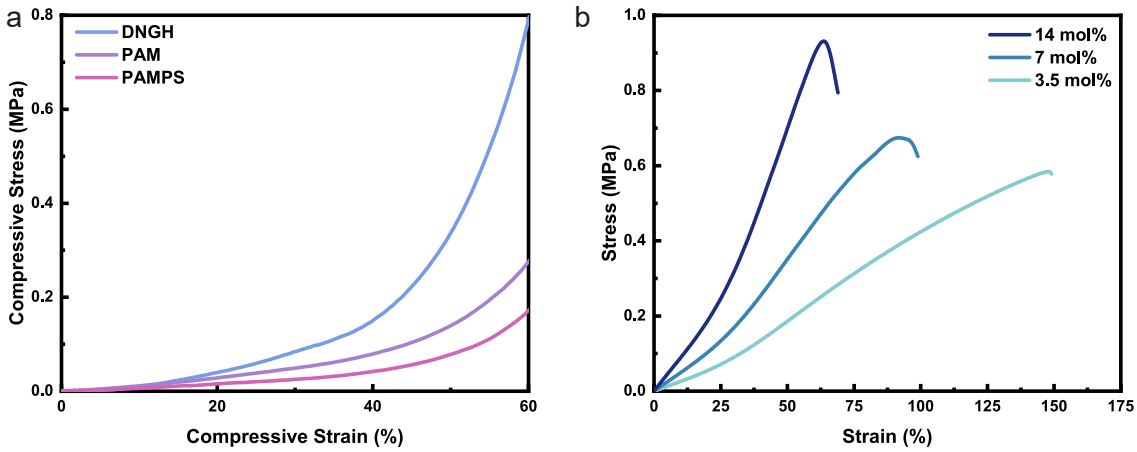

Figure 5.7: Mechanical characterization of DNGHs. (**a**) Compression measurements of DNGH and those of bulk corresponding PAM and PAMPS single network hydrogels. The compressive strength of the DNGH is at least 3-fold higher than that of both bulk hydrogels. (**b**) Tensile measurements of DNGH with different primary network crosslinker densities. The material shows an increase in elasticity with no significant change in toughness. Adapted with permission from [271].

poles of the microgels due to a substantial mismatch in elasticity of the two interpenetrating networks, as has been described for microgel reinforced hydrogels [274]. These results demonstrate the potential of granular hydrogels possessing locally varying compositions for load-bearing applications and as dampers.

Most soft natural materials are subjected to complex loading profiles [275]. To test if our DNGH is sufficiently robust to sustain more demanding loading profiles, we perform compression measurements on DNGH, PAMPS, and PAM samples. The compressive modulus of the DNGH is 2-fold higher than that of PAM, as shown in Figure 5.7a. The compressive stress increases even more: it reaches 0.8 MPa at 60% strain which is 3 times higher than that of the PAM network. Furthermore, we test its ability to lift a 1 kg weight through a folded rectangular stripe with a cross section of 10 mm x 2 mm, as shown in Figure 5.8b. Remarkably, the stripe is able to support the applied load for at least 5 loading cycles with no appreciable weakening. These results demonstrate the potential of our DNGHs to be used for load bearing applications.

The elasticity of DN hydrogels depends on the initial polymer content and crosslinker concentration of the first network [60]. To test if this is also the case for our DNGH where the first network is not percolating, we fabricate microgels containing different polymer contents and perform tensile tests on them. Indeed, the Young's modulus of the DNGH increases from 0.10 MPa to 0.48 MPa with increasing polymer content until it reaches a plateau at 25 wt% AMPS, as shown in Figure 5.8c. The lower mechanical performance

of the DNGH at 30 wt% AMPS is related to the poor swelling of the microgels in the second AM solution. A similar behavior is observed if we fix the polymer content of the AMPS microgels and vary the crosslinker concentrations. For example, DNGHs prepared with 14 mol% MBA crosslinker possess a Young's modulus four-fold higher than the corresponding sample containing only 3.5 mol% MBA, as shown in Figure 5.7b. However, the increase in the microgel crosslinker density decreases the fracture strain of the DNGH from 150% to 65%. To ensure good elasticity of the printed construct while maintaining good mechanical integrity, we keep the crosslink density of the microgels constant at 3.5 mol% in the following experiments.

Our results indicate that the mechanical properties of DNGHs strongly depend on the polymer content of the microgels and the second percolating network. To determine the best combination of the polymer contents of the microgels and the percolating network, we systematically and independently vary these two parameters and quantify the Young's modulus and toughness of the resulting materials from tensile tests. The Young's modulus of our DNGHs increases with increasing AMPS concentration, independent of the AM concentration used to form the second percolating network, as summarized in Figure 5.8e. This finding is in agreement with unstructured DN where the elasticity is mainly determined by the first network [58, 66]. The Young's modulus of our DNGHs can reach values up to 0.57 MPa if they are composed of 30 wt% AMPS and 20 wt% AM.

The toughness of unstructured DNs is mainly determined by the loosely crosslinked secondary network [58, 66]. To test if this is also the case for our DNGHs, we quantify the toughness, calculated as the area under the stress-strain curve, for all the tested samples. Indeed, the toughness of our DNGHs increases with increasing AM concentration, as summarized in Figure 5.8d. The one clear exception to this trend presents the stiffest DNGHs that we formed, that also displays a high toughness of 0.53 MJ/m^3. The maximum toughness of 0.66 MJ/m^3 is achieved for DNGHs prepared with 25% AMPS and 30% AM, as summarized in the color map in Figure 5.8f. The color maps of the Young's moduli and toughnesses of DNGHs nicely show that their mechanical properties can be tuned over a wide range by adjusting the concentrations of monomers used to form the microgels and the secondary network respectively.

An additional parameter that strongly influences the mechanical properties of unstructured DNs is the crosslinker density of the second network. To test if this is also the case for our DNGHs, we fabricate DNGHs with two different AM crosslinker densities and test them under tension. At 0.02 mol% crosslinker concentration, the material displays the yielding behavior that is characteristic for conventional DN hydrogels, as shown in Figure 5.9a. However, because of the low crosslink density, the bonds between microgels are weak such that the material easily ruptures along the grain boundaries, as shown in

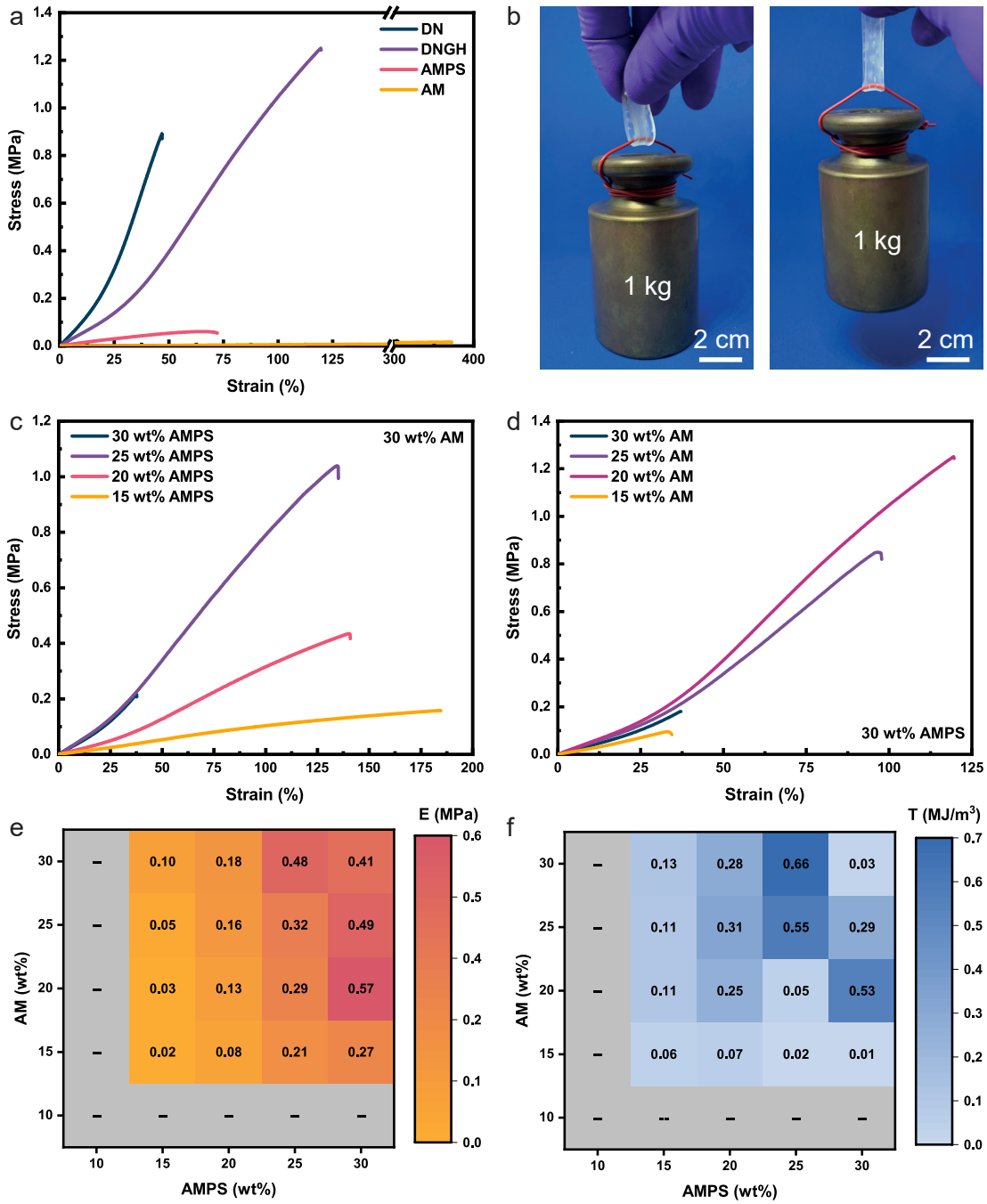

Figure 5.8: Mechanical characterization of DNGHs. (**a**) Tensile tests of DNGH are compared to those of bulk PAMPS-PAM DN, single PAM and PAMPS hydrogels. The granular material displays a toughening behavior typical of DN hydrogels that is threefold higher than the bulk DN counterpart. (**b**) Photograph of a hydrogel stripe with a cross section of 10×2 mm^2 that has been loaded with a 1 kg weight. (**c**) Tensile measurements of DNGHs prepared with 30 wt% AMPS microgels and a PAM second network made from varying AM concentrations. The toughness of the samples increases

Figure 5.8: with increasing AM concentration until it peaks at 25 wt% AM. (**d**) Tensile measurements of DNGHs made of PAMPS microgels synthesized with varying AMPS concentrations that are embedded in a percolating network made from 30 wt% AM. The elasticity of the DNGHs increases with increasing AMPS concentration. (**e,f**) Color maps of the Young's moduli (**e**) and toughness (**f**) calculated as the area under the stress–strain curve of DNGHs as a function of the concentration of AMPS contained in the microgels and that of AM that forms the second percolating network. Reported values represent the mean of five repeated measurements. Adapted with permission from [271].

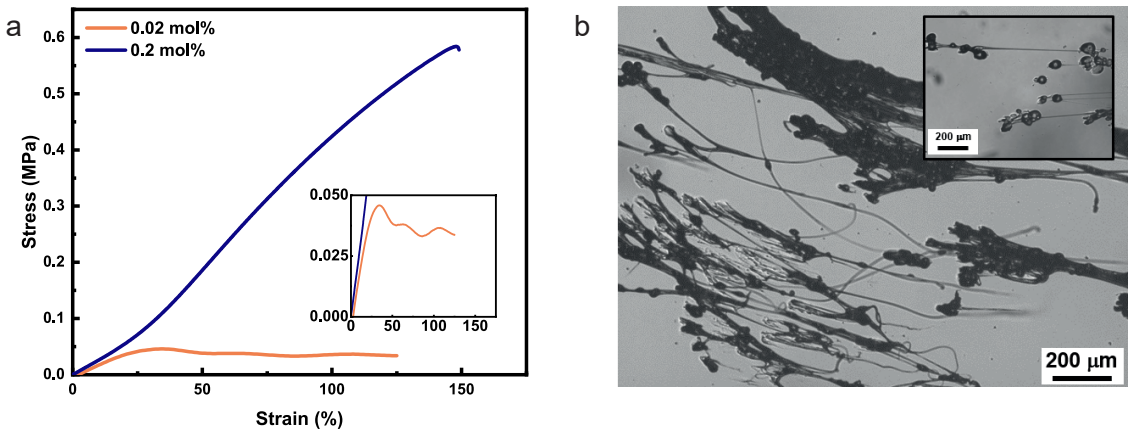

Figure 5.9: Influence of the crosslink density of the percolating second network on the mechanical properties of DNGH. (**a**) Tensile measurements performed on DNGH with a crosslink density of the secondary network of 0.02 mol% (**orange**) and 0.2 mol% (**blue**). The Young's modulus of both samples is 0.28 MPa. DNGHs containing 0.02 mol% crosslinker display a typical yielding behavior, as illustrated in the inset. (**b**) Optical micrograph of a fractured sample containing 0.02 mol% crosslinker. The loosely crosslinked secondary network hinders good interparticle adhesion such that individual PAMPS microgels are bridged by fibrous PAM filaments, as highlighted in the inset. Adapted with permission from [271].

Figure 5.9b. These results suggest a weak interparticle adhesion. The toughness strongly increases, if we increase the AM crosslink density: by increasing it ten-fold, the fracture strength increases from 50 kPa to 600 kPa. Importantly, the increase in toughness does not compromise the stiffness of the DNGH: the Young's modulus remains unchanged at 0.28 MPa. As a consequence, the fracture toughness of the DNGH increases more than 10-fold if we increase the AM concentration to 0.2 mol%. These results demonstrate that the mechanical properties of DNGH can be tuned with the crosslink density of the percolating network, by analogy to DN materials that contain individually dispersed microgels in them [221]. However, by contrast to the DN materials, our DNGH can be 3D printed into complex shapes. To ensure good shape-retaining properties of the ink and a good stability of the additive manufactured materials, we employ the formulation containing

0.2 mol% crosslinker for the following experiments.

5.4.4 Printability and post-curing stability of DNGHs

An important asset of our DNGHs is their fabrication from jammed microgels that shear thin and rapidly recover when stress is relieved. We expect this rheological behavior to render our jammed microgels well-suited inks for 3D printing. When the ink is extruded through a 410 µm diameter nozzle, it is subjected to significant shear stresses that lower the viscosity of the ink locally. The fast recovery of the elastic properties upon relaxation of the stress allows extruding a stable filament whose diameter is similar to that of the nozzle, as shown in the photograph in Figure 5.10a. Importantly, the extruded filament maintains the characteristic granularity of the ink, as evidenced form the fluorescent micrograph in Figure 5.10b.

Macroscopic 3D structures are typically printed by depositing multiple layers on top of each other. To ensure good integrity of the 3D printed structures, subsequent layers must partially merge. Our ink is fundamentally different in that it is composed of jammed microgels that can re-arrange before a second percolating network is formed such that we expect it to enable printing junctions with good interconnections. To test our expectation, we print two perpendicular filaments in a grid-like geometry. Indeed, the junctions display good interconnectivity between adjacent layers already before the second percolating network is formed, as shown in Figure 5.10c. After the second percolating network is formed, the grid retains its shape and integrity even if removed from the substrate, as shown in Figure 5.10d.

The mechanical properties of additive manufactured materials are typically inferior to those of the corresponding bulk materials. This discrepancy is often related to a weak adhesion between sequentially deposited layers. Our ink offers an elegant possibility to overcome this limitation as the second, percolating network is formed after the ink is 3D printed. Therefore, we expect the interfaces between sequentially deposited layers to be equally strong as the grain boundaries within the printing plane. To test this hypothesis, we print a solid DNGH rectangular stripe where the printing direction is along its length and one where the printing direction is perpendicular to it, as schematically shown in Figure 5.11a. Remarkably, we do not observe any significant influence of the printing direction on the mechanical properties of these stripes, as shown in Figure 5.11b. This is in stark contrast to polymers that are 3D printed using conventional, homogeneous inks [276]. Indeed, the Young's modulus is the same as the one measured for molded samples, 0.28 MPa. Interestingly, the additive manufactured samples possess a higher toughness than the corresponding molded ones: DNGH printed stripes reach a fracture strength of

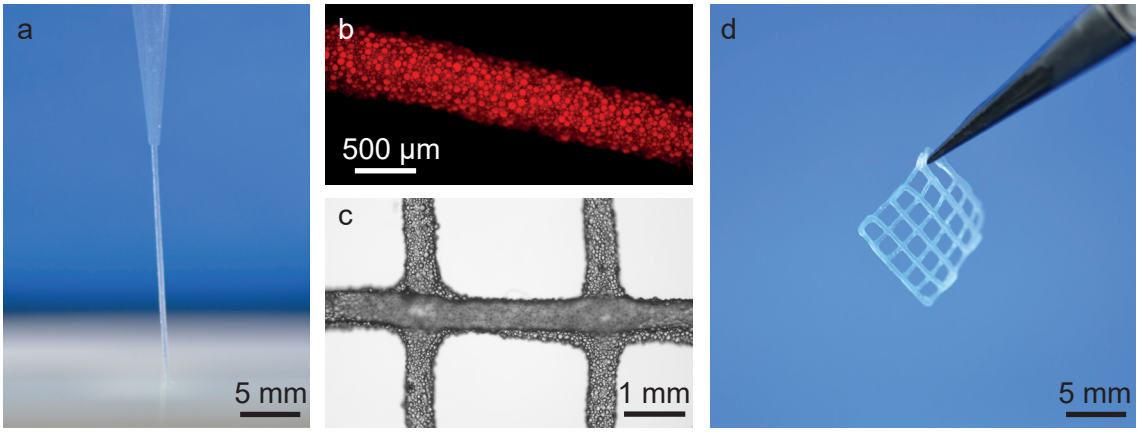

Figure 5.10: Printing of jammed microgels. (**a**) Photograph of the jammed microgel filament while it is extruded from a 410 µm conical nozzle. The material can be printed continuously without rupture yielding a filament with high shape fidelity. (**b**) Fluorescent micrograph of the extruded granular filament. Microgels are labeled with sulforhodamine B sodium salt. The resulting granular filament has an average diameter of 500 µm. (**c**) Optical micrograph of a printed grid demonstrating the high shape-retaining properties of the extruded layers. The curvature between crossing filaments suggests partial merging of subsequent layers. (**d**) Photograph of a free-standing DNGH grid. Upon UV curing, the printed object can be removed from the substrate while retaining its shape, demonstrating the good interconnectivity between layers that is caused by the percolating second PAM network. Adapted with permission from [271].

more than 0.8 MPa, and a maximum elongation of around 290%, compared to the molded samples whose fracture strength is 0.6 MPa and the maximum elongation is 150%. The superior mechanical properties are likely related to the more homogeneous distribution of microgels in printed samples and the lower density of defects such as air inclusions.

To put the mechanical performance of our 3D printed DNGHs in perspective with previously reported 3D printed hydrogel, we compare the Young's moduli of these systems. Our DNGHs are stiffer than any of the previously reported formulation, as summarized in Figure 5.12 [203, 26, 277, 278, 279, 280, 64, 281, 282]. We assign this difference to the processing: our DNGHs are fabricated from jammed microgels such that we can independently optimize the rheological properties of the ink and the composition of the microgels. This is in stark contrast to most 3D printed hydrogels where these two parameters are closely coupled. Taking advantage of this important aspect, we can combine the extraordinary mechanical properties of DN hydrogels with an additive manufacturing process, without compromising the printability and resolution of the ink.

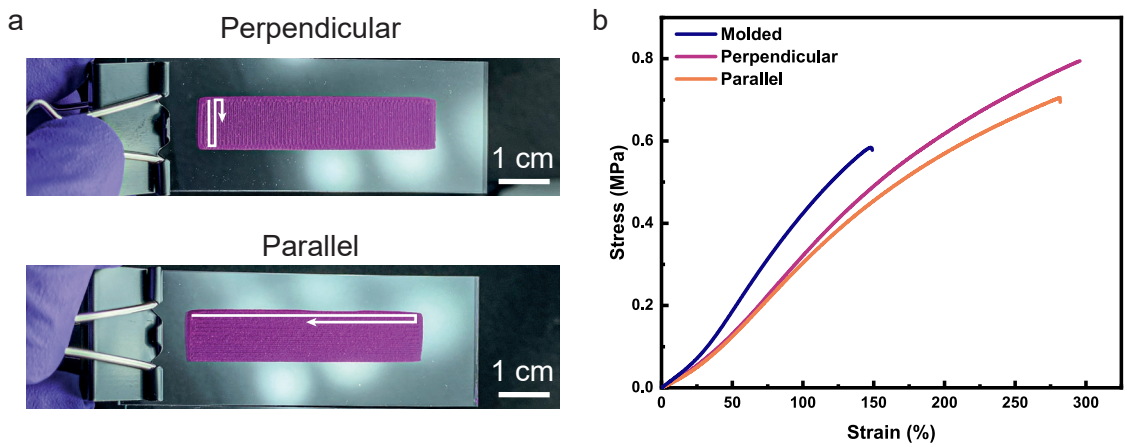

Figure 5.11: Effect of printing direction on mechanical properties. (**a**) Photograph of DNGH stripes printed with perpendicular (**top**) or parallel (**bottom**) filament orientation. Microgels are labeled with sulforhodamine B sodium salt for visualization. (**b**) Tensile measurements of DNGH stripes printed parallel and perpendicular to the long axis of the stripe. We cannot observe any influence of the printing direction on the mechanical properties. The toughness of additive manufactured DNGHs is significantly higher than that of molded samples. Adapted with permission from [271].

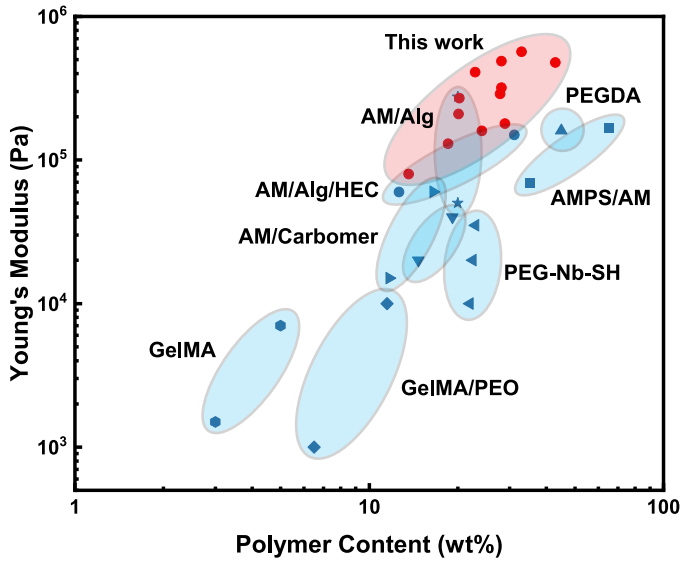

Figure 5.12: Ashby plot. Young's moduli of various hydrogel inks plotted as a function of the total polymer content. DNGHs reported here are stiffer than any other previously reported 3D printed hydrogel. Adapted with permission from [271].

5.4.5 Potential applications of DNGHs

Our results suggest that jammed microgels soaked in a monomer solution are well-suited inks to 3D print strong and tough hydrogels. This is an asset that has been difficult to achieve with previously reported 3D printed hydrogels [283, 284, 285]. To exploit this new feature, we 3D print our jammed microgels into high aspect ratio hollow cylinders, as shown in Figure 5.13a. Indeed, the additive manufactured DNGH structure can be repetitively compressed up to 80%, where it buckles, and retains its initial shape when the stress is released. Importantly, we do not observe any signs of damage, even after samples have been unloaded, as shown in Figure 5.13b. The exceptional shape fidelity and mechanical stability of the construct hints at the potential of the jammed microgel-based ink to design mechanically robust granular materials possessing complex geometries.

A key feature of the ink introduced here is its ability to vary the composition of 3D printed objects locally without risking the introduction of weak interfaces that would sacrifice their mechanical properties. This feature can be achieved if materials are 3D printed from multiple inks, each one composed of jammed microgels possessing a well-defined composition that varies between the different inks and all microgels are soaked in the same type of monomer solution. This ink formulation allows covalent crosslinking of adjacent microgels even if these microgels originate from different types of inks and hence possess different compositions after they have been processed into complex 3D structures. To demonstrate feasibility, we print an ink containing red microgels and one containing green microgels into a grid where the two types of hydrogels remain spatially separated, as illustrated in Figure 5.13c. To demonstrate the importance of the second percolating network for the mechanical stability of the DNGHs, we print the EPFL logo from a structural ink composed of microgels that are soaked in a monomer-containing solution and fill the interstices with a sacrificial ink, namely one composed of jammed microgels that do not contain any monomers. After the second percolating network is formed through exposure to UV-light, we selectively remove the sacrificial ink by immersing the 3D printed structure into an aqueous solution. We obtain an integral material possessing well-defined cm-sized structures, as illustrated in Figure 5.13d.

To demonstrate the advantage of co-printing inks composed of microgels possessing different properties we 3D print shape-morphing DNGHs. Shape-morphing properties can be imparted to complex structures if they display anisotropic swelling behaviors [286, 287, 288]. To obtain this property, we employ microgels with different crosslink densities such that their swelling behavior varies. Indeed, if we print a flower whose first layer is composed of microgels possessing a lower crosslink density than those contained in the second layer, the flower folds into opposite directions upon drying and soaking, as exemplified

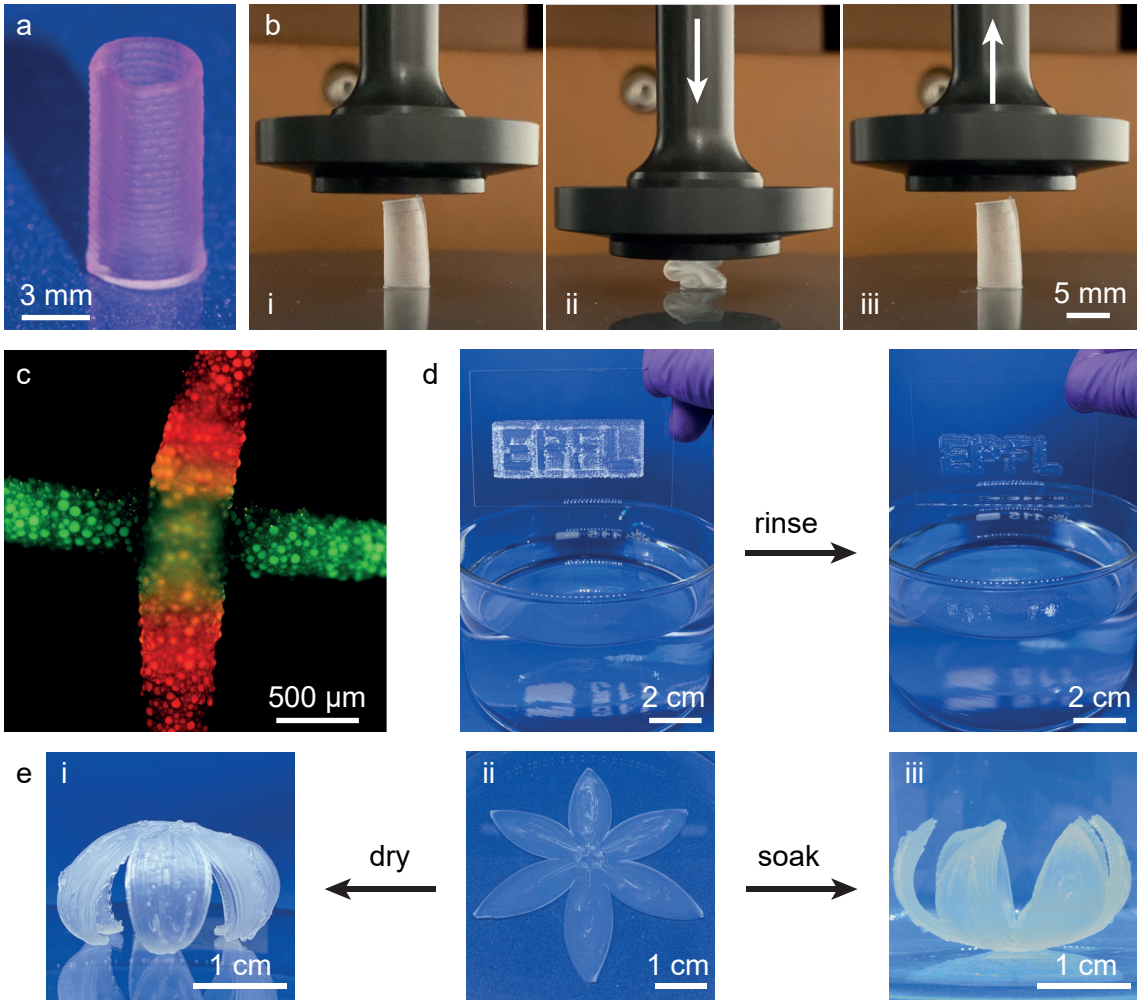

Figure 5.13: 3D printing of DNGHs. (**a**) Photograph of a hollow cylinder with an aspect ratio of 2 that can be printed with high shape fidelity. Microgels are labeled with sulforhodamine B for better visualization. (**b**) Photographs of the hollow DNGH cylinder under compression. While compressed, the cylinder experiences strong deformation and buckling. The good elasticity of DNGH allows the cylinder to return to its initial shape when the stress is released. (**c**) Fluorescent micrograph of two filaments labeled with different dyes, demonstrating the ability to control the composition locally. (**d**) Photographs of an object that has been 3D printed with a structural and sacrificial ink. The sacrificial ink can be removed after the secondary network of the structural ink has been formed by immersing the material into an aqueous solution. (**e**) Photographs of dual-ink printing of a shape-morphing flower. The object is fabricated from two layers with different swelling behaviors. The first layer is composed of microgels containing 3.5 mol% cross-linker, the microgels contained in the second layer contain 14 mol% cross-linker. As a result of the different swelling behaviors of the microgels and the secondary network, that ensures a good integrity of the overall structure, the DNGH flower can repetitively fold in opposite directions upon drying and immersion in water. Adapted with permission from [271].

in Figure 5.13e. This example demonstrates the power and versatility of the presented method to fabricate responsive, smart soft materials that are sufficiently strong and stiff to bear significant loads.

5.5 Conclusion

We introduce a modular, versatile method to 3D print strong and tough complex hydrogels. The hydrogels are composed of jammed microgels that are connected through a second covalently crosslinked percolating network. Our approach combines the advantageous rheological properties of jammed microgels with the excellent mechanical properties of double network hydrogels to additive manufacture strong and tough granular hydrogels that can optionally be rendered adaptive. Because adjacent microgels are embedded in a percolating 3D network, the mechanical properties of the 3D printed materials are isotropic and independent of the printing direction. Importantly, the two-step approach to fabricate DNGH is not limited to hydrogel particles but can be extended to a broad range of materials that can be processed into porous particles. Thereby, it significantly enlarges the range of materials that can be 3D printed into complex mechanically robust materials. The flexibility in the granular ink design and excellent control over the micrometer length scale structure opens up new possibilities to design the next generation of strong and tough soft robots and implants that can adapt their properties locally in response to external stimuli.

CHAPTER 6

3D printing of recyclable double network granular hydrogels

In this chapter, I present a recyclable double network granular hydrogel, composed of non-degradable microparticles that are contained in a degradable percolating second network. The microparticles constituting the first network can be recovered, and re-used for the fabrication of new recycled double network granular hydrogel.

This chapter is adapted from a manuscript in preparation entitled "3D printing of Recyclable Double Network Granular Hydrogels" authored by Alvaro Charlet, Matteo Hirsch, Sanjay Schreiber and Esther Amstad. A. Charlet and M. Hirsch are equally contributing co-first authors. A. Charlet, M. Hirsch and E. Amstad designed the experiments. A. Charlet performed the degradation experiments, the Raman spectroscopy, and the rheological study. M. Hirsch performed the 3D printing of the material. S. Schreiber performed preliminary experiments that were essential to establish the final protocol used in this work. All remaining experiments are performed by A. Charlet and M. Hirsch collectively. A. Charlet, M. Hirsch and E. Amstad analyzed the data and wrote the manuscript.

Contents

6.1 Abstract

Sustainable materials, such as degradable and recyclable polymers, become increasingly important as they are often environmentally more friendly than their one-time-use counterparts. In parallel, the trend towards more customized products demands for fast prototyping methods that allow processing materials into well-defined 3D objects that are mechanically sufficiently robust to bear significant loads. Soft materials that satisfy the two rather contradictory needs remain to be shown. Here, we introduce a material that simultaneously fulfills both requirements, a 3D printable and recyclable double network granular hydrogel (rDNGH). This hydrogel is composed of PAMPS microparticles that are covalently crosslinked through a disulfide-based percolating network after they have been 3D printed. The possibility to independently degrade the percolating network, with no harm to the primary network contained within the microgels, renders the recovery of the microgel paste efficient. As a result, the recycled material pertains mechanical properties that are similar to those of the pristine material. Importantly, this process can be extended to the fabrication of recyclable hard plastics made of, for example, dried rDNGHs. We envision this approach to not only benefit the field of soft materials but also serve as foundation for a paradigm shift in the design of new sustainable plastics.

6.2 Introduction

Plastic pollution represents one of the largest sources of environmental threat [289]. Every year, more than 40 million tons of plastic waste is released into the environment [290].

Because the majority of these materials cannot be degraded, the plastic rapidly accumulates. To address the urgent need to reduce plastic waste, a lot of work has been devoted towards recyclable plastics [291, 292, 293, 294]. For example, the increased awareness of the environmental impact of plastic waste motivated excellent work devoted to degradable and recyclable elastomers [295, 296], and hydrogels [297, 298, 299]. The ability to degrade hydrogels also offers new possibilities to use them as adhesive layers between other hydrogels and biological tissues or synthetic substrates where the adhesive layer selectively degrades over time, thereby enabling a safe removal of the coating [163, 300, 301, 5]. Unfortunately, these degradable hydrogels cannot be used for load-bearing applications because they are mechanically too weak. Another approach to reduce the ecological impact of plastic and hydrogel waste is the use of novel processing technologies that enable shorter and more localized value chains [302]. In this context, additive manufacturing has gained tremendous interest in the field of hydrogel for its efficient use of resources, fast prototyping capability, and on-demand production [303]. Among various manufacturing techniques, extrusion printing has been widely adopted thanks to its easy implementation and low material waste [304, 13, 305, 306].

As was presented in chapter 5, the use of jammed microgels enables the 3D printing of strong and tough double network granular hydrogels. Here, we introduce a double network granular hydrogel, which can be selectively degraded and recycled several times. This is achieved by synergistically combining the favorable 3D printing properties of jammed microgels, the high mechanical performance of double-network hydrogels, and the degradability of covalent reversible bonds. Our material is composed of microgels loaded with a second precursor that contains cleavable crosslinks. Once printed, the granular structure is stabilized by initiating the polymerization reaction of the second precursor to form a percolating network that interpenetrates the microgels and simultaneously crosslinks them. The resulting rDNGH can bear loads up to 0.7 MPa. At the end of its life, it can be disassembled into its microgel components upon exposure to an aqueous solution containing an agent that degrades the dynamic covalent bonds of the second percolating network, TCEP, as described in section 1.6.4. The ability to recover the microgels, that can then be reused for the preparation of a new rDNGH ink, renders this process thrifty and sustainable. Our new rDNGHs demonstrate the possibility to combine good mechanical properties and recyclability. We envision this material to serve as a source of inspiration for the fabrication of the next generation of additive manufactured sustainable hydrogel materials and maybe even for more sustainable plastic replacements.

6.3 Experimental section

Details about the experimental procedure are presented in chapter 3 from section 3.4.1 on page 48 to section 3.4.8 on page 49.

6.4 Results and discussion

6.4.1 Microgel ink design and rDNGH fabrication

To decouple the rheological properties of the hydrogel precursor solution from that of the 3D printable ink, we produce microgels in a similar way to what was presented in chapter 5. Briefly, microgels are produced from aqueous emulsion drop templates that contain AMPS precursors. They are converted into microparticles by initiating the polymerization reaction of the precursors using UV illumination. The microgels are washed and transferred into an aqueous solution containing AM, N,N′-bis(acryloyl)cystamine (BAC), and 2-hydroxy-2-methylpropiophenone that serves as a photoinitiator (PI) before they are jammed to obtain the rheological properties required for 3D printing. The 3D printed structure is solidified by initiating the polymerization reaction of AM and BAC which form a percolating network that interpenetrates the microgels and simultaneously crosslinks them, as schematically illustrated in Figure 6.1a.

The key novelty of our system is its ability to be recycled at the end of its life. Importantly, the disassembly of 3D printed materials can be done under benign conditions in an aqueous solution: the intrinsic reversibility of disulfide linkages enables selective de-crosslinking of the secondary network, while the microgel primary structure is preserved, as schematically shown in Figure 6.1b. The microgels can be purified from the de-crosslinked PAM chains, loaded with new AM, BAC, and PI and jammed such that it can be used as a new ink, as shown in Figure 6.1c. This process can be iterated several times without major microgel deterioration thus making this material suitable for recycling, as detailed in Figure 6.1d.

6.4.2 Dynamic covalent bonds as degradable crosslinks

For recyclable materials to be truly useful, they must degrade upon exposure to an externally controllable trigger [307]. Furthermore, the degradation process should occur under benign conditions. To satisfy these requirements, we introduce a degradation protocol that bases on a naturally occurring hydrolysis. We employ a covalently crosslinked percolating network that entails disulfide bonds, each of which is hydrolyzed into two thiol moieties by

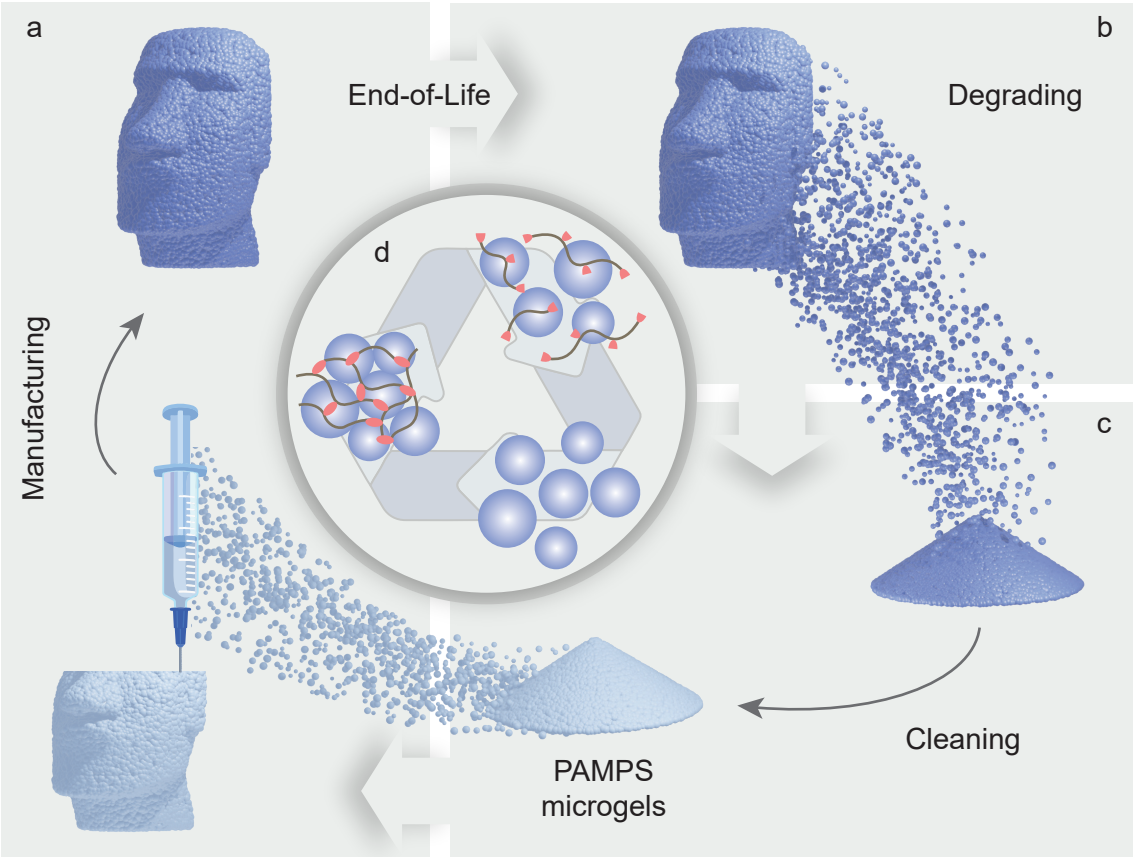

Figure 6.1: Life cycle of rDNGHs. (**a**) Schematic representation of the manufacturing process of rDNGHs. Jammed microgels loaded with AM monomers and the degradable crosslinker BAC are 3D printed or molded into an arbitrary shape, and stabilized through UV exposure. (**b**) Upon object failure or wear, the structure can be disassembled into its microgel components by a green degradation reaction, performed in an aqueous environment. (**c**) The recovered microgels are washed to remove the former percolating network. The purified microgels are recycled into a fully functional ink by re-soaking them in a monomer-containing solution. (**d**) The inset shows a schematic representation of the degradable and recyclable crosslink mechanism. Microgels (**blue**) are held together by a percolating PAM network (**brown**) crosslinked by a cleavable disulfide linkage (**red**).

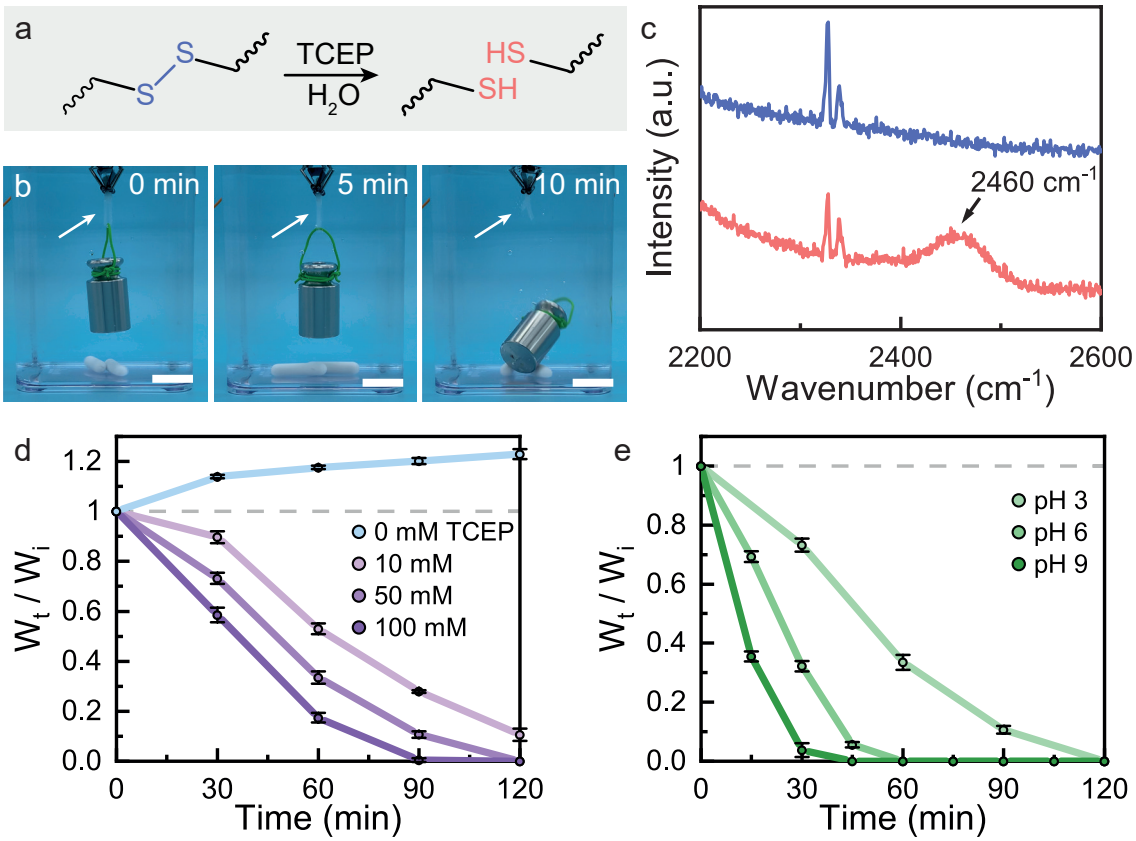

Figure 6.2: Degradability of rDNGHs. (**a**) Schematic representation of the degradation reaction. Upon rDNGH immersion in a TCEP solution, the disulfide bonds are reduced into individual thiols, thus breaking the percolating network. (**b**) Time lapse of a rDNGH thread holding a 100 g weight in a solution containing 50 mM TCEP. After 10 min incubation, the hydrogel thread breaks, releasing the weight. Scale bars are 20 mm. (**c**) The degradation mechanism is confirmed with Raman spectroscopy, by the appearance of the characteristic -SH peak at 2460 cm^{-1} in the degraded sample (**red**), that is absent in the pristine rDNGH (**blue**). (**d**) Degradation kinetics of rDNGHs as a function of the TCEP concentration. Samples immersed in solutions containing increasing TCEP concentrations are monitored through gravimetric analysis over time. In the absence of TCEP, swelling is observed resulting in an increased weight. With increasing TCEP concentrations the degradation rate increases. e, Degradation kinetics of rDNGHs in 50 mM TCEP as a function of pH. Increasing pH results in faster degradation.

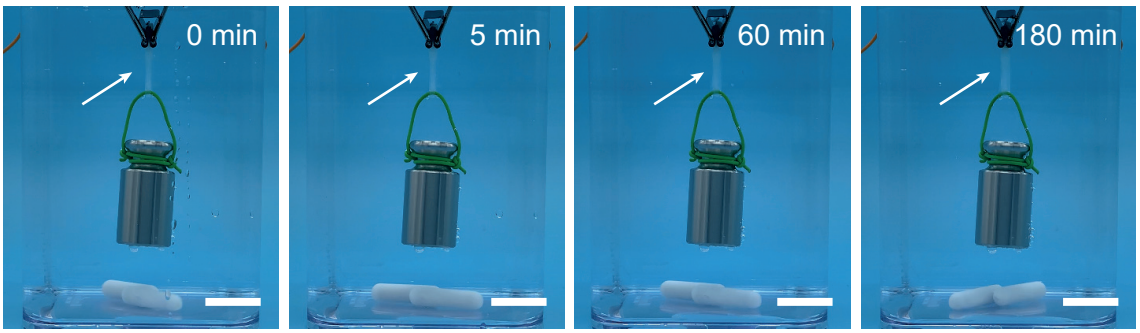

Figure 6.3: Stability in aqueous environment of rDNGH. Time lapse of a rDNGH thread holding a 100 g weight in deionized water. Scale bars are 20 mm.

immersing the material in a TCEP containing aqueous solution, as schematically shown in Figure 6.2a. Hence, we expect that rDNGHs decompose into individual microgels if immersed in such a solution. To test this expectation, we attach a 100 g weight to one of the ends of a rDNGH thread and immerse it in an aqueous solution containing 50 mM of TCEP. Indeed, within 10 min, the weight is released because the rDNGH starts to degrade, as shown in Figure 6.2b. To demonstrate that the degradation of the rDNGH is caused by the hydrolysis of the disulfide bonds, we immerse a rDNGH that is again loaded with a 100 g weight into deionized water. We do not observe any sign of degradation, even after 3 hours, as shown in Figure 6.3. We verify that the decomposition of the rDNGH is caused by the hydrolysis of disulfide bonds by monitoring their conversion into individual thiol groups using resonance Raman spectroscopy. Indeed, upon 30 min incubation of the rDNGH in the TCEP containing solution, we observe the appearance of a peak at 2460 cm^{-1} which is attributed to the vibration of thiol groups [308], as shown in Figure 6.2c.

An important factor that determines the potential of recyclable materials to be broadly used is the time needed for recycling: this time should be similar or shorter than currently used commercial recycling processes. To assess this parameter, we measure the recycling time of our material as a function of the TCEP concentration. If rDNGHs are immersed in an aqueous solution containing 100 mM TCEP, they degrade within 90 min. A two-fold reduction in the TCEP concentration prolongs the degradation by 30 min. The material can be decomposed under even more benign conditions: if immersed in aqueous solutions containing only 10 mM TCEP, they still degrade within the experimental observation time of 120 min, as shown in Figure 6.2d. Note that the degradation kinetics also depends on the solution pH: if we keep the TCEP concentration constant at 50 mM and increase the pH from 3 to 9, we reduce the degradation time from 120 to 45 min, as shown in Figure 6.2e. This degradation time is much faster than the time needed to degrade biodegradable plastic, which can take up to 6 months, illustrating the potential of our material [309].

6.4.3 Mechanical characterization of rDNGHs

Another key parameter for the quality of a recyclable material is its recovery yield. To evaluate this property, we quantify the microgel amount that is recovered as a function of the number or recycles the microgels have been subjected to. After each recycle, the process is monitored by weighing the purified microgels and evaluated by normalizing this value with the original microgel weight. We recover close to 100% of the microgels such that we obtain a recovery yield close to 1, as shown in Figure 6.4a. We assign this very high recovery yield to the size of our microgels: they have diameters of order 10-100 µm such that they readily sediment if centrifuged at 4500 rpm and thus, can easily be extracted from the solution.

Recyclable materials are only truly useful if their mechanical properties do not deteriorate upon recycling [291]. In a first approximation, we expect the mechanical properties of our rDNGH to be independent of the number of recycles the microgels have been subjected to. To test this expectation, we quantify the mechanical properties of pristine rDNGHs and compare them to recycled counterparts using tensile tests. The stiffness of rDNGHs containing microgels made from a 25% AMPS solution remains unchanged. By contrast, their maximum elongation decreases after the first recycle by approximately 30% and after the following four recycles by another 30%, as shown in Figure 6.4b. The decrease in maximum elongation with increasing recycles hints at a non-perfect removal of the degraded PAM chains. We assign the hindered removal to the physical entanglement of PAM chains within the microgels such that part of these degraded chains remain trapped in the microgel network, thus increasing the overall crosslink density. As a result, subsequent cycles suffer from reduced diffusion of the secondary precursor solution which yields rDNGHs with lower maximum elongation.

The stiffness of double network granular hydrogels is dictated by the polymer content and crosslink density of the microgels [221, 274, 310, 311]. We observe an increase in stiffness of the rDNGHs with increasing number of recycles, as shown in Figure 6.4a. To test if this increase is indeed caused by the increase in microgel stiffness, we fabricate microgels from solutions containing different concentrations of AMPS and assess the mechanical properties of rDNGHs made from them. Indeed, rDNGHs containing microgels produced from an aqueous solution containing 20 wt% AMPS possess a lower stiffness compared to those containing microgels made from an aqueous solution containing 25 wt% AMPS, as already established in chapter 5. The stiffness is further increased if we fabricate rDNGHs containing microgels produced from a 30% AMPS containing solution, as shown in Figure 6.5. Upon recycling, we observe a decrease in stiffness for rDNGHs made from a solution containing 20 wt% AMPS with increasing number of recycles, as shown in Figure 6.6a.

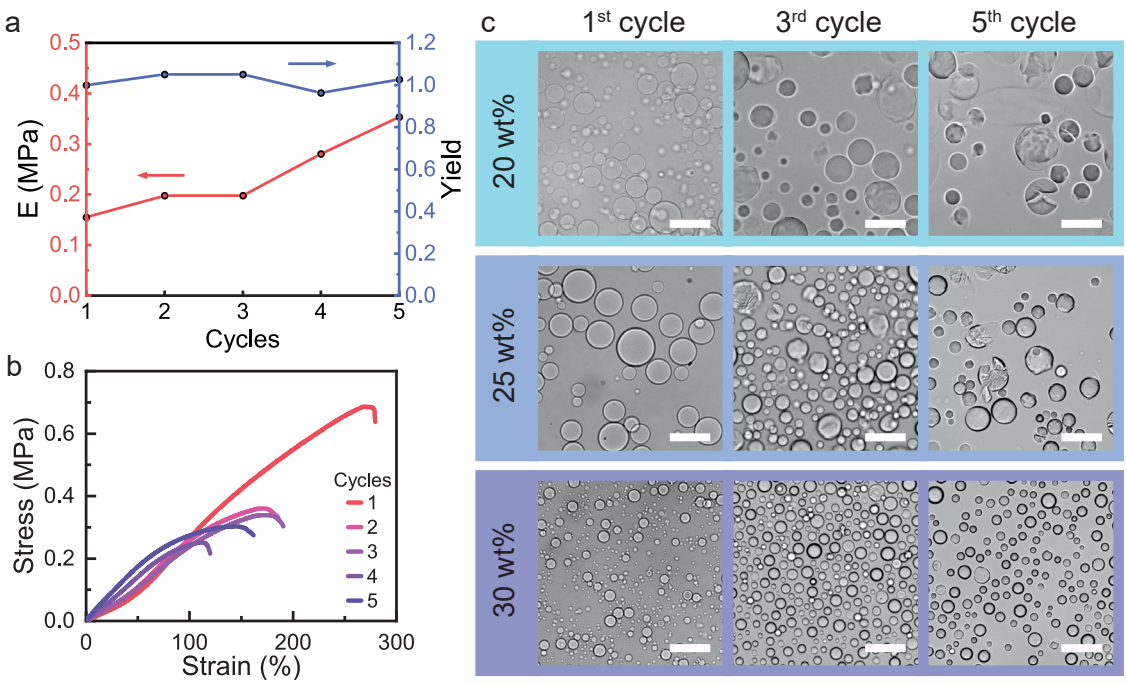

Figure 6.4: Mechanical performance of rDNGHs. (**a**) The Young's modulus of the rDNGHs (**red**) and recovery yield of the microgels (**blue**) as a function of the number of recycles microgels have been subjected to. The small increase in Young's modulus is attributed to AM residues that are crosslinked during recycling. The resulting recycled microgels have a higher polymer content that results in a higher stiffness of the double network. The recovery yield of the degraded microgels, measured by gravimetry, is close to 100 % even after 5 cycles. (**b**) Tensile curves of rDNGHs containing microgels prepared from an aqueous solution containing 25 wt% AMPS as a function of recycling. (**c**) Optical micrographs of PAMPS microgels with varying polymer contents as a function of the degradation cycle. Microgels prepared from solutions containing 20 wt% monomers are damaged as they are recycled multiple times. With increasing polymer content, the microgels display better shape fidelity and reduced damage over multiple recycling iterations. Scale bars are 100 µm.

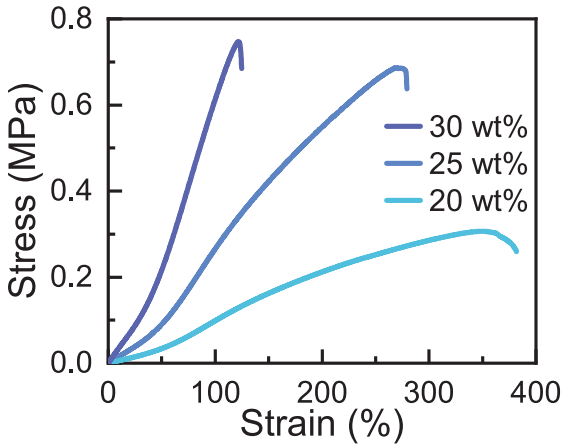

Figure 6.5: Mechanical performance of rDNGHs. Tensile curves of rDNGHs as a function of microgel polymer content.

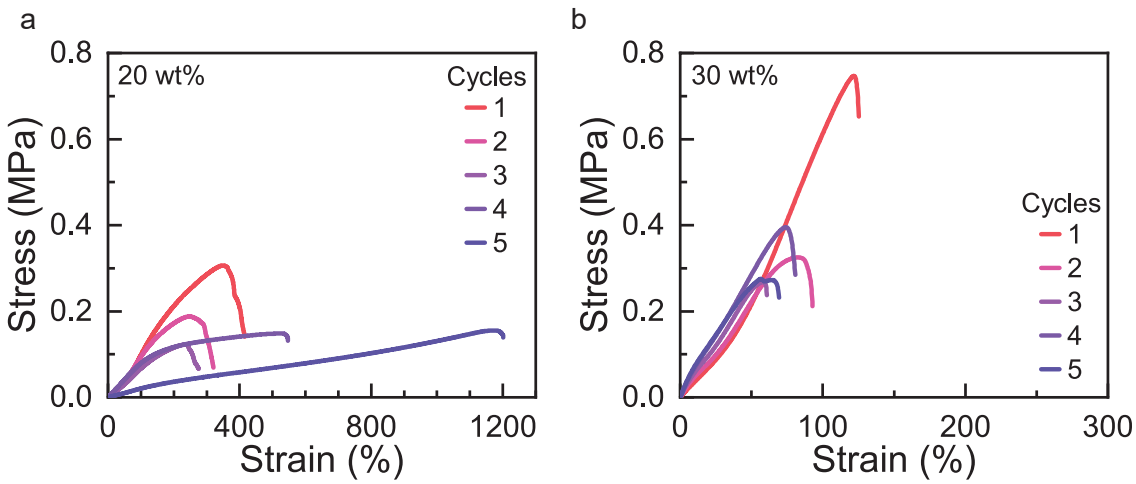

Figure 6.6: Mechanical performance of rDNGHs. (**a**) Tensile curves of rDNGHs containing microgels prepared from an aqueous solution containing 20 wt% AMPS as a function of recycling. (**b**) Tensile curves of rDNGHs containing microgels prepared from an aqueous solution containing 30 wt% AMPS as a function of recycling.

By contrast, rDNGHs containing microgels made from 30 wt% AMPS solutions show no appreciable stiffness change throughout cycles, as shown in Figure 6.6b. This difference in stiffness of rDNGHs composed of microgels made from a 20 wt% AMPS solution is attributed to an ever-increasing internal damage of these microgels, that influences the mechanical performance of rDNGHs throughout the cycles, as observed from the optical images in Figure 6.4c. The internal damage is much lower for recycled microgels that have been prepared from a 25 wt% AMPS solution, and almost no damage is observed for recycled microgels prepared from a 30 wt% AMPS solution. While rDNGHs prepared from a 30 wt% AMPS solution appear to be the least damaged throughout the recycles, the high polymer content within the microgels limits their swelling capability and therefore their capacity to load AM precursor. As a result, the density of PAM within 30 wt% AMPS rDNGHs is lower, resulting in lower maximum elongation in the pristine sample, as shown in Figure 6.6b. Hence, the maximum elongation must be traded off with the structural integrity. For this reason, we fix the AMPS concentration in the solution used to make microgels to 25 wt% for the following experiments.

6.4.4 3D printing of rDNGHs

As investigated in chapter 5, jammed microgels are well-suited for 3D printing because they are shear thinning and display a low yield stress [21, 312]. To test, if this is also the case for our ink based on AM and BAC precursors, we assess its rheological properties. As expected, our jammed microgels are shear thinning and have a yield stress as low as 5 kPa. Note that the rheological properties are independent of the number of recycles the microgels have been subjected to, as shown in Figure 6.7a, suggesting that the recycling does not affect the 3D printability of the ink.

The ease to 3D print depends on the pressure required to extrude the ink through the nozzle. This parameter is determined by the characteristic rheological flow point, defined as the crossover between storage modulus (G') and loss modulus (G"), beyond which the material will flow through the nozzle. Furthermore, the quality of the 3D printed object depends on its shape fidelity, a parameter that is determined by the amplitude of the plateau G' at low strain [177, 207, 313]. To assess whether the recycling affects the ease of printing and the quality of the resulting object, we monitor the characteristic rheological flow point and the plateau storage modulus at 0.1% as a function of the recycles. We observe no appreciable change in these two parameters even if microgels are recycled up to 5 times, as shown in Figure 6.7b, indicating that the ease and precision of the 3D printing remains unchanged even if microgels are recycled several times. To highlight this feature, we print a 3D rDNGH construct representing a Moai head, as displayed in Figure

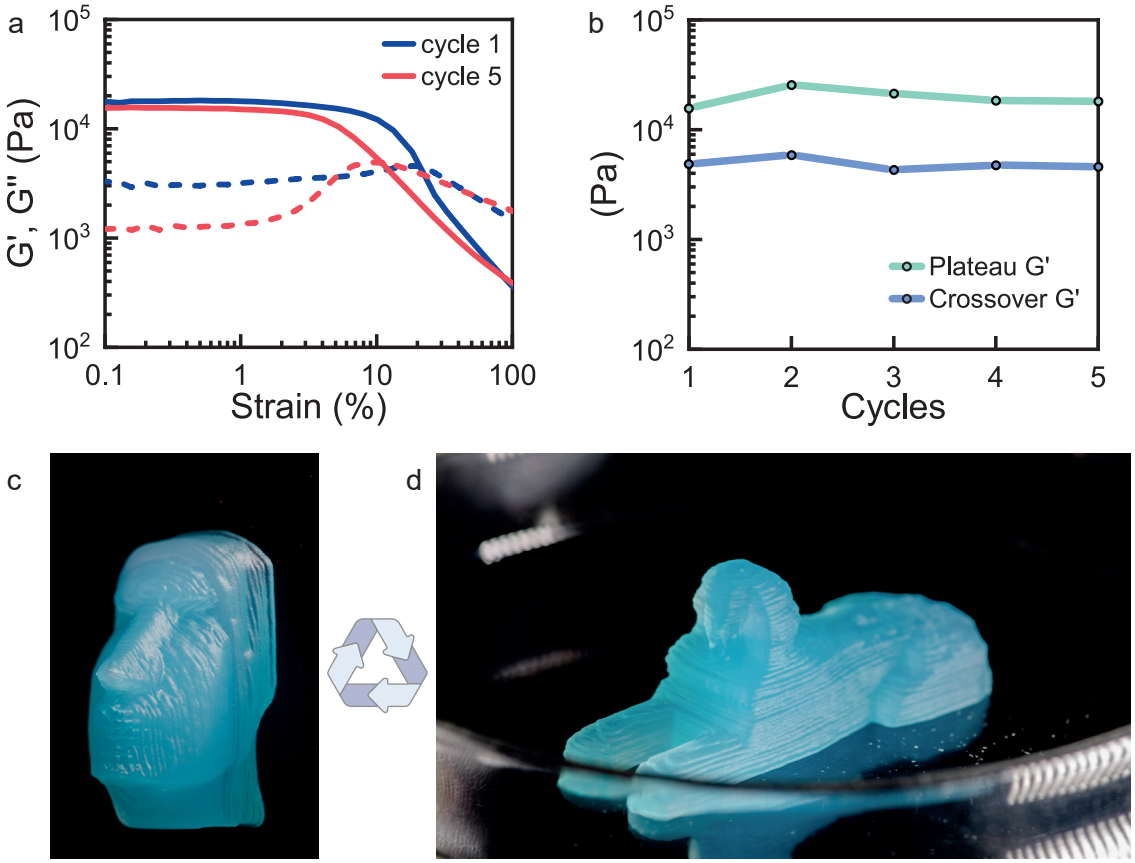

Figure 6.7: Printing and recycling of rDNGHs. (**a**) Rheological characterization of pristine and recovered jammed microgels. The amplitude sweep shows good printability of the jammed microgels even after 5 cycles. (**b**) Storage modulus (plateau G') and flow point (crossover G' with G") demonstrate no appreciable decrease in rheological performance over several recycling iterations. (**c**) Pristine jammed microgels are printed into a Moai figure, and polymerized into a rDNGH. Microgels are colored with methylene blue for visualization. Scale bar is 10 mm. (**d**) After degradation of the Moai figure, the recovered microgels can be regenerated into a fully functional ink and 3D printed again. To better elucidate the recycling process, a sphinx is chosen as the new print. Scale bar is 10 mm.

6.7c. We subsequently degrade the Moai head, recover the microgels, and re-print another rDNGH construct representing a sphinx that displays a similar printing resolution, as seen in Figure 6.7d.

6.4.5 Dried rDNGHs as recyclable plastics

Hydrogels are well-suited for biomedical applications. However, their mechanical properties can only be tuned over a limited range. To broaden the range of mechanical properties that can be accessed with our rDNGHs, we dehydrate 3D printed rDNGHs in a vacuum chamber to obtain a hard integral plastic material, as shown in Figure 6.8a and well in agreement with existing literature on dehydrated polyelectrolyte gels [314]. The mechanical properties of the resulting material are assessed using three-point bending. Dried rDNGHs display a bending modulus as high as 1.92 GPa with a maximum flexural stress of 130 MPa at 6% strain. These values are similar to those of commercial plastics, such as acrylonitrile butadiene styrene (ABS), polyethylene (PE), and polyethylene terephthalate (PET) [315]. To recycle the material at the end of its life, we immerse it in an aqueous solution containing TCEP until it is fully degraded, which takes approximately 2 hours. The recovered material is swollen in an aqueous solution containing acrylamide before it is processed into a new rDNGH sample. After drying, the bending modulus increases by 10% whereas the flexural strain decreases by 50%, as shown in Figure 6.8b. We assign the changes in mechanical properties to the increase in the PAM density within the microgel that stiffens them.

To demonstrate the potential of the dried rDNGHs to act as load-bearing materials, we fabricate a wrench to screw in a stainless-steel nut. Like in conventional manufacturing processes, poor design can result in an unfunctional tool, as shown in Figure 6.8c. Thanks to the intrinsic recyclability of our material, it is possible to reprocess our plastic within the same day and adapt the design to better fit the nut, as shown in Figure 6.8d. As a result, the final tool can easily tighten the nut to the bolt.

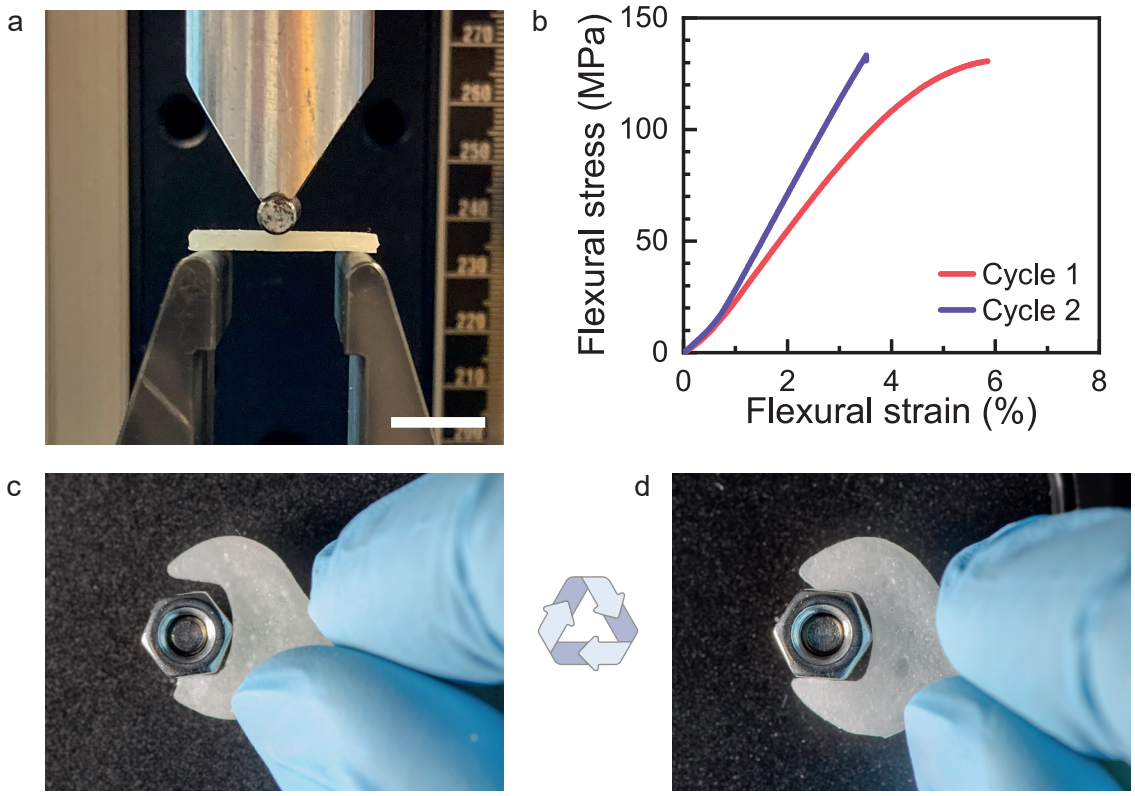

Figure 6.8: The new paradigm of rDNGH-based plastics. (**a**) Picture of 3-point bending test of a dried rDNGH slab (20.0 x 10.2 x 1.4 mm^3). Scale bar is 10 mm. (**b**) Flexural stress-strain curves of dried pristine and recycled rDNGH. The solid material behaves as a hard plastic with a flexural modulus of 1.92 GPa. The recycled material displays an increase in modulus of 10 % with respect to the pristine sample, while the flexural strain decreases by 50 %. (**c,d**), Proof of concept of fast prototyping of dried rDNGHs. As an example, a M5 molded wrench cannot tighten a M4 bolt (**c**). The wrench is therefore recycled and casted into a new M4 wrench, enabling us to tighten the bolt (**d**). Scale bars are 5 mm.

6.5 Conclusion

We introduce a 3D printable, recyclable double network granular hydrogel that can bear loads up to 0.7 MPa. The material is composed of microgels that are connected through a degradable covalently crosslinked network that interpenetrates the microgels and covalently crosslinks them. The ability to selectively degrade the percolating secondary network enables a fast, benign material disassembly. The microgels can be recovered at a yield close to 1, purified and loaded with new reagents, before they are again processed into a rDNGH whose mechanical properties closely resemble those of the pristine counterpart. Importantly, the degradation procedure is not limited to hydrogels or disulfide-based

linkers but can be extended to a broader range of materials and reversible chemistries, thus making this process generalizable. Finally, we showcase a proof of concept for the translation of rDNGHs to the fabrication of recyclable hard plastics. We envisage this approach to have the potential to shift the paradigm of recyclable polymeric materials and serve the bigger purpose of fighting global environmental pollution.

CHAPTER 7

Conclusion

At the beginning of this thesis, I identified two major challenges in the development of strategies to mechanically reinforce hydrogels:

- Bio-inspired metal-coordination hydrogels lack solid-like mechanical properties, due to the relatively short lifetime of the crosslinking bonds.
- Double network hydrogels lack good manufacturability beyond simple casting methods, due to the liquid state of the precursor solutions.

Throughout the remainder of this work, I presented solutions to address these problems. In this chapter, I summarize the findings collected across the thesis. I conclude by giving general directions for future research.

In chapter 4, I introduced a metal-coordinated hydrogel based on high functionality crosslinks. The simple one-step gelation is achieved by a simultaneous precipitation of inorganic ions, and the attractive interaction between the precipitates and the polymers functionalized with pyrogallol ligands. The advantage of using pyrogallols is their strong chelation of trivalent ions at neutral pH, due to the low pKa of the molecule. The competition between nucleation and growth of inorganic precipitates, and the chelation of the ligands to available ions, leads to an arrested growth of the precipitates. As a result, polydisperse nanoparticles act as high functionality crosslinks for a mechanically reinforced metal-coordinated hydrogel based on linear end-functionalized PEG.

In chapters 5 and 6, I introduced microgel-based inks as 3D printable precursors to fabricate strong and tough double network granular hydrogels. The advantage of using microgels to fabricate hydrogels is two-fold:

1. Jammed microgel-based inks have ideal viscoelastic properties that are compatible with precision manufacturing techniques, such as injection and 3D printing.

2. microgels with varying compositions can be embedded into a single granular hydrogel.

These keys aspects enable the precise fabrication of hydrogels with locally varying compositions. However, a limitation of our method presented in chapter 5 is the permanent nature of the percolating network. I demonstrate in chapter 6 that this limitation can be overcome using a degradable second network.

In conclusion, in this thesis I have introduced two distinctive strategies to mechanically reinforce hydrogels for load-bearing applications. First, I have demonstrated that metal-coordinated hydrogels can have solid-like properties, through a simple one-step precipitation of high functionality crosslinks. Second, I introduced the use of granular hydrogels to fabricate 3D printable double network hydrogels, that have high strength and toughness. As a result, I can locally vary the composition of the material, and induce stimuli responsiveness. Finally, I showed that the latter approach can be used with a degradable second network, thereby achieving the recycling of the microgels, without significant loss in mechanical properties of the granular hydrogel. I have demonstrated that this technique can be extended to form rigid plastics, that are recyclable under mild aqueous conditions. I conceptualized that granular hydrogels yield many promising applications, for their versatility, robust production, and easy cutomization. Furthermore, I believe that the presented methods provide a significant contribution to the field of load-bearing hydrogels, to expand the range of possible future applications beyond the biomedical field. While significant progress is being made in this field of research, I warn that substantial legal approval remains to be overcome before I can effectively foresee a use of these materials within the human body as soft load-bearing implants.

CHAPTER 8

Outlook

In this chapter, I propose an outlook on promissing future work that could greatly contribute to the field of load-bearing hydrogels. I present some preliminary results, for each of the explored directions.

8.0.1 Metal-coordinated hydrogels

In chapter 4, I presented a method to fabricate a metal-coordinated hydrogel based on the precipitation of high functionality crosslinks. While the resulting mechanical properties are increased as compared to a classical metal-coordinated hydrogels based on single ion crosslinks, the material lacks good stretchability. I attribute this behavior to the high number of defects, resulting in a far from ideal network. This leads to a poor cohesion within the hydrogel at large scale. I postulate that a highly stretchable percolating network would greatly improve the cohesion of the material. Furthermore the metal-coordinated network could act as a reversible first network in a double network architecture, rendering it self-healing.

In chapter 1, I introduced the concepts behind the remarkable mechanical properties of double networks. In chapters 5 and 6, I demonstrated the use of the double network architecture to enable the 3D printing of strong and tough hydrogels. However, the impressive mechanical properties are partially owed to the irreversible breaking of covalent bonds in the first network. As a result, the material is irreversibly damaged beyond the critical elastic regime, leading to a decay in mechanical properties over several large strain cycles.

This limitation can be overcome if the first network contains reversible bonds that break during loading, yet re-bond thereafter, such as metal-coordination bonds used in chapter 4. The rupture of these bonds enables to dissipate energy, effectively contributing as

sacrificial crosslinks in the first network. It is worth mentioning that the requirements for this are two fold:

1. the crosslinking degree of the first network is substantially higher than that of the second network, such that the elongation of the material is limited by the first network.
2. the bonding energy of the sacrificial reversible bonds is smaller than that of the second network.

As mentioned in section 1.6.6, this strategy has been first demonstrated using alginate ionically crosslinked by Ca^{2+} ions as first network, and AM covalently crosslinked by MBA [79]. However, the slow re-crosslinking of the trapped alginate network leads to a recovery of only 50% of its original toughness within a day. To overcome this limitation, reversible bonds with faster relaxation, yet high bonding energy are required. Coordination bonds fulfill these requirements, and have effectively been used in dually crosslinked single networks, as sacrificial bonds [256, 55]. For example, the use of catechols and Fe^{3+} ions as secondary crosslinks in elastomers greatly improved the mechanics of the covalently crosslinked network [253]. Additionally, the material recovers 50% of its original toughness within 10 min. However, true metal coordinated double networks, where the primary network is entirely crosslinked by coodination bonds remain to be shown.

In an attempt to achieve this, I fabricate a double network based on a 2cPEG 1 kDa crosslinked by Fe^{3+} as first network, and covalently crosslinked PAM second network. All reactants are mixed under acidic conditions, and the solution is exposed to UV in a mold. The crosslinking of metal-coordinated network is triggered by exposure of the solid samples to ammonia.

To investigate whether the presence of the metal-coordinated network is affected by the second network, I perform frequency sweep rheological measurements on the double network, on the covalent single network, and on the metal-coordinated single network, as shown in Figure 8.1a,b. I substract the storage and loss modulus of the covalent network, to those of the double network, to obtain the rheological contribution of the metal-coordinated network within the double network. Remarkably, the obtained artificial storage and loss moduli resemble those of the measured metal-coordinated single network, as shown in Figure 8.1c. I attribute this finding to the fast reversible bonding of the metal-coordination bonds, which remains nearly unchanged by the presence of the covalent second network. However, the material did not reach a high stretchability, strength or toughness. I attribute this to the non-ideal second network, that does not meet the requirements stated above. In conclusion, from the remarkable rheological observation, I postulate that metal-coordination bonds yield promising use as sacrifical crosslinks in

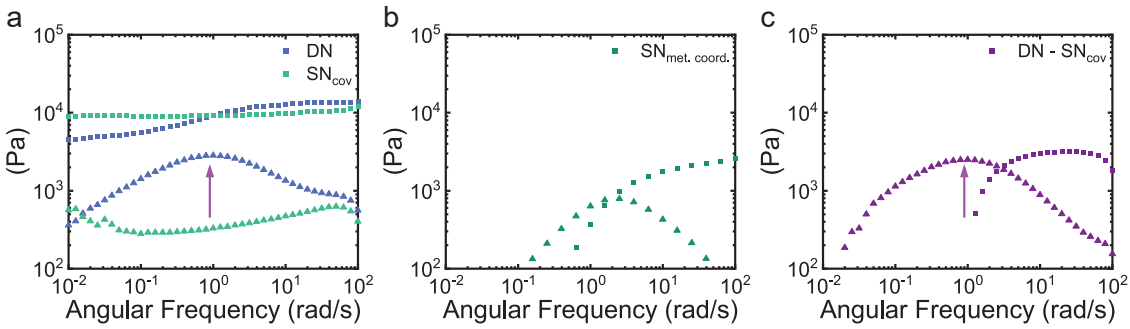

Figure 8.1: Rheological tests of metal-coordinated double network. (**a**) Frequency sweep of a metal-coordinated double network and of a covalent single network. The arrow shows the resonance frequency of the metal-coordination bond. At frequencies higher than the resonance, the metal-coordination bonds strongly contribute elastically to the network, as observed by an increased storage modulus. (**b**) Frequency sweep of a metal-coordinated single network of 2cPEG - Fe^{3+}, depicting a classical Maxwell model. (**c**) Artificial frequency sweep from the metal-coordination contribution in the double network. Remarkably, this frequency sweep ressembles that of a metal-coordinated single network. Squares represent storage moduli, triangles represent loss moduli.

healable double networks. Part of this work was performed by Paolo Pedrazzini, as part of his semester project, and subsequent internship.

8.0.2 Granular hydrogels

In chapter 6, I presented a method to selectively trigger the dissolution of the percolating network in double network granular hydrogels. While the triggerable breaking of the bonds is ideal to fabricate degradable materials, recovered microgels need to be re-soaked in a pristine AM + MBA precursor solution, thereby not achieving "full" recyclability.

An alternative to this is the use of coordination bonds as dynamic reversible bonds to link microgels together. I attempt to fabricate simple self-healable microgels, by decorating them with ligands. To do so, I synthesized dopamine acrylamide, a short molecule containing both an acrylate group and a catechol group. I validated the covalent decoration of PMPTC microgels with catechols by performing hyperspectral Raman imaging, as shown in Figure 8.2a. PMPTC microgels were selected for their lack of interaction with Fe^{3+} ions. I exposed the microgels to Fe^{3+} ions and an increase in pH in an attempt to create bridging coordination bonds across microgels. While the resulting jammed microgels, shown in Figure 8.2b had an increased viscosity, the material did not solidify. I attribute this to a limited amount of metal coordination bonds, leading to a poor inter-microgel adhesion. I believe that a hybrid approach between a percolating covalent network, and interparticle metal coordination bonds yields promissing avenues for the future. Part of this work was

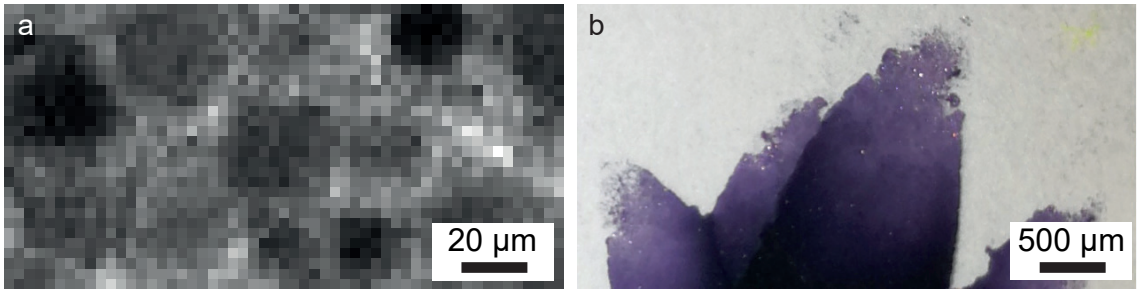

Figure 8.2: Imaging of catechol decorated microgels that are exposed to Fe^{3+}. (**a**) Hyperspectral Raman image of microgels. The resonance peak of the coordination bond is chosen as color gradient. Individual microgels can be observed, revealing the presence of catechol - Fe^{3+} coordination bonds on the microgels. (**b**) Picture of jammed microgels. The catechol - Fe^{3+} coordination bonds lead to a purple color.

performed by Stella Laperrousaz and Joëlle Piot during their semester projects, and by Francesca Bono, as part of her master thesis. Francesca Bono will pursue these ideas as part of her PhD.

APPENDIX A

Abbreviations

$2cPEG$	di-catechol functionalised poly (ethylene glycol)
$2gPEG$	di-pyrogallol functionalised poly (ethylene glycol)
$3D$	three dimensional
α	Kohlraush exponent
AM	acrylamide
$AMPS$	2-acrylamido-2-methylpropane sulfonic acid
d	diameter
D_2O	deuterium oxide
DAT	data file extension
DCM	dichloromethane
$DIPEA$	N,N-diisopropylethylamine
DMF	dimethylformaldehyde
DN	double network
$DNGH$	double network granular hydrogel
E_a	activation energy
ECM	extracellular matrix
EWC	equilibrium water content
$FeCl_3$	iron III chloride
$FTIR$	fourier-transform infrared spectroscopy
γ	shear
G	stress relaxation modulus
G_i	initial stress relaxation modulus
G_0	plateau stress relaxation modulus
G'	viscoelastic storage modulus
G''	viscoelastic loss modulus
h	height

H	relaxation spectrum
H_2O	water
HCl	hydrogen chloride
I	scattering intensity
k_B	Boltzmann constant
$mol\%$	molar percentage
MBA	N,N′-methylene bisacrylamide
$MgSO_4$	magnesium sulfate
$NaBr$	sodium bromide
$NaCl$	sodium chloride
$NaClO$	sodium hypochlorite
$NaOH$	sodium hydroxide
NMR	nuclear magnetic resonance
ξ	short correlation length
PAA	poly(acrylic acid)
PAM	poly(acrylamide)
$PAMPS$	poly(sodium 2-acrylamido-2-methyl-1-propanesulfonate)
PEG	poly(ethylene glycol)
$PEG-COOH$	carboxylic functionalised poly(ethylene glycol)
$PHEMA$	poly(hydroxyethylmethacrylate)
PI	photoinitiator
$PMPTC$	poly((3-(methacryloylamino)propyl)trimethylammonium chloride)
$PNIPAM$	poly(N-isopropylacrylamide)
$PyBOP$	benzotriazole-1-yl-oxy-tris-pyrrolidino-phosphonium hexafluorophosphate
PVA	poly(vinyl alcool)
q	scattering vector
rpm	rotation per minute
$SAXS$	small-angle X-ray scattering
τ	relaxation time
t	time
T	temperature
TEM	transmission electron microscopy
$TEMPO$	2,2,6,6-tetramethylpiperidine 1-oxyl, 2,2,6,6-tetramethyl-1-piperidinyloxy
UV	ultraviolet
V	volume
W_{ap}	as-prepared sample weight

W_d	dry sample weight
$wt\%$	weight percentage
χ	electronegativity
XRD	X-ray diffraction
ψ	long correlation length

APPENDIX B

Units

cm	centimeter
Da	dalton
g	gram
h	hour
J	joule
kDa	kilodalton
kg	kilogram
kPa	kilopascal
L	litter
μg	microgram
μL	microlitter
μm	micrometer
mg	milligram
min	minute
mL	milliliter
mm	millimeter
M	molar
MHz	megahertz
MPa	megapascal
$mmol$	millimollar
mW	milliwatt
N	newton
nm	nanometer
Pa	pascal
rad	radian
s	second

t	time
W	watt

Bibliography

[1] Jean P. Mercier, Gérald Zambelli, and Wilfried Kurz. Chapter 1 - Materials. In Jean P. Mercier, Gérald Zambelli, and Wilfried Kurz, editors, *Introduction to Materials Science*, pages 1–16. Elsevier, Oxford, January 2002.

[2] Shan Cecilia Cao, Jiabin Liu, Linli Zhu, Ling Li, Ming Dao, Jian Lu, and Robert O. Ritchie. Nature-Inspired Hierarchical Steels. *Scientific Reports*, 8(1):5088, March 2018.

[3] Jean P. Mercier, Gérald Zambelli, and Wilfried Kurz. Chapter 10 - Microstructures. In Jean P. Mercier, Gérald Zambelli, and Wilfried Kurz, editors, *Introduction to Materials Science*, pages 239–259. Elsevier, Oxford, January 2002.

[4] Paul Calvert. Hydrogels for Soft Machines. *Advanced Materials*, 21(7):743–756, 2009.

[5] Hyunwoo Yuk, Claudia E. Varela, Christoph S. Nabzdyk, Xinyu Mao, Robert F. Padera, Ellen T. Roche, and Xuanhe Zhao. Dry double-sided tape for adhesion of wet tissues and devices. *Nature*, 575(7781):169–174, November 2019.

[6] Jun Fang, Jaekyung Koh, Qizhi Fang, Huiliang Qiu, Maani M. Archang, Mohammad Mahdi Hasani-Sadrabadi, Hiromi Miwa, Xintong Zhong, Richard Sievers, Dong-Wei Gao, Randall Lee, Dino Di Carlo, and Song Li. Injectable Drug-Releasing Microporous Annealed Particle Scaffolds for Treating Myocardial Infarction. *Advanced Functional Materials*, 30(43):2004307, 2020.

[7] Jonathan A. Brassard, Mike Nikolaev, Tania Hübscher, Moritz Hofer, and Matthias P. Lutolf. Recapitulating macro-scale tissue self-organization through organoid bioprinting. *Nature Materials*, 20(1):22–29, January 2021.

[8] Brandon V. Slaughter, Shahana S. Khurshid, Omar Z. Fisher, Ali Khademhosseini, and Nicholas A. Peppas. Hydrogels in Regenerative Medicine. *Advanced Materials*, 21(32-33):3307–3329, 2009.

[9] Ye Sun, Yongqing You, Wenbo Jiang, Bo Wang, Qiang Wu, and Kerong Dai. 3D bioprinting dual-factor releasing and gradient-structured constructs ready to implant for anisotropic cartilage regeneration. *Science Advances*, 6(37):eaay1422, September 2020.

[10] Yanyu Zhang and Yishun Huang. Rational Design of Smart Hydrogels for Biomedical Applications. *Frontiers in Chemistry*, 8:1288, 2021.

[11] Steven R. Caliari and Jason A. Burdick. A practical guide to hydrogels for cell culture. *Nature Methods*, 13(5):405–414, May 2016.

[12] Joshua E. Mealy, Jennifer J. Chung, Heon-Ho Jeong, David Issadore, Daeyeon Lee, Pavan Atluri, and Jason A. Burdick. Injectable Granular Hydrogels with Multifunctional Properties for Biomedical Applications. *Advanced Materials*, 30(20):1705912, 2018.

[13] Wei Sun, Binil Starly, Andrew C. Daly, Jason A. Burdick, Jürgen Groll, Gregor Skeldon, Wenmiao Shu, Yasuyuki Sakai, Marie Shinohara, Masaki Nishikawa, Jinah Jang, Dong-Woo Cho, Minghao Nie, Shoji Takeuchi, Serge Ostrovidov, Ali Khademhosseini, Roger D. Kamm, Vladimir Mironov, Lorenzo Moroni, and Ibrahim T. Ozbolat. The bioprinting roadmap. *Biofabrication*, 12(2):022002, February 2020.

[14] Jonas C. Rose and Laura De Laporte. Hierarchical Design of Tissue Regenerative Constructs. *Advanced Healthcare Materials*, 7(6):1701067, 2018.

[15] Danqing Zhu, Pavin Trinh, Elisa Liu, and Fan Yang. Biochemical and Mechanical Gradients Synergize To Enhance Cartilage Zonal Organization in 3D. *ACS Biomaterials Science & Engineering*, 4(10):3561–3569, October 2018.

[16] Justin R Tse and Adam J Engler. Stiffness Gradients Mimicking In Vivo Tissue Variation Regulate Mesenchymal Stem Cell Fate. *PLoS ONE*, 6(1), 2011.

[17] Ovijit Chaudhuri. Viscoelastic hydrogels for 3D cell culture. *Biomaterials Science*, 5, 2017.

[18] Jenna L. Balestrini, Sidharth Chaudhry, Vincent Sarrazy, Anne Koehler, and Boris Hinz. The mechanical memory of lung myofibroblasts. *Integrative Biology*, 4(4):410–421, April 2012.

[19] Ovijit Chaudhuri, Luo Gu, Darinka Klumpers, Max Darnell, Sidi A. Bencherif, James C. Weaver, Nathaniel Huebsch, Hong-pyo Lee, Evi Lippens, Georg N. Duda, and David J. Mooney. Hydrogels with tunable stress relaxation regulate stem cell fate and activity. *Nature Materials*, 15(3):326–334, March 2016.

[20] Andrew C. Daly, Lindsay Riley, Tatiana Segura, and Jason A. Burdick. Hydrogel microparticles for biomedical applications. *Nature Reviews Materials*, 5(1):20–43, January 2020.

[21] Lindsay Riley, Lucas Schirmer, and Tatiana Segura. Granular hydrogels: Emergent properties of jammed hydrogel microparticles and their applications in tissue repair and regeneration. *Current Opinion in Biotechnology*, 60:1–8, December 2019.

[22] Mikhail Nikolaev, Olga Mitrofanova, Nicolas Broguiere, Sara Geraldo, Devanjali Dutta, Yoji Tabata, Bilge Elci, Nathalie Brandenberg, Irina Kolotuev, Nikolce Gjorevski, Hans Clevers, and Matthias P. Lutolf. Homeostatic mini-intestines through scaffold-guided organoid morphogenesis. *Nature*, 585(7826):574–578, September 2020.

[23] Michael Shur, Florian Fallegger, Elvira Pirondini, Adrien Roux, Arnaud Bichat, Quentin Barraud, Grégoire Courtine, and Stéphanie P. Lacour. Soft Printable Electrode Coating for Neural Interfaces. *ACS Applied Bio Materials*, 3(7):4388–4397, July 2020.

[24] Jingzhou Yang, Yu Shrike Zhang, Kan Yue, and Ali Khademhosseini. Cell-laden hydrogels for osteochondral and cartilage tissue engineering. *Acta Biomaterialia*, 57:1–25, July 2017.

[25] Thomas Billiet, Mieke Vandenhaute, Jorg Schelfhout, Sandra Van Vlierberghe, and Peter Dubruel. A review of trends and limitations in hydrogel-rapid prototyping for tissue engineering. *Biomaterials*, 33(26):6020–6041, September 2012.

[26] Mei Liu, Xin Zeng, Chao Ma, Huan Yi, Zeeshan Ali, Xianbo Mou, Song Li, Yan Deng, and Nongyue He. Injectable hydrogels for cartilage and bone tissue engineering. *Bone Research*, 5:17014, 2017.

[27] Xuanhe Zhao, Xiaoyu Chen, Hyunwoo Yuk, Shaoting Lin, Xinyue Liu, and German Parada. Soft Materials by Design: Unconventional Polymer Networks Give Extreme Properties. *Chemical Reviews*, 121(8):4309–4372, April 2021.

[28] Hyunwoo Yuk, Jingjing Wu, Tiffany L. Sarrafian, Xinyu Mao, Claudia E. Varela, Ellen T. Roche, Leigh G. Griffiths, Christoph S. Nabzdyk, and Xuanhe Zhao. Rapid and coagulation-independent haemostatic sealing by a paste inspired by barnacle glue. *Nature Biomedical Engineering*, August 2021.

[29] Melanie Baumgartner, Florian Hartmann, Michael Drack, David Preninger, Daniela Wirthl, Robert Gerstmayr, Lukas Lehner, Guoyong Mao, Roland Pruckner, Stepan Demchyshyn, Lisa Reiter, Moritz Strobel, Thomas Stockinger, David Schiller, Susanne Kimeswenger, Florian Greibich, Gerda Buchberger, Elke Bradt, Sabine Hild, Siegfried Bauer, and Martin Kaltenbrunner. Resilient yet entirely degradable gelatin-based biogels for soft robots and electronics. *Nature Materials*, 19(10):1102–1109, October 2020.

[30] Wenhuan Sun, Saul Schaffer, Kevin Dai, Lining Yao, Adam Feinberg, and Victoria Webster-Wood. 3D Printing Hydrogel-Based Soft and Biohybrid Actuators: A Mini-Review on Fabrication Techniques, Applications, and Challenges. *Frontiers in Robotics and AI*, 8:120, 2021.

[31] E. Acome, S. K. Mitchell, T. G. Morrissey, M. B. Emmett, C. Benjamin, M. King, M. Radakovitz, and C. Keplinger. Hydraulically amplified self-healing electrostatic actuators with muscle-like performance. *Science*, 359(6371):61–65, January 2018.

[32] Canhui Yang and Zhigang Suo. Hydrogel ionotronics. *Nature Reviews Materials*, 3(6):125–142, June 2018.

[33] Wen Jiang Zheng, Ning An, Jian Hai Yang, Jinxiong Zhou, and Yong Mei Chen. Tough Al-alginate/Poly(N-isopropylacrylamide) Hydrogel with Tunable LCST for Soft Robotics. *ACS Applied Materials & Interfaces*, 7(3):1758–1764, January 2015.

[34] Bruce P Lee and Shari Konst. Novel Hydrogel Actuator Inspired by Reversible Mussel Adhesive Protein Chemistry COMMUNICATION. *Advanced Materials*, 26:3415–3419, 2014.

[35] Hyunwoo Yuk, Shaoting Lin, Chu Ma, Mahdi Takaffoli, Nicolas X. Fang, and Xuanhe Zhao. Hydraulic hydrogel actuators and robots optically and sonically camouflaged in water. *Nature Communications*, 8(1):14230, February 2017.

[36] Guorui Li, Xiangping Chen, Fanghao Zhou, Yiming Liang, Youhua Xiao, Xunuo Cao, Zhen Zhang, Mingqi Zhang, Baosheng Wu, Shunyu Yin, Yi Xu, Hongbo Fan, Zheng Chen, Wei Song, Wenjing Yang, Binbin Pan, Jiaoyi Hou, Weifeng Zou, Shunping He, Xuxu Yang, Guoyong Mao, Zheng Jia, Haofei Zhou, Tiefeng Li, Shaoxing Qu, Zhongbin Xu, Zhilong Huang, Yingwu Luo, Tao Xie, Jason Gu, Shiqiang Zhu, and Wei Yang. Self-powered soft robot in the Mariana Trench. *Nature*, 591(7848):66–71, March 2021.

[37] Xinyue Liu, Ji Liu, Shaoting Lin, and Xuanhe Zhao. Hydrogel machines. *Materials Today*, January 2020.

[38] The soft touch of robots. *Nature Reviews Materials*, 3(6):71–71, June 2018.

[39] Matteo Cianchetti, Cecilia Laschi, Arianna Menciassi, and Paolo Dario. Biomedical applications of soft robotics. *Nature Reviews Materials*, 3(6):143–153, June 2018.

[40] Guoying Gu, Ningbin Zhang, Haipeng Xu, Shaoting Lin, Yang Yu, Guohong Chai, Lisen Ge, Houle Yang, Qiwen Shao, Xinjun Sheng, Xiangyang Zhu, and Xuanhe Zhao. A soft neuroprosthetic hand providing simultaneous myoelectric control and tactile feedback. *Nature Biomedical Engineering*, pages 1–10, August 2021.

[41] Panagiotis Polygerinos, Zheng Wang, Kevin C. Galloway, Robert J. Wood, and Conor J. Walsh. Soft robotic glove for combined assistance and at-home rehabilitation. *Robotics and Autonomous Systems*, 73:135–143, November 2015.

[42] N. A. Peppas, J. Z. Hilt, A. Khademhosseini, and R. Langer. Hydrogels in Biology and Medicine: From Molecular Principles to Bionanotechnology. *Advanced Materials*, 18(11):1345–1360, 2006.

[43] Ferdinand Ruedinger, Antonina Lavrentieva, Cornelia Blume, Iliyana Pepelanova, and Thomas Scheper. Hydrogels for 3D mammalian cell culture: A starting guide for laboratory practice. *Applied Microbiology and Biotechnology*, 99(2):623–636, January 2015.

[44] Junsoo Kim, Guogao Zhang, Meixuanzi Shi, and Zhigang Suo. Fracture, fatigue, and friction of polymers in which entanglements greatly outnumber cross-links. *Science*, 374(6564):212–216, October 2021.

[45] Ji Liu, Shaoting Lin, Xinyue Liu, Zhao Qin, Yueying Yang, Jianfeng Zang, and Xuanhe Zhao. Fatigue-resistant adhesion of hydrogels. *Nature Communications*, 11(1):1–9, February 2020.

[46] Huachuan Du, Alice Cont, Mathias Steinacher, and Esther Amstad. Fabrication of Hexagonal-Prismatic Granular Hydrogel Sheets. *Langmuir*, 34:3459–3466, 2018.

[47] Donald L. Elbert and Jeffrey A. Hubbell. Conjugate Addition Reactions Combined with Free-Radical Cross-Linking for the Design of Materials for Tissue Engineering. *Biomacromolecules*, 2(2):430–441, June 2001.

[48] Takamasa Sakai, Takuro Matsunaga, Yuji Yamamoto, Chika Ito, Ryo Yoshida, Shigeki Suzuki, Nobuo Sasaki, Mitsuhiro Shibayama, and Ung-il Chung. Design and Fabrication of a High-Strength Hydrogel with Ideally Homogeneous Network Structure from Tetrahedron-like Macromonomers. *Macromolecules*, 41(14):5379–5384, July 2008.

[49] Lauren E. Jansen, Lenny J. Negrón-Piñeiro, Sualyneth Galarza, and Shelly R. Peyton. Control of thiol-maleimide reaction kinetics in PEG hydrogel networks. *Acta Biomaterialia*, 70:120–128, April 2018.

[50] Michael Malkoch, Robert Vestberg, Nalini Gupta, Laetitia Mespouille, Philipe Dubois, Andrew F. Mason, James L. Hedrick, Qi Liao, Curtis W. Frank, Kevin Kingsbury, and Craig J. Hawker. Synthesis of well-defined hydrogel networks using Click chemistry. *Chemical Communications*, (26):2774–2776, June 2006.

[51] Hiroyuki Kamata, Yuki Akagi, Yuko Kayasuga-Kariya, Ung-il Chung, and Takamasa Sakai. "Nonswellable" Hydrogel Without Mechanical Hysteresis. *Science*, 343(6173):873–875, February 2014.

[52] Huaping Tan, Chao Xiao, Jinchen Sun, Dangsheng Xiong, and Xiaohong Hu. Biological self-assembly of injectable hydrogel as cell scaffold via specific nucleobase pairing. *Chemical Communications*, 48(83):10289–10291, September 2012.

[53] Xiaoyu Chen, Chaoqun Dong, Kongchang Wei, Yifei Yao, Qian Feng, Kunyu Zhang, Fengxuan Han, Arthur Fuk-Tat Mak, Bin Li, and Liming Bian. Supramolecular hydrogels cross-linked by preassembled host–guest PEG cross-linkers resist excessive, ultrafast, and non-resting cyclic compression. *NPG Asia Materials*, 10(8):788–799, August 2018.

[54] Bruce P. Lee, Jeffrey L. Dalsin, and Phillip B. Messersmith. Synthesis and Gelation of DOPA-Modified Poly(ethylene glycol) Hydrogels. *Biomacromolecules*, 3(5):1038–1047, September 2002.

[55] S.C. Scott C Grindy, Robert Learsch, Davoud Mozhdehi, Jing Cheng, D.G. Devin G Barrett, Zhibin Guan, P.B. Phillip B Messersmith, and Niels Holten-Andersen. Control of hierarchical polymer mechanics with bioinspired metal-coordination dynamics. *Nature Materials*, 14(12):1210–1216, 2015.

[56] Jeannine E. Elliott, Mara Macdonald, Jun Nie, and Christopher N. Bowman. Structure and swelling of poly(acrylic acid) hydrogels: Effect of pH, ionic strength, and dilution on the crosslinked polymer structure. *Polymer*, 45(5):1503–1510, March 2004.

[57] L. Bilmes. A Rheological Chart. *Nature*, 150(3806):432–433, October 1942.

[58] Jian Ping Gong. Materials both Tough and Soft. *Science*, 344(6180):161–162, April 2014.

[59] Multi-scale multi-mechanism design of tough hydrogels: Building dissipation into stretchy networks - Soft Matter (RSC Publishing). https://pubs.rsc.org/en/content/articlelanding/2014/sm/c3sm52272e#!divAbstract.

[60] J. P. Gong, Y. Katsuyama, T. Kurokawa, and Y. Osada. Double-Network Hydrogels with Extremely High Mechanical Strength. *Advanced Materials*, 15(14):1155–1158, 2003.

[61] Yanning Zeng, Weiming Yang, Shuxin Liu, Xiahui Shi, Aoqian Xi, and Faai Zhang. Dynamic Semi IPNs with Duple Dynamic Linkers: Self-Healing, Reprocessing, Welding, and Shape Memory Behaviors. *Polymers*, 13(11):1679, January 2021.

[62] Dong Zhang, Yingchun Yao, Jiahui Wu, Iryna Protsak, Wei Lu, Xiaomin He, Shengwei Xiao, Mingqiang Zhong, Tao Chen, and Jintao Yang. Super Hydrophilic Semi-IPN Fluorescent Poly(N-(2-hydroxyethyl)acrylamide) Hydrogel for Ultrafast, Selective, and Long-Term Effective Mercury(II) Detection in a Bacteria-Laden System. *ACS Applied Bio Materials*, 2(2):906–915, February 2019.

[63] Jian Ping Gong. Why are double network hydrogels so tough? *Soft Matter*, 6(12):2583–2590, June 2010.

[64] Feichen Yang, Vaibhav Tadepalli, and Benjamin J Wiley. 3D Printing of a Double Network Hydrogel with a Compression Strength and Elastic Modulus Greater than those of Cartilage. page 7, 2017.

[65] Tomáš Sedlačík, Takayuki Nonoyama, Honglei Guo, Ryuji Kiyama, Tasuku Nakajima, Yoshihiro Takeda, Takayuki Kurokawa, and Jian Ping Gong. Preparation of

Tough Double- and Triple-Network Supermacroporous Hydrogels through Repeated Cryogelation. *Chemistry of Materials*, September 2020.

[66] Etienne Ducrot, Yulan Chen, Markus Bulters, Rint P. Sijbesma, and Costantino Creton. Toughening Elastomers with Sacrificial Bonds and Watching Them Break. *Science*, 344(6180):186–189, April 2014.

[67] Juan Du, Shimei Xu, Shun Feng, Lina Yu, Jide Wang, and Yumei Liu. Tough dual nanocomposite hydrogels with inorganic hybrid crosslinking. *Soft Matter*, 12(6):1649–1654, February 2016.

[68] Elizabeth M. Foster, Erin E. Lensmeyer, Borui Zhang, Progyateg Chakma, Jacob A. Flum, Jeremy J. Via, Jessica L. Sparks, and Dominik Konkolewicz. Effect of Polymer Network Architecture, Enhancing Soft Materials Using Orthogonal Dynamic Bonds in an Interpenetrating Network. *ACS Macro Letters*, 6(5):495–499, May 2017.

[69] Liming Cao, Jianfeng Fan, Jiarong Huang, and Yukun Chen. A robust and stretchable cross-linked rubber network with recyclable and self-healable capabilities based on dynamic covalent bonds. *Journal of Materials Chemistry A*, 7(9):4922–4933, February 2019.

[70] K. Haraguchi and T. Takehisa. Nanocomposite Hydrogels: A Unique Organic–Inorganic Network Structure with Extraordinary Mechanical, Optical, and Swelling/De-swelling Properties. *Advanced Materials*, 14(16):1120, August 2002.

[71] Yaoyao Chen and Kenneth R. Shull. High-Toughness Polycation Cross-Linked Triblock Copolymer Hydrogels. *Macromolecules*, 50(9):3637–3646, May 2017.

[72] Yuan-na Sun, Guo-rong Gao, Gao-lai Du, Ya-jun Cheng, and Jun Fu. Super Tough, Ultrastretchable, and Thermoresponsive Hydrogels with Functionalized Triblock Copolymer Micelles as Macro-Cross-Linkers. *ACS Macro Letters*, 3(5):496–500, May 2014.

[73] Ming Zhong, Xiao-Ying Liu, Fu-Kuan Shi, Li-Qin Zhang, Xi-Ping Wang, Andrew G. Cheetham, Honggang Cui, and Xu-Ming Xie. Self-healable, tough and highly stretchable ionic nanocomposite physical hydrogels. *Soft Matter*, 11(21):4235–4241, May 2015.

[74] Jun Fu. Strong and tough hydrogels crosslinked by multi-functional polymer colloids. *Journal of Polymer Science Part B: Polymer Physics*, 56(19):1336–1350, 2018.

[75] A. Nakayama, A. Kakugo, J. P. Gong, Y. Osada, M. Takai, T. Erata, and S. Kawano. High Mechanical Strength Double-Network Hydrogel with Bacterial Cellulose. *Advanced Functional Materials*, 14(11):1124–1128, 2004.

[76] Dongdong Ye, Qiaoyun Cheng, Qianlei Zhang, Yixiang Wang, Chunyu Chang, Liangbin Li, Haiyan Peng, and Lina Zhang. Deformation Drives Alignment of Nanofibers in Framework for Inducing Anisotropic Cellulose Hydrogels with High Toughness. *ACS Applied Materials & Interfaces*, 9(49):43154–43162, December 2017.

[77] André E. X. Brown, Rustem I. Litvinov, Dennis E. Discher, Prashant K. Purohit, and John W. Weisel. Multiscale Mechanics of Fibrin Polymer: Gel Stretching with Protein Unfolding and Loss of Water. *Science*, 325(5941):741–744, August 2009.

[78] Matteo Hirsch, Mathias Steinacher, Ran Zhao, and Esther Amstad. Load-bearing hydrogels ionically reinforced through competitive ligand exchanges. *Biomaterials Science*, August 2021.

[79] Jeong-Yun Sun, Xuanhe Zhao, Widusha R. K. Illeperuma, Ovijit Chaudhuri, Kyu Hwan Oh, David J. Mooney, Joost J. Vlassak, and Zhigang Suo. Highly stretchable and tough hydrogels. *Nature*, 489(7414):133–136, September 2012.

[80] Yanyu Yang, Xing Wang, Fei Yang, Luning Wang, and Decheng Wu. Highly Elastic and Ultratough Hybrid Ionic–Covalent Hydrogels with Tunable Structures and Mechanics. *Advanced Materials*, 30(18):1707071, 2018.

[81] Shannon E. Bakarich, Robert Gorkin, Marc in het Panhuis, and Geoffrey M. Spinks. 4D Printing with Mechanically Robust, Thermally Actuating Hydrogels. *Macromolecular Rapid Communications*, 36(12):1211–1217, 2015.

[82] Jianyu Li, Widusha R K Illeperuma, Zhigang Suo, and Joost J Vlassak. Hybrid Hydrogels with Extremely High Stiffness and Toughness. *ACS Macro Letters*, 3:520–523, 2014.

[83] Xiaobo Hu, Mohammad Vatankhah-Varnoosfaderani, Jing Zhou, Qiaoxi Li, and Sergei S. Sheiko. Weak Hydrogen Bonding Enables Hard, Strong, Tough, and Elastic Hydrogels. *Advanced Materials*, 27(43):6899–6905, 2015.

[84] Chuang Li, Matthew J. Rowland, Yu Shao, Tianyang Cao, Chun Chen, Haoyang Jia, Xu Zhou, Zhongqiang Yang, Oren A. Scherman, and Dongsheng Liu. Responsive Double Network Hydrogels of Interpenetrating DNA and CB[8] Host–Guest Supramolecular Systems. *Advanced Materials*, 27(21):3298–3304, 2015.

[85] Qiang Chen, Xiaoqiang Yan, Lin Zhu, Hong Chen, Bing Jiang, Dandan Wei, Lina Huang, Jia Yang, Baozhong Liu, and Jie Zheng. Improvement of Mechanical Strength and Fatigue Resistance of Double Network Hydrogels by Ionic Coordination Interactions. *Chemistry of Materials*, 28(16):5710–5720, August 2016.

[86] Haiyan Jia, Zhangjun Huang, Zhaofu Fei, Paul J. Dyson, Zhen Zheng, and Xinling Wang. Unconventional Tough Double-Network Hydrogels with Rapid Mechanical Recovery, Self-Healing, and Self-Gluing Properties. *ACS Applied Materials & Interfaces*, 8(45):31339–31347, November 2016.

[87] Xuanhe Zhao. Designing toughness and strength for soft materials. *Proceedings of the National Academy of Sciences*, 114(31):8138–8140, August 2017.

[88] Shaoting Lin, Xinyue Liu, Ji Liu, Hyunwoo Yuk, Hyun-Chae Loh, German A. Parada, Charles Settens, Jake Song, Admir Masic, Gareth H. McKinley, and Xuanhe Zhao. Anti-fatigue-fracture hydrogels. *Science Advances*, 5(1):eaau8528.

[89] Shaoting Lin, Ji Liu, Xinyue Liu, and Xuanhe Zhao. Muscle-like fatigue-resistant hydrogels by mechanical training. *Proceedings of the National Academy of Sciences*, 116(21):10244–10249, May 2019.

[90] Qingyan He, Yan Huang, and Shaoyun Wang. Hofmeister Effect-Assisted One Step Fabrication of Ductile and Strong Gelatin Hydrogels. *Advanced Functional Materials*, 28(5):1705069, 2018.

[91] Sinan Keten, Zhiping Xu, Britni Ihle, and Markus J. Buehler. Nanoconfinement controls stiffness, strength and mechanical toughness of β-sheet crystals in silk. *Nature Materials*, 9(4):359–367, April 2010.

[92] Greg A. Johnson, Dawn M. Tramaglini, Rebecca E. Levine, Kazunori Ohno, Nam-Yong Choi, and Savio L.-Y. Woo. Tensile and viscoelastic properties of human patellar tendon. *Journal of Orthopaedic Research*, 12(6):796–803, 1994.

[93] R. E. Shadwick. Elastic energy storage in tendons: Mechanical differences related to function and age. *Journal of Applied Physiology*, 68(3):1033–1040, March 1990.

[94] Ji Liu, Shaoting Lin, Xinyue Liu, Zhao Qin, Yueying Yang, Jianfeng Zang, and Xuanhe Zhao. Fatigue-resistant adhesion of hydrogels. *Nature Communications*, 11(1):1071, February 2020.

[95] Janine M. Benyus. *Biomimicry: Innovation Inspired by Nature*. Perennial, New York, NY, nachdr. edition, 2002.

[96] Kui Huang, Bruce P. Lee, Dale R. Ingram, and Phillip B. Messersmith. Synthesis and Characterization of Self-Assembling Block Copolymers Containing Bioadhesive End Groups. *Biomacromolecules*, 3(2):397–406, March 2002.

[97] Bruce P. Lee, Kui Huang, F. Nelson Nunalee, Kenneth R. Shull, and Phillip B. Messersmith. Synthesis of 3,4-dihydroxyphenylalanine (DOPA) containing monomers and their co-polymerization with PEG-diacrylate to form hydrogels. *Journal of Biomaterials Science, Polymer Edition*, 15(4):449–464, January 2004.

[98] N. Holten-Andersen, M. J. Harrington, H. Birkedal, B. P. Lee, P. B. Messersmith, K. Y. C. Lee, and J. H. Waite. pH-induced metal-ligand cross-links inspired by mussel yield self-healing polymer networks with near-covalent elastic moduli. *Proceedings of the National Academy of Sciences*, 108(7):2651–2655, 2011.

[99] Zahid Shafiq, Jiaxi Cui, Lourdes Pastor-Pérez, Verónica San Miguel, Radu A. Gropeanu, Cristina Serrano, and Aránzazu del Campo. Bioinspired Underwater Bonding and Debonding on Demand. *Angewandte Chemie International Edition*, 51(18):4332–4335, 2012.

[100] Matthew S. Menyo, Craig J. Hawker, and J. Herbert Waite. Versatile tuning of supramolecular hydrogels through metal complexation of oxidation-resistant catechol-inspired ligands. *Soft Matter*, 9(43):10314–10323, October 2013.

[101] Niels Holten-Andersen, Aditya Jaishankar, Matthew J. Harrington, Dominic E. Fullenkamp, Genevieve DiMarco, Lihong He, Gareth H. McKinley, Phillip B. Messersmith, and Ka Yee C. Lee. Metal-coordination: Using one of nature's tricks to control soft material mechanics. *Journal of Materials Chemistry B*, 2(17):2467–2467, 2014.

[102] Scott C Grindy, Martin Lenz, and Niels Holten-Andersen. Engineering Elasticity and Relaxation Time in Metal-Coordinate Cross-Linked Hydrogels. *Macromolecules*, 49:8306–8312, 2016.

[103] Tobias Priemel, Elena Degtyar, Mason N Dean, and Matthew J Harrington. Rapid self-assembly of complex biomolecular architectures during mussel byssus biofabrication. *Nature Communications*, 8:14539–14539, 2017.

[104] Antje Reinecke, Luca Bertinetti, Peter Fratzl, and Matthew J. Harrington. Cooperative behavior of a sacrificial bond network and elastic framework in providing self-healing capacity in mussel byssal threads. *Journal of Structural Biology*, 196(3):329–339, December 2016.

[105] Matthew J. Harrington, Franziska Jehle, and Tobias Priemel. Mussel Byssus Structure-Function and Fabrication as Inspiration for Biotechnological Production of Advanced Materials. *Biotechnology Journal*, 13(12):1800133, 2018.

[106] Franziska Jehle, Elena Macías-Sánchez, Sanja Sviben, Peter Fratzl, Luca Bertinetti, and Matthew J. Harrington. Hierarchically-structured metalloprotein composite coatings biofabricated from co-existing condensed liquid phases. *Nature Communications*, 11(1), December 2020.

[107] Matthew J Harrington, Admir Masic, and Niels Holten-andersen. Iron-Clad Fibers : A Metal-Based. *Science*, 328(April):216–220, 2010.

[108] Niels Holten-Andersen, Hua Zhao, and J Herbert Waite. Stiff Coatings on Compliant Biofibers: The Cuticle of Mytilus californianus Byssal Threads. *Biochemistry*, 48:2752–2759, 2009.

[109] Esther Amstad and Matthew J. Harrington. From vesicles to materials: Bioinspired strategies for fabricating hierarchically structured soft matter. *Philosophical Transactions of the Royal Society A: Mathematical, Physical and Engineering Sciences*, 379(2206):20200338, September 2021.

[110] Franziska Jehle, Peter Fratzl, and Matthew J. Harrington. Metal-Tunable Self-Assembly of Hierarchical Structure in Mussel-Inspired Peptide Films. *ACS Nano*, 12(3):2160–2168, March 2018.

[111] Florence G. Downs, David J. Lunn, Michael J. Booth, Joshua B. Sauer, William J. Ramsay, R. George Klemperer, Craig J. Hawker, and Hagan Bayley. Multi-responsive hydrogel structures from patterned droplet networks. *Nature Chemistry*, 12(4):363–371, April 2020.

[112] Eesha Khare, Niels Holten-Andersen, and Markus J. Buehler. Transition-metal coordinate bonds for bioinspired macromolecules with tunable mechanical properties. *Nature Reviews Materials*, pages 1–16, February 2021.

[113] Martin K. Beyer. The mechanical strength of a covalent bond calculated by density functional theory. *The Journal of Chemical Physics*, 112(17):7307–7312, May 2000.

[114] Faheem Ullah, Muhammad Bisyrul Hafi Othman, Fatima Javed, Zulkifli Ahmad, and Hazizan Md. Akil. Classification, processing and application of hydrogels: A review. *Materials Science and Engineering: C*, 57:414–433, December 2015.

[115] Alexander Jans, Jonas Lölsberg, Abdolrahman Omidinia-Anarkoli, Robin Viermann, Martin Möller, Laura De Laporte, Matthias Wessling, and Alexander J. C. Kuehne. High-Throughput Production of Micrometer Sized Double Emulsions and Microgel Capsules in Parallelized 3D Printed Microfluidic Devices. *Polymers*, 11(11):1887, November 2019.

[116] Narendra Reddy, Roopa Reddy, and Qiuran Jiang. Crosslinking biopolymers for biomedical applications. *Trends in Biotechnology*, 33(6):362–369, June 2015.

[117] Janarthanan Gopinathan and Insup Noh. Click Chemistry-Based Injectable Hydrogels and Bioprinting Inks for Tissue Engineering Applications. *Tissue Engineering and Regenerative Medicine*, 15(5):531–546, August 2018.

[118] Anne Duconseille, Thierry Astruc, Naira Quintana, Filip Meersman, and Véronique Sante-Lhoutellier. Gelatin structure and composition linked to hard capsule dissolution: A review. *Food Hydrocolloids*, 43:360–376, January 2015.

[119] K. P. Pratt, H. C. F. Cote, D. W. Chung, R. E. Stenkamp, and E. W. Davie. The primary fibrin polymerization pocket: Three-dimensional structure of a 30-kDa C-terminal chain fragment complexed with the peptide Gly-Pro-Arg-Pro. *Proceedings of the National Academy of Sciences*, 94(14):7176–7181, July 1997.

[120] Shauna R. Stauffer and Nikolaos A. Peppast. Poly(vinyl alcohol) hydrogels prepared by freezing-thawing cyclic processing. *Polymer*, 33(18):3932–3936, September 1992.

[121] Guangzhao Zhang, Yunhua Chen, Yonghong Deng, To Ngai, and Chaoyang Wang. Dynamic Supramolecular Hydrogels: Regulating Hydrogel Properties through Self-Complementary Quadruple Hydrogen Bonds and Thermo-Switch. *ACS Macro Letters*, 6(7):641–646, July 2017.

[122] Lenny Voorhaar and Richard Hoogenboom. Supramolecular polymer networks: Hydrogels and bulk materials. *Chemical Society Reviews*, 45(14):4013–4031, July 2016.

[123] Akira Harada, Yoshinori Takashima, and Masaki Nakahata. Supramolecular Polymeric Materials via Cyclodextrin–Guest Interactions. *Accounts of Chemical Research*, 47(7):2128–2140, July 2014.

[124] Eric A. Appel, Jesús del Barrio, Xian Jun Loh, and Oren A. Scherman. Supramolecular polymeric hydrogels. *Chemical Society Reviews*, 41(18):6195–6214, August 2012.

[125] Yoshinori Takashima, Yuki Sawa, Kazuhisa Iwaso, Masaki Nakahata, Hiroyasu Yamaguchi, and Akira Harada. Supramolecular Materials Cross-Linked by Host–Guest

Inclusion Complexes: The Effect of Side Chain Molecules on Mechanical Properties. *Macromolecules*, 50(8):3254–3261, April 2017.

[126] Steven E. Wheeler. Understanding Substituent Effects in Noncovalent Interactions Involving Aromatic Rings. *Accounts of Chemical Research*, 46(4):1029–1038, April 2013.

[127] Fang Li, Yingchun Zhu, Bo You, Donghui Zhao, Qichao Ruan, Yi Zeng, and Chuanxian Ding. Smart Hydrogels Co-switched by Hydrogen Bonds and π–π Stacking for Continuously Regulated Controlled-Release System. *Advanced Functional Materials*, 20(4):669–676, 2010.

[128] Wan-Ru Zhuang, Yi Wang, Peng-Fei Cui, Lei Xing, Jaiwoo Lee, Dongyoon Kim, Hu-Lin Jiang, and Yu-Kyoung Oh. Applications of π-π stacking interactions in the design of drug-delivery systems. *Journal of Controlled Release*, 294:311–326, January 2019.

[129] Kuen Yong Lee and David J. Mooney. Hydrogels for Tissue Engineering. *Chemical Reviews*, 101(7):1869–1880, July 2001.

[130] Kuen Yong Lee and David J. Mooney. Alginate: Properties and biomedical applications. *Progress in Polymer Science*, 37(1):106–126, January 2012.

[131] Feng Luo, Tao Lin Sun, Tasuku Nakajima, Takayuki Kurokawa, Yu Zhao, Koshiro Sato, Abu Bin Ihsan, Xufeng Li, Honglei Guo, and Jian Ping Gong. Oppositely Charged Polyelectrolytes Form Tough, Self-Healing, and Rebuildable Hydrogels. *Advanced Materials*, 27(17):2722–2727, 2015.

[132] Feng Luo, Tao Lin Sun, Tasuku Nakajima, Daniel R. King, Takayuki Kurokawa, Yu Zhao, Abu Bin Ihsan, Xufeng Li, Honglei Guo, and Jian Ping Gong. Strong and Tough Polyion-Complex Hydrogels from Oppositely Charged Polyelectrolytes: A Comparative Study with Polyampholyte Hydrogels. *Macromolecules*, 49(7):2750–2760, April 2016.

[133] Chris C. Broomell, Mike A. Mattoni, Frank W. Zok, and J. Herbert Waite. Critical role of zinc in hardening of Nereis jaws. *Journal of Experimental Biology*, 209(16):3219–3225, August 2006.

[134] Helga C. Lichtenegger, Thomas Schöberl, Michael H. Bartl, Herbert Waite, and Galen D. Stucky. High Abrasion Resistance with Sparse Mineralization: Copper Biomineral in Worm Jaws. *Science*, 298(5592):389–392, October 2002.

[135] H. C. Lichtenegger, T. Schoberl, J. T. Ruokolainen, J. O. Cross, S. M. Heald, H. Birkedal, J. H. Waite, and G. D. Stucky. Zinc and mechanical prowess in the jaws of Nereis, a marine worm. *Proceedings of the National Academy of Sciences*, 100(16):9144–9149, August 2003.

[136] C. C. Broomell, F. W. Zok, and J. H. Waite. Role of transition metals in sclerotization of biological tissue. *Acta Biomaterialia*, 4(6):2045–2051, November 2008.

[137] R. M. S Schofield, M. H Nesson, K. A Richardson, and P Wyeth. Zinc is incorporated into cuticular "tools" after ecdysis: The time course of the zinc distribution in "tools" and whole bodies of an ant and a scorpion. *Journal of Insect Physiology*, 49(1):31–44, January 2003.

[138] Marie Krogsgaard, Manja A. Behrens, Jan Skov Pedersen, and Henrik Birkedal. Self-Healing Mussel-Inspired Multi-pH-Responsive Hydrogels. *Biomacromolecules*, 14(2):297–301, February 2013.

[139] Jeongwook Lee, Kyeol Chang, Sunhye Kim, Vikas Gite, Hoeil Chung, and Daewon Sohn. Phase Controllable Hyaluronic Acid Hydrogel with Iron III Ion Catechol Induced Dual Cross Linking by Utilizing the Gap of Gelation Kinetics. *Macromolecules*, 49:7450–7459, 2016.

[140] M. Reza Nejadnik, Xia Yang, Matilde Bongio, Hamdan S. Alghamdi, Jeroen J. J. P. van den Beucken, Marie C. Huysmans, John A. Jansen, Jöns Hilborn, Dmitri Ossipov, and Sander C. G. Leeuwenburgh. Self-healing hybrid nanocomposites consisting of bisphosphonated hyaluronan and calcium phosphate nanoparticles. *Biomaterials*, 35(25):6918–6929, August 2014.

[141] Haili Qin, Tan Zhang, He-Nan Li, Huai-Ping Cong, Markus Antonietti, and Shu-Hong Yu. Dynamic Au-Thiolate Interaction Induced Rapid Self-Healing Nanocomposite Hydrogels with Remarkable Mechanical Behaviors. *Chem*, 3(4):691–705, October 2017.

[142] Si Yu Zheng, Hongyao Ding, Jin Qian, Jun Yin, Zi Liang Wu, Yihu Song, and Qiang Zheng. Metal-Coordination Complexes Mediated Physical Hydrogels with High Toughness, Stick–Slip Tearing Behavior, and Good Processability. *Macromolecules*, 49(24):9637–9646, December 2016.

[143] Sytze J. Buwalda, Pieter J. Dijkstra, and Jan Feijen. Poly(ethylene glycol)–poly(L-lactide) star block copolymer hydrogels crosslinked by metal–ligand coordination. *Journal of Polymer Science Part A: Polymer Chemistry*, 50(9):1783–1791, 2012.

[144] Yoshiki Chujo, Kazuki Sada, and Takeo Saegusa. Iron(II) bipyridyl-branched poly-oxazoline complex as a thermally reversible hydrogel. *Macromolecules*, 26(24):6315–6319, November 1993.

[145] Matthew S. Menyo, Craig J. Hawker, and J. Herbert Waite. Rate-Dependent Stiffness and Recovery in Interpenetrating Network Hydrogels through Sacrificial Metal Coordination Bonds. *ACS Macro Letters*, 4(11):1200–1204, November 2015.

[146] Gengsheng Weng, Srinivas Thanneeru, and Jie He. Dynamic Coordination of Eu–Iminodiacetate to Control Fluorochromic Response of Polymer Hydrogels to Multistimuli. *Advanced Materials*, 30(11):1706526, 2018.

[147] Mathew Patenaude, Niels M. B. Smeets, and Todd Hoare. Designing Injectable, Covalently Cross-Linked Hydrogels for Biomedical Applications. *Macromolecular Rapid Communications*, 35(6):598–617, 2014.

[148] Sepehr Talebian, Mehdi Mehrali, Nayere Taebnia, Cristian Pablo Pennisi, Firoz Babu Kadumudi, Javad Foroughi, Masoud Hasany, Mehdi Nikkhah, Mohsen Akbari, Gorka Orive, and Alireza Dolatshahi-Pirouz. Self-Healing Hydrogels: The Next Paradigm Shift in Tissue Engineering? *Advanced Science*, 6(16):1801664, 2019.

[149] Yi Liu and Shan-hui Hsu. Synthesis and Biomedical Applications of Self-healing Hydrogels. *Frontiers in Chemistry*, 6:449, 2018.

[150] Jing Ye, Shuwen Fu, Shiya Zhou, Mohan Li, Kaiyu Li, Wei Sun, and Yinglei Zhai. Advances in hydrogels based on dynamic covalent bonding and prospects for its biomedical application. *European Polymer Journal*, 139:110024, October 2020.

[151] Fuyuan Ding, Shuping Wu, Shishuai Wang, Yuan Xiong, Yan Li, Bin Li, Hongbing Deng, Yumin Du, Ling Xiao, and Xiaowen Shi. A dynamic and self-crosslinked polysaccharide hydrogel with autonomous self-healing ability. *Soft Matter*, 11(20):3971–3976, May 2015.

[152] Natalie Boehnke, Cynthia Cam, Erhan Bat, Tatiana Segura, and Heather D. Maynard. Imine Hydrogels with Tunable Degradability for Tissue Engineering. *Biomacromolecules*, 16(7):2101–2108, July 2015.

[153] Ying Guan and Yongjun Zhang. Boronic acid-containing hydrogels: Synthesis and their applications. *Chemical Society Reviews*, 42(20):8106–8121, September 2013.

[154] Susanne Kirchhof, Ferdinand P. Brandl, Nadine Hammer, and Achim M. Goepferich. Investigation of the Diels–Alder reaction as a cross-linking mechanism for degradable poly(ethylene glycol) based hydrogels. *Journal of Materials Chemistry B*, 1(37):4855–4864, August 2013.

[155] Changyou Shao, Meng Wang, Huanliang Chang, Feng Xu, and Jun Yang. A Self-Healing Cellulose Nanocrystal-Poly(ethylene glycol) Nanocomposite Hydrogel via Diels–Alder Click Reaction. *ACS Sustainable Chemistry & Engineering*, 5(7):6167–6174, July 2017.

[156] Chelsea M. Nimmo, Shawn C. Owen, and Molly S. Shoichet. Diels-Alder Click Cross-Linked Hyaluronic Acid Hydrogels for Tissue Engineering. *Biomacromolecules*, 12(3):824–830, March 2011.

[157] Xiao Zheng Shu, Yanchun Liu, Yi Luo, Meredith C. Roberts, and Glenn D. Prestwich. Disulfide Cross-Linked Hyaluronan Hydrogels. *Biomacromolecules*, 3(6):1304–1311, November 2002.

[158] Haeshin Lee and Tae Gwan Park. Reduction/Oxidation Induced Cleavable/Crosslinkable Temperature-Sensitive Hydrogel Network Containing Disulfide Linkages. *Polymer Journal*, 30(12):976–980, December 1998.

[159] Yu Zhang, Philipp Heher, Jöns Hilborn, Heinz Redl, and Dmitri A. Ossipov. Hyaluronic acid-fibrin interpenetrating double network hydrogel prepared in situ by orthogonal disulfide cross-linking reaction for biomedical applications. *Acta Biomaterialia*, 38:23–32, July 2016.

[160] Joel Madrazo, Jerry H. Brown, Sergei Litvinovich, Roberto Dominguez, Sergei Yakovlev, Leonid Medved, and Carolyn Cohen. Crystal structure of the central region of bovine fibrinogen (E5 fragment) at 1.4-Å resolution. *Proceedings of the National Academy of Sciences*, 98(21):11967–11972, October 2001.

[161] D T Cheung, P DiCesare, P D Benya, E Libaw, and M E Nimni. The presence of intermolecular disulfide cross-links in type III collagen. *Journal of Biological Chemistry*, 258(12):7774–7778, June 1983.

[162] Sun-Young Choh, Daisy Cross, and Chun Wang. Facile Synthesis and Characterization of Disulfide-Cross-Linked Hyaluronic Acid Hydrogels for Protein Delivery and Cell Encapsulation. *Biomacromolecules*, 12(4):1126–1136, April 2011.

[163] Hang Yang, Chenghai Li, Jingda Tang, and Zhigang Suo. Strong and Degradable Adhesion of Hydrogels. *ACS Applied Bio Materials*, 2(5):1781–1786, May 2019.

[164] John A. Burns, James C. Butler, John Moran, and George M. Whitesides. Selective reduction of disulfides by tris(2-carboxyethyl)phosphine. *The Journal of Organic Chemistry*, 56(8):2648–2650, April 1991.

[165] William Konigsberg. [13] Reduction of disulfide bonds in proteins with dithiothreitol. In *Methods in Enzymology*, volume 25 of *Enzyme Structure, Part B*, pages 185–188. Academic Press, January 1972.

[166] Zhou Qiao Lei, Hong Ping Xiang, Yong Jian Yuan, Min Zhi Rong, and Ming Qiu Zhang. Room-Temperature Self-Healable and Remoldable Cross-linked Polymer Based on the Dynamic Exchange of Disulfide Bonds. *Chemistry of Materials*, 26(6):2038–2046, March 2014.

[167] Tetsuo Yamaguchi, Yudai Onoue, and Yoshinori Sawae. Topology and Toughening of Sparse Elastic Networks. *Physical Review Letters*, 124(6):068002, February 2020.

[168] Etienne Ducrot and Costantino Creton. Characterizing Large Strain Elasticity of Brittle Elastomeric Networks by Embedding Them in a Soft Extensible Matrix. *Advanced Functional Materials*, 26(15):2482–2492, 2016.

[169] Rebecca E. Webber, Costantino Creton, Hugh R. Brown, and Jian Ping Gong. Large Strain Hysteresis and Mullins Effect of Tough Double-Network Hydrogels. *Macromolecules*, 40(8):2919–2927, April 2007.

[170] Taiki Tominaga, Vijay R. Tirumala, Eric K. Lin, Jian Ping Gong, Hidemitsu Furukawa, Yoshihito Osada, and Wen-li Wu. The molecular origin of enhanced toughness in double-network hydrogels: A neutron scattering study. *Polymer*, 48(26):7449–7454, December 2007.

[171] Qiaochu Li, Devin G Barrett, Phillip B Messersmith, and Niels Holten-Andersen. Controlling Hydrogel Mechanics via Bio-Inspired Polymer–Nanoparticle Bond Dynamics. *ACS Nano*, 10(1):1317–1324, 2016.

[172] Sungjin Kim, Abigail U. Regitsky, Jake Song, Jan Ilavsky, Gareth H. McKinley, and Niels Holten-Andersen. In situ mechanical reinforcement of polymer hydrogels via metal-coordinated crosslink mineralization. *Nature Communications*, 12(1):667, January 2021.

[173] Riku Takahashi, Kouichi Shimano, Haruka Okazaki, Takayuki Kurokawa, Tasuku Nakajima, Takayuki Nonoyama, Daniel R. King, and Jian Ping Gong. Tough Particle-Based Double Network Hydrogels for Functional Solid Surface Coatings. *Advanced Materials Interfaces*, 5(23):1801018, 2018.

[174] Nicole J. Darling, Elias Sideris, Naomi Hamada, S. Thomas Carmichael, and Tatiana Segura. Injectable and Spatially Patterned Microporous Annealed Particle (MAP) Hydrogels for Tissue Repair Applications. *Advanced Science*, 5(11):1801046, 2018.

[175] Minna H. Chen, Jennifer J. Chung, Joshua E. Mealy, Samir Zaman, Elizabeth C. Li, Maria F. Arisi, Pavan Atluri, and Jason A. Burdick. Injectable Supramolecular Hydrogel/Microgel Composites for Therapeutic Delivery. *Macromolecular Bioscience*, 19(1):1800248, 2019.

[176] Mikyung Shin, Kwang Hoon Song, Justin C. Burrell, D. Kacy Cullen, and Jason A. Burdick. Injectable and Conductive Granular Hydrogels for 3D Printing and Electroactive Tissue Support. *Advanced Science*, 6(20):1901229, 2019.

[177] Christopher B. Highley, Kwang Hoon Song, Andrew C. Daly, and Jason A. Burdick. Jammed Microgel Inks for 3D Printing Applications. *Advanced Science*, 6(1):1801076, January 2019.

[178] O. Jeon, Y. B. Lee, T. J. Hinton, A. W. Feinberg, and E. Alsberg. Cryopreserved cell-laden alginate microgel bioink for 3D bioprinting of living tissues. *Materials Today Chemistry*, 12:61–70, June 2019.

[179] Andrew C. Daly, Lindsay Riley, Tatiana Segura, and Jason A. Burdick. Hydrogel microparticles for biomedical applications. *Nature Reviews Materials*, November 2019.

[180] Andrea J. Liu and Sidney R. Nagel. Jamming is not just cool any more. *Nature*, 396(6706):21–22, November 1998.

[181] Paul Menut, Sebastian Seiffert, Joris Sprakel, and David A. Weitz. Does size matter? elasticity of compressed suspensions of colloidal- and granular-scale microgels. *Soft Matter*, 8(1):156–164, December 2011.

[182] D. J. Hornbaker, R. Albert, I. Albert, A.-L. Barabási, and P. Schiffer. What keeps sandcastles standing? *Nature*, 387(6635):765–765, June 1997.

[183] Thomas J. Hinton, Quentin Jallerat, Rachelle N. Palchesko, Joon Hyung Park, Martin S. Grodzicki, Hao-Jan Shue, Mohamed H. Ramadan, Andrew R. Hudson, and Adam W. Feinberg. Three-dimensional printing of complex biological structures by freeform reversible embedding of suspended hydrogels. *Science Advances*, 1(9):e1500758, October 2015.

[184] Jason W. Nichol, Sandeep T. Koshy, Hojae Bae, Chang M. Hwang, Seda Yamanlar, and Ali Khademhosseini. Cell-laden microengineered gelatin methacrylate hydrogels. *Biomaterials*, 31(21):5536–5544, July 2010.

[185] T. Y. Lee, C. A. Guymon, E. Sonny Jönsson, and C. E. Hoyle. The effect of monomer structure on oxygen inhibition of (meth)acrylates photopolymerization. *Polymer*, 45(18):6155–6162, August 2004.

[186] Ru-Siou Hsu, Pei-Yueh Chen, Jen-Hung Fang, You-Yin Chen, Chien-Wen Chang, Yu-Jen Lu, and Shang-Hsiu Hu. Adaptable Microporous Hydrogels of Propagating NGF-Gradient by Injectable Building Blocks for Accelerated Axonal Outgrowth. *Advanced Science*, 6(16):1900520, 2019.

[187] Amir Sheikhi, Joseph de Rutte, Reihaneh Haghniaz, Outman Akouissi, Alireza Sohrabi, Dino Di Carlo, and Ali Khademhosseini. Microfluidic-enabled bottom-up hydrogels from annealable naturally-derived protein microbeads. *Biomaterials*, 192:560–568, February 2019.

[188] Blaise N. Pfaff, Lauren J. Pruett, Nicholas J. Cornell, Joseph de Rutte, Dino Di Carlo, Christopher B. Highley, and Donald R. Griffin. Selective and Improved Photoannealing of Microporous Annealed Particle (MAP) Scaffolds. *ACS Biomaterials Science & Engineering*, January 2021.

[189] Elias Sideris, Donald R. Griffin, Yichen Ding, Shuoran Li, Westbrook M. Weaver, Dino Di Carlo, Tzung Hsiai, and Tatiana Segura. Particle Hydrogels Based on Hyaluronic Acid Building Blocks. *ACS Biomaterials Science & Engineering*, 2(11):2034–2041, November 2016.

[190] Nicole Zoratto, Donatella Di Lisa, Joseph de Rutte, Md Nurus Sakib, Angelo Roncalli Alves e Silva, Ali Tamayol, Dino Di Carlo, Ali Khademhosseini, and Amir Sheikhi. In situ forming microporous gelatin methacryloyl hydrogel scaffolds from thermostable microgels for tissue engineering. *Bioengineering & Translational Medicine*, 5(3):e10180, 2020.

[191] Mounika Choppadandi, Namdev More, and Govinda Kapusetti. Detoxification of poly(methyl methacrylate) bone cement by natural antioxidant intervention. *Journal of Biomedical Materials Research Part A*, 107(12):2835–2847, 2019.

[192] Nicholas A. Kurniawan, Thomas H. S. van Kempen, Stijn Sonneveld, Tilaï T. Rosalina, Bart E. Vos, Karin A. Jansen, Gerrit W. M. Peters, Frans N. van de Vosse,

and Gijsje H. Koenderink. Buffers Strongly Modulate Fibrin Self-Assembly into Fibrous Networks. *Langmuir*, 33(25):6342–6352, June 2017.

[193] Lina R. Nih, Elias Sideris, S. Thomas Carmichael, and Tatiana Segura. Injection of Microporous Annealing Particle (MAP) Hydrogels in the Stroke Cavity Reduces Gliosis and Inflammation and Promotes NPC Migration to the Lesion. *Advanced Materials*, 29(32):1606471, 2017.

[194] Donald R. Griffin, Westbrook M. Weaver, Philip O. Scumpia, Dino Di Carlo, and Tatiana Segura. Accelerated wound healing by injectable microporous gel scaffolds assembled from annealed building blocks. *Nature Materials*, 14(7):737–744, July 2015.

[195] Jaekyung Koh, Donald R. Griffin, Maani M. Archang, An-Chieh Feng, Thomas Horn, Michael Margolis, David Zalazar, Tatiana Segura, Philip O. Scumpia, and Dino Di Carlo. Enhanced In Vivo Delivery of Stem Cells using Microporous Annealed Particle Scaffolds. *Small*, 15(39):1903147, 2019.

[196] Joseph Michael de Rutte, Jaekyung Koh, and Dino Di Carlo. Scalable High-Throughput Production of Modular Microgels for In Situ Assembly of Microporous Tissue Scaffolds. *Advanced Functional Materials*, 29(25):1900071, 2019.

[197] Donald R. Griffin, Maani M. Archang, Chen-Hsiang Kuan, Westbrook M. Weaver, Jason S. Weinstein, An Chieh Feng, Amber Ruccia, Elias Sideris, Vasileios Ragkousis, Jaekyung Koh, Maksim V. Plikus, Dino Di Carlo, Tatiana Segura, and Philip O. Scumpia. Activating an adaptive immune response from a hydrogel scaffold imparts regenerative wound healing. *Nature Materials*, pages 1–10, November 2020.

[198] Lauren Pruett, Heather Koehn, Teresa Martz, Ian Churnin, Sergio Ferrante, Lisa Salopek, Patrick Cottler, Donald R. Griffin, and James J. Daniero. Development of a microporous annealed particle hydrogel for long-term vocal fold augmentation. *The Laryngoscope*, 130(10):2432–2441, 2020.

[199] Norman F. Truong, Sasha Cai Lesher-Pérez, Evan Kurt, and Tatiana Segura. Pathways Governing Polyethylenimine Polyplex Transfection in Microporous Annealed Particle Scaffolds. *Bioconjugate Chemistry*, 30(2):476–486, February 2019.

[200] Norman F. Truong, Evan Kurt, Nairi Tahmizyan, Sasha Cai Lesher-Pérez, Mabel Chen, Nicole J. Darling, Weixian Xi, and Tatiana Segura. Microporous annealed

particle hydrogel stiffness, void space size, and adhesion properties impact cell proliferation, cell spreading, and gene transfer. *Acta Biomaterialia*, 94:160–172, August 2019.

[201] Nicole J. Darling, Weixian Xi, Elias Sideris, Alexa R. Anderson, Cassie Pong, S. Thomas Carmichael, and Tatiana Segura. Click by Click Microporous Annealed Particle (MAP) Scaffolds. *Advanced Healthcare Materials*, 9(10):1901391, 2020.

[202] Shangjing Xin, Omar M. Wyman, and Daniel L. Alge. Assembly of PEG Microgels into Porous Cell-Instructive 3D Scaffolds via Thiol-Ene Click Chemistry. *Advanced Healthcare Materials*, 7(11):1800160, 2018.

[203] Shangjing Xin, David Chimene, Jay E. Garza, Akhilesh K. Gaharwar, and Daniel L. Alge. Clickable PEG hydrogel microspheres as building blocks for 3D bioprinting. *Biomaterials Science*, 7(3):1179–1187, 2019.

[204] Fanyi Li, Vinh X. Truong, Philipp Fisch, Clara Levinson, Veronica Glattauer, Marcy Zenobi-Wong, Helmut Thissen, John S. Forsythe, and Jessica E. Frith. Cartilage tissue formation through assembly of microgels containing mesenchymal stem cells. *Acta Biomaterialia*, 77:48–62, September 2018.

[205] Kaidong Song, Ashley M. Compaan, Wenxuan Chai, and Yong Huang. Injectable Gelatin Microgel-Based Composite Ink for 3D Bioprinting in Air. *ACS Applied Materials & Interfaces*, 12(20):22453–22466, May 2020.

[206] David B. Gehlen, Niklas Jürgens, Abdolrahman Omidinia-Anarkoli, Tamás Haraszti, Julian George, Andreas Walther, Hua Ye, and Laura De Laporte. Granular Cellulose Nanofibril Hydrogel Scaffolds for 3D Cell Cultivation. *Macromolecular Rapid Communications*, 41(18):2000191, 2020.

[207] Matteo Hirsch, Alvaro Charlet, and Esther Amstad. 3D Printing of Strong and Tough Double Network Granular Hydrogels. *Advanced Functional Materials*, 31(5):2005929, January 2021.

[208] Hartmuth C. Kolb, M. G. Finn, and K. Barry Sharpless. Click Chemistry: Diverse Chemical Function from a Few Good Reactions. *Angewandte Chemie International Edition*, 40(11):2004–2021, 2001.

[209] Faraz Jivan, Ramanathan Yegappan, Hannah Pearce, James K. Carrow, Michael McShane, Akhilesh K. Gaharwar, and Daniel L. Alge. Sequential Thiol–Ene and Tetrazine Click Reactions for the Polymerization and Functionalization of Hydrogel Microparticles. *Biomacromolecules*, 17(11):3516–3523, November 2016.

[210] Tobin E. Brown and Kristi S. Anseth. Spatiotemporal hydrogel biomaterials for regenerative medicine. *Chemical Society Reviews*, 46(21):6532–6552, 2017.

[211] M. P. Lutolf, N. Tirelli, S. Cerritelli, L. Cavalli, and J. A. Hubbell. Systematic Modulation of Michael-Type Reactivity of Thiols through the Use of Charged Amino Acids. *Bioconjugate Chemistry*, 12(6):1051–1056, November 2001.

[212] M. P. Lutolf and J. A. Hubbell. Synthesis and Physicochemical Characterization of End-Linked Poly(ethylene glycol)- *co* -peptide Hydrogels Formed by Michael-Type Addition. *Biomacromolecules*, 4(3):713–722, May 2003.

[213] Devatha P. Nair, Maciej Podgórski, Shunsuke Chatani, Tao Gong, Weixian Xi, Christopher R. Fenoli, and Christopher N. Bowman. The Thiol-Michael Addition Click Reaction: A Powerful and Widely Used Tool in Materials Chemistry. *Chemistry of Materials*, 26(1):724–744, January 2014.

[214] Ricardo Cruz-Acuña, Miguel Quirós, Attila E. Farkas, Priya H. Dedhia, Sha Huang, Dorothée Siuda, Vicky García-Hernández, Alyssa J. Miller, Jason R. Spence, Asma Nusrat, and Andrés J. García. Synthetic hydrogels for human intestinal organoid generation and colonic wound repair. *Nature Cell Biology*, 19(11):1326–1335, November 2017.

[215] Edward A. Phelps, Nduka O. Enemchukwu, Vincent F. Fiore, Jay C. Sy, Niren Murthy, Todd A. Sulchek, Thomas H. Barker, and Andrés J. García. Maleimide cross-linked bioactive PEG hydrogel exhibits improved reaction kinetics and cross-linking for cell encapsulation and in situ delivery. *Advanced Materials (Deerfield Beach, Fla.)*, 24(1):64–70, 2, January 2012.

[216] Lauren Pruett, Christian Jenkins, Neharika Singh, Katarina Catallo, and Donald Griffin. Heparin MicroIslands to Promote Enhanced Diabetic Wound Healing Outcomes. *bioRxiv*, page 2020.10.31.363531, November 2020.

[217] Alexander S. Caldwell, Gavin T. Campbell, Kelly M. T. Shekiro, and Kristi S. Anseth. Clickable Microgel Scaffolds as Platforms for 3D Cell Encapsulation. *Advanced Healthcare Materials*, 6(15):1700254, 2017.

[218] Rienk Eelkema and Andrij Pich. Pros and Cons: Supramolecular or Macromolecular: What Is Best for Functional Hydrogels with Advanced Properties? *Advanced Materials*, n/a(n/a):1906012, 2020.

[219] Nicolas Rauner, Monika Meuris, Mirjana Zoric, and Joerg C Tiller. Enzymatic mineralization generates ultrastiff and tough hydrogels with tunable mechanics. 2017.

[220] Haeshin Lee, Norbert F. Scherer, and Phillip B. Messersmith. Single-molecule mechanics of mussel adhesion. *Proceedings of the National Academy of Sciences*, 103(35):12999–13003, August 2006.

[221] Jian Hu, Kenta Hiwatashi, Takayuki Kurokawa, Song Miao Liang, Zi Liang Wu, and Jian Ping Gong. Microgel-Reinforced Hydrogel Films with High Mechanical Strength and Their Visible Mesoscale Fracture Structure. *Macromolecules*, 44(19):7775–7781, October 2011.

[222] Pier Lucio Anelli, Carlo Biffi, Fernando Montanari, and Silvio Quici. General Oxygenation Procedure. An apparently hetero-Fast and Selective Oxidation of Primary Alcohols to Aldehydes or to Carboxylic Acids and of Secondary Alcohols to Ketones Mediated by Oxoammonium Salts under Two-Phase Conditions. *J. Am. Chem. Soc*, 52(5):4492, 1987.

[223] Simon Mallam, Ferenc Horkay, Anne Marie Hecht, Adrian R. Rennie, and Erik Geissler. Microscopic and macroscopic thermodynamic observations in swollen poly(dimethylsiloxane) networks. *Macromolecules*, 24(2):543–548, January 1991.

[224] G. Evmenenko, E. Theunissen, K. Mortensen, and H. Reynaers. SANS study of surfactant ordering in κ-carrageenan/cetylpyridinium chloride complexes. *Polymer*, 42(7):2907–2913, March 2001.

[225] E A Sagitova, K A Prokhorov, G Yu Nikolaeva, A V Baimova, P P Pashinin, A Yu Yarysheva, and D I Mendeleev. Raman analysis of polyethylene glycols and polyethylene oxides. *Journal of Physics: Conference Series*, 999:012002, April 2018.

[226] Luis García-Fernández, Jiaxi Cui, Cristina Serrano, Zahid Shafiq, Radu A. Gropeanu, Verónica San Miguel, Jagoba Iturri Ramos, Miao Wang, Gunther K. Auernhammer, Sandra Ritz, Ali A. Golriz, Rüdiger Berger, Manfred Wagner, and Aránzazu del Campo. Antibacterial Strategies from the Sea: Polymer-Bound Cl-Catechols for Prevention of Biofilm Formation. *Advanced Materials*, 25(4):529–533, 2013.

[227] Marie Krogsgaard, Vicki Nue, and Henrik Birkedal. Mussel-Inspired Materials: Self-Healing through Coordination Chemistry. *Chemistry – A European Journal*, 22(3):844–857, 2016.

[228] Joseph P. Park, In Taek Song, Juwon Lee, Ji Hyun Ryu, Yunho Lee, and Haeshin Lee. Vanadyl–Catecholamine Hydrogels Inspired by Ascidians and Mussels. *Chemistry of Materials*, 27(1):105–111, January 2015.

[229] Dongyeop X. Oh, Sangsik Kim, Dohoon Lee, and Dong Soo Hwang. Tunicate-mimetic nanofibrous hydrogel adhesive with improved wet adhesion. *Acta Biomaterialia*, 20:104–112, July 2015.

[230] Zhongwei Guo, Shengli Mi, and Wei Sun. A Facile Strategy for Preparing Tough, Self-Healing Double-Network Hyaluronic Acid Hydrogels Inspired by Mussel Cuticles. *Macromolecular Materials and Engineering*, 304(4):1800715, 2019.

[231] Ji Hyun Ryu, Seonki Hong, and Haeshin Lee. Bio-inspired adhesive catechol-conjugated chitosan for biomedical applications: A mini review. *Acta Biomaterialia*, 27:101–115, November 2015.

[232] Marie Krogsgaard, Michael Ryan Hansen, and Henrik Birkedal. Metals & polymers in the mix: Fine-tuning the mechanical properties & color of self-healing mussel-inspired hydrogels. *Journal of Materials Chemistry B*, 2(47):8292–8297, November 2014.

[233] Prabhu S. Yavvari and Aasheesh Srivastava. Robust, self-healing hydrogels synthesised from catechol rich polymers. *Journal of Materials Chemistry B*, 3(5):899–910, January 2015.

[234] Matthew J. Harrington, Himadri S. Gupta, Peter Fratzl, and J. Herbert Waite. Collagen insulated from tensile damage by domains that unfold reversibly: In situ X-ray investigation of mechanical yield and damage repair in the mussel byssus. *Journal of Structural Biology*, 167(1):47–54, July 2009.

[235] Matthew J. Harrington and J. Herbert Waite. pH-Dependent Locking of Giant Mesogens in Fibers Drawn from Mussel Byssal Collagens. *Biomacromolecules*, 9(5):1480–1486, May 2008.

[236] Ellen Kime-Hunt, K. Spartalian, Stephen Holmes, Madan Mohan, and Carl J. Carrano. Vanadium metabolism in tunicates: The coordination chemistry of V(III), V(IV), and V(V) with models for the tunichromes. *Journal of Inorganic Biochemistry*, 41(2):125–141, February 1991.

[237] Steven W. Taylor, Mark M. Ross, and J. Herbert Waite. Novel 3,4-Di- and 3,4,5-Trihydroxyphenylalanine-Containing Polypeptides from the Blood Cells of the AscidiansAscidia ceratodesandMolgula manhattensis. *Archives of Biochemistry and Biophysics*, 324(2):228–240, December 1995.

[238] Steven W. Taylor, Bernd Kammerer, and Ernst Bayer. New Perspectives in the Chemistry and Biochemistry of the Tunichromes and Related Compounds. *Chemical Reviews*, 97(1):333–346, February 1997.

[239] A. Üçer, A. Uyanik, and Ş. F. Aygün. Adsorption of Cu(II), Cd(II), Zn(II), Mn(II) and Fe(III) ions by tannic acid immobilised activated carbon. *Separation and Purification Technology*, 47(3):113–118, January 2006.

[240] Hirotaka Ejima, Joseph J. Richardson, Kang Liang, James P. Best, Martin P. van Koeverden, Georgina K. Such, Jiwei Cui, and Frank Caruso. One-Step Assembly of Coordination Complexes for Versatile Film and Particle Engineering. *Science*, 341(6142):154–157, July 2013.

[241] Qi-Zhi Zhong, Shuaijun Pan, Md. Arifur Rahim, Gyeongwon Yun, Jianhua Li, Yi Ju, Zhixing Lin, Yiyuan Han, Yutian Ma, Joseph J. Richardson, and Frank Caruso. Spray Assembly of Metal–Phenolic Networks: Formation, Growth, and Applications. *ACS Applied Materials & Interfaces*, 10(39):33721–33729, October 2018.

[242] Hee Joong Kim, Dong-Gyun Kim, Hongsik Yoon, Yong-Seok Choi, Jeyong Yoon, and Jong-Chan Lee. Polyphenol/FeIII Complex Coated Membranes Having Multifunctional Properties Prepared by a One-Step Fast Assembly. *Advanced Materials Interfaces*, 2(14):1500298, 2015.

[243] Ann-Kathrin Koopmann, Christian Schuster, Jorge Torres-Rodríguez, Stefan Kain, Heidi Pertl-Obermeyer, Alexander Petutschnigg, and Nicola Hüsing. Tannin-Based Hybrid Materials and Their Applications: A Review. *Molecules*, 25(21):4910, January 2020.

[244] Md Arifur Rahim, Mattias Björnmalm, Tomoya Suma, Matthew Faria, Yi Ju, Kristian Kempe, Markus Müllner, Hirotaka Ejima, Anthony D. Stickland, and Frank Caruso. Metal–Phenolic Supramolecular Gelation. *Angewandte Chemie International Edition*, 55(44):13803–13807, 2016.

[245] M. Krogsgaard, A. Andersen, and H. Birkedal. Gels and threads: Mussel-inspired one-pot route to advanced responsive materials. *Chemical Communications*, 50(87):13278–13281, October 2014.

[246] Beom Jin Kim, Sol Han, Kyung-Bok Lee, and Insung S. Choi. Biphasic Supramolecular Self-Assembly of Ferric Ions and Tannic Acid across Interfaces for Nanofilm Formation. *Advanced Materials*, 29(28):1700784, July 2017.

[247] Jung Seung Lee, Jung Ho Cho, Soohwan An, Jisoo Shin, Soojeong Choi, Eun Je Jeon, and Seung-Woo Cho. In Situ Self-Cross-Linkable, Long-Term Stable Hyaluronic Acid Filler by Gallol Autoxidation for Tissue Augmentation and Wrinkle Correction. *Chemistry of Materials*, 31(23):9614–9624, December 2019.

[248] Seth Allen Cazzell and Niels Holten-Andersen. Expanding the stoichiometric window for metal cross-linked gel assembly using competition. *Proceedings of the National Academy of Sciences*, page 201906349, October 2019.

[249] Alvaro Charlet, Viviane Lutz, Raffaele Mezzenga, and Esther Amstad. Shape retaining self-healing metal-coordinated hydrogels. *Nanoscale*, January 2021.

[250] S. Palato, N. Metatla, and A. Soldera. Temperature behavior of the Kohlrausch exponent for a series of vinylic polymers modelled by an all-atomistic approach. *The European Physical Journal E*, 34(9):90, September 2011.

[251] Grzegorz Milczarek, Tomasz Rebis, and Justyna Fabianska. One-step synthesis of lignosulfonate-stabilized silver nanoparticles. *Colloids and Surfaces B: Biointerfaces*, 105:335–341, May 2013.

[252] Donglin Gan, Wensi Xing, Lili Jiang, Ju Fang, Cancan Zhao, Fuzeng Ren, Liming Fang, Kefeng Wang, and Xiong Lu. Plant-inspired adhesive and tough hydrogel based on Ag-Lignin nanoparticles-triggered dynamic redox catechol chemistry. *Nature Communications*, 10(1), December 2019.

[253] Emmanouela Filippidi, Thomas R. Cristiani, Claus D. Eisenbach, J. Herbert Waite, Jacob N. Israelachvili, B. Kollbe Ahn, and Megan T. Valentine. Toughening elastomers using mussel-inspired iron-catechol complexes. *Science*, 358(6362):502–505, 2017.

[254] Diederik W. R. Balkenende, Sally M. Winkler, and Phillip B. Messersmith. Marine-inspired polymers in medical adhesion. *European Polymer Journal*, 116:134–143, July 2019.

[255] Sang-Bae Lee, Carlos González-Cabezas, Kwang-Mahn Kim, Kyoung-Nam Kim, and Kenichi Kuroda. Catechol-Functionalized Synthetic Polymer as a Dental Adhesive to Contaminated Dentin Surface for a Composite Restoration. *Biomacromolecules*, 16(8):2265–2275, August 2015.

[256] Changyou Shao, Meng Wang, Lei Meng, Huanliang Chang, Bo Wang, Feng Xu, Jun Yang, and Pengbo Wan. Mussel-Inspired Cellulose Nanocomposite Tough Hydrogels

with Synergistic Self-Healing, Adhesive, and Strain-Sensitive Properties. *Chemistry of Materials*, 30(9):3110–3121, May 2018.

[257] Daiheon Lee, Honggu Hwang, Jun-Sung Kim, Jongmin Park, Donghwan Youn, Duhwan Kim, Jungseok Hahn, Myungeun Seo, and Haeshin Lee. VATA: Poly(vinyl alcohol)- and Tannic Acid-based Nontoxic Underwater Adhesive. *ACS Applied Materials & Interfaces*, March 2020.

[258] Dominic E. Fullenkamp, Lihong He, Devin G. Barrett, Wesley R. Burghardt, and Phillip B. Messersmith. Mussel-Inspired Histidine-Based Transient Network Metal Coordination Hydrogels. *Macromolecules*, 46(3):1167–1174, February 2013.

[259] Abu Bin Imran, Kenta Esaki, Hiroaki Gotoh, Takahiro Seki, Kohzo Ito, Yasuhiro Sakai, and Yukikazu Takeoka. Extremely stretchable thermosensitive hydrogels by introducing slide-ring polyrotaxane cross-linkers and ionic groups into the polymer network. *Nature Communications*, 5(1):5124, October 2014.

[260] Lu Han, Xiong Lu, Kezhi Liu, Kefeng Wang, Liming Fang, Lu-Tao Weng, Hongping Zhang, Youhong Tang, Fuzeng Ren, Cancan Zhao, Guoxing Sun, Rui Liang, and Zongjin Li. Mussel-Inspired Adhesive and Tough Hydrogel Based on Nanoclay Confined Dopamine Polymerization. *ACS nano*, 11(3):2561–2574, March 2017.

[261] Lu Han, Xiong Lu, Menghao Wang, Donglin Gan, Weili Deng, Kefeng Wang, Liming Fang, Kezhi Liu, Chun Wai Chan, Youhong Tang, Lu-Tao Weng, and Huipin Yuan. A Mussel-Inspired Conductive, Self-Adhesive, and Self-Healable Tough Hydrogel as Cell Stimulators and Implantable Bioelectronics. *Small*, 13(2):1601916, 2017.

[262] Zhen Tao, Hailong Fan, Junchao Huang, Taolin Sun, Takayuki Kurokawa, and Jian Ping Gong. Fabrication of Tough Hydrogel Composites from Photoresponsive Polymers to Show Double-Network Effect. *ACS Applied Materials & Interfaces*, 11(40):37139–37146, October 2019.

[263] Takayuki Nonoyama, Susumu Wada, Ryuji Kiyama, Nobuto Kitamura, Md Tariful Islam Mredha, Xi Zhang, Takayuki Kurokawa, Tasuku Nakajima, Yasuaki Takagi, Kazunori Yasuda, and Jian Ping Gong. Double-Network Hydrogels Strongly Bondable to Bones by Spontaneous Osteogenesis Penetration. *Advanced Materials*, 28(31):6740–6745, 2016.

[264] Zhengzhi Wang. Spatial and temporal tunability of magnetically-actuated gradient nanocomposites. *Soft Matter*, 15(15):3133–3148, April 2019.

[265] William M. Gramlich, Iris L. Kim, and Jason A. Burdick. Synthesis and orthogonal photopatterning of hyaluronic acid hydrogels with thiol-norbornene chemistry. *Biomaterials*, 34(38):9803–9811, December 2013.

[266] Hyemin Lee, Jun-Hyun Kim, Gaoxiang Wu, Hae-Min Lee, Jaekyoung Kim, Dokyeong Kwon, Shu Yang, Chang-Koo Kim, and Hyunsik Yoon. Clustering and Self-Recovery of Slanted Hydrogel Micropillars. *Advanced Materials Interfaces*, 5(24):1801142, 2018.

[267] Wenwei Lei, Shuanhu Qi, Qinfeng Rong, Jin Huang, Yichao Xu, Ruochen Fang, Kesong Liu, Lei Jiang, and Mingjie Liu. Diffusion–Freezing-Induced Microphase Separation for Constructing Large-Area Multiscale Structures on Hydrogel Surfaces. *Advanced Materials*, 31(32):1808217, 2019.

[268] Benjamin Kessel, Mihyun Lee, Angela Bonato, Yann Tinguely, Enrico Tosoratti, and Marcy Zenobi-Wong. 3D Bioprinting of Macroporous Materials Based on Entangled Hydrogel Microstrands. *Advanced Science*, 7(18):2001419, 2020.

[269] Amir Sheikhi, Joseph de Rutte, Reihaneh Haghniaz, Outman Akouissi, Alireza Sohrabi, Dino Di Carlo, and Ali Khademhosseini. Modular microporous hydrogels formed from microgel beads with orthogonal thermo-chemical responsivity: Microfluidic fabrication and characterization. *MethodsX*, 6:1747–1752, January 2019.

[270] Junji Saito, Hidemitsu Furukawa, Takayuki Kurokawa, Rikimaru Kuwabara, Shinya Kuroda, Jian Hu, Yoshimi Tanaka, Jian Ping Gong, Nobuto Kitamura, and Kazunori Yasuda. Robust bonding and one-step facile synthesis of tough hydrogels with desirable shape by virtue of the double network structure. *Polymer Chemistry*, 2(3):575–580, February 2011.

[271] Matteo Hirsch, Alvaro Charlet, and Esther Amstad. 3D Printing of Strong and Tough Double Network Granular Hydrogels. *Advanced Functional Materials*, n/a(n/a):2005929, 2020.

[272] David Chimene, Charles W. Peak, James L. Gentry, James K. Carrow, Lauren M. Cross, Eli Mondragon, Guinea B. Cardoso, Roland Kaunas, and Akhilesh K. Gaharwar. Nanoengineered Ionic–Covalent Entanglement (NICE) Bioinks for 3D Bioprinting. *ACS Applied Materials & Interfaces*, 10(12):9957–9968, March 2018.

[273] David Chimene, Logan Miller, Lauren M. Cross, Manish K. Jaiswal, Irtisha Singh, and Akhilesh K. Gaharwar. Nanoengineered Osteoinductive Bioink for 3D Bioprint-

ing Bone Tissue. *ACS Applied Materials & Interfaces*, 12(14):15976–15988, April 2020.

[274] Jian Hu, Takayuki Kurokawa, Kenta Hiwatashi, Tasuku Nakajima, Zi Liang Wu, Song Miao Liang, and Jian Ping Gong. Structure Optimization and Mechanical Model for Microgel-Reinforced Hydrogels with High Strength and Toughness. *Macromolecules*, 45(12):5218–5228, June 2012.

[275] Carlos F. Guimarães, Luca Gasperini, Alexandra P. Marques, and Rui L. Reis. The stiffness of living tissues and its implications for tissue engineering. *Nature Reviews Materials*, 5(5):351–370, May 2020.

[276] Shouling Ding, Bin Zou, Peng Wang, and Hongjian Ding. Effects of nozzle temperature and building orientation on mechanical properties and microstructure of PEEK and PEI printed by 3D-FDM. *Polymer Testing*, 78:105948, September 2019.

[277] Guo-Liang Ying, Nan Jiang, Sushila Maharjan, Yi-Xia Yin, Rong-Rong Chai, Xia Cao, Jing-Zhou Yang, Amir K. Miri, Shabir Hassan, and Yu Shrike Zhang. Aqueous Two-Phase Emulsion Bioink-Enabled 3D Bioprinting of Porous Hydrogels. *Advanced Materials*, 30(50):1805460, 2018.

[278] Zhe Chen, Donghao Zhao, Binhong Liu, Guodong Nian, Xiaokeng Li, Jun Yin, Shaoxing Qu, and Wei Yang. 3D Printing of Multifunctional Hydrogels. *Advanced Functional Materials*, 29(20):1900971, 2019.

[279] Wangqu Liu, Ozan Erol, and David H. Gracias. 3D Printing of an In Situ Grown MOF Hydrogel with Tunable Mechanical Properties. *ACS Applied Materials & Interfaces*, 12(29):33267–33275, July 2020.

[280] Yin Cheng, Kwok Hoe Chan, Xiao-Qiao Wang, Tianpeng Ding, Tongtao Li, Xin Lu, and Ghim Wei Ho. Direct-Ink-Write 3D Printing of Hydrogels into Biomimetic Soft Robots. *ACS Nano*, 13(11):13176–13184, November 2019.

[281] L. A. Hockaday, K. H. Kang, N. W. Colangelo, P. Y. C. Cheung, B. Duan, E. Malone, J. Wu, L. N. Girardi, L. J. Bonassar, H. Lipson, C. C. Chu, and J. T. Butcher. Rapid 3D printing of anatomically accurate and mechanically heterogeneous aortic valve hydrogel scaffolds. *Biofabrication*, 4(3):035005, August 2012.

[282] Junhua Wei, Jilong Wang, Siheng Su, Shiren Wang, Jingjing Qiu, Zhenhuan Zhang, Gordon Christopher, Fuda Ning, and Weilong Cong. 3D printing of an extremely tough hydrogel. *RSC Advances*, 5(99):81324–81329, September 2015.

[283] Sungmin Hong, Dalton Sycks, Hon Fai Chan, Shaoting Lin, Gabriel P. Lopez, Farshid Guilak, Kam W. Leong, and Xuanhe Zhao. 3D Printing of Highly Stretchable and Tough Hydrogels into Complex, Cellularized Structures. *Advanced Materials*, 27(27):4035–4040, 2015.

[284] Elia A. Guzzi, Giovanni Bovone, and Mark W. Tibbitt. Universal Nanocarrier Ink Platform for Biomaterials Additive Manufacturing. *Small*, 15(51):1905421, 2019.

[285] Biao Zhang, Shiya Li, Hardik Hingorani, Ahmad Serjouei, Liraz Larush, Amol A. Pawar, Wei Huang Goh, Amir Hosein Sakhaei, Michinao Hashimoto, Kavin Kowsari, Shlomo Magdassi, and Qi Ge. Highly stretchable hydrogels for UV curing based high-resolution multimaterial 3D printing. *Journal of Materials Chemistry B*, 6(20):3246–3253, May 2018.

[286] A. Sydney Gladman, Elisabetta A. Matsumoto, Ralph G. Nuzzo, L. Mahadevan, and Jennifer A. Lewis. Biomimetic 4D printing. *Nature Materials*, 15(4):413–418, April 2016.

[287] Ozan Erol, Aishwarya Pantula, Wangqu Liu, and David H. Gracias. Transformer Hydrogels: A Review. *Advanced Materials Technologies*, 4(4):1900043, April 2019.

[288] Yoonho Kim, Hyunwoo Yuk, Ruike Zhao, Shawn A. Chester, and Xuanhe Zhao. Printing ferromagnetic domains for untethered fast-transforming soft materials. *Nature*, 558(7709):274–279, June 2018.

[289] Lili Jia, Steve Evans, and Sander van der Linden. Motivating actions to mitigate plastic pollution. *Nature Communications*, 10(1):4582, October 2019.

[290] Matthew MacLeod, Hans Peter H. Arp, Mine B. Tekman, and Annika Jahnke. The global threat from plastic pollution. *Science*, 373(6550):61–65, July 2021.

[291] Zoé O. G. Schyns and Michael P. Shaver. Mechanical Recycling of Packaging Plastics: A Review. *Macromolecular Rapid Communications*, 42(3):2000415, 2021.

[292] AliReza Rahimi and Jeannette M. García. Chemical recycling of waste plastics for new materials production. *Nature Reviews Chemistry*, 1(6):1–11, June 2017.

[293] Simone Giaveri, Adeline M. Schmitt, Laura Roset Julià, Anna Murello, Laure Menin, Daniel Ortiz, Luc Patiny, Sreenath Bolisetty, Raffaele Mezzenga, Sebastian J. Maerkl, and Francesco Stellacci. Nature-inspired Circular-economy Recycling (NaCRe) for Proteins: Proof of Concept, September 2020.

[294] Weina Liu, Simone Giaveri, Daniel Ortiz, and Francesco Stellacci. DNA as a Recyclable Natural Polymer, September 2021.

[295] Alan M. Wemyss, Chris Bowen, Cédric Plesse, Cédric Vancaeyzeele, Giao T. M. Nguyen, Frédéric Vidal, and Chaoying Wan. Dynamic crosslinked rubbers for a green future: A material perspective. *Materials Science and Engineering: R: Reports*, 141:100561, July 2020.

[296] Lucie Imbernon and Sophie Norvez. From landfilling to vitrimer chemistry in rubber life cycle. *European Polymer Journal*, 82:347–376, September 2016.

[297] Lijing Teng, Yunhua Chen, Yong-Guang Jia, and Li Ren. Supramolecular and dynamic covalent hydrogel scaffolds: From gelation chemistry to enhanced cell retention and cartilage regeneration. *Journal of Materials Chemistry B*, 7(43):6705–6736, November 2019.

[298] Yi Li, Hong Yu Yang, and Doo Sung Lee. Advances in biodegradable and injectable hydrogels for biomedical applications. *Journal of Controlled Release*, 330:151–160, February 2021.

[299] M. Mario Perera and Neil Ayres. Dynamic covalent bonds in self-healing, shape memory, and controllable stiffness hydrogels. *Polymer Chemistry*, 11(8):1410–1423, February 2020.

[300] Benjamin R. Freedman, Oktay Uzun, Nadja M. Maldonado Luna, Anna Rock, Charles Clifford, Emily Stoler, Gabrielle Östlund-Sholars, Christopher Johnson, and David J. Mooney. Degradable and Removable Tough Adhesive Hydrogels. *Advanced Materials*, 33(17):2008553, 2021.

[301] Yang Gao, Kangling Wu, and Zhigang Suo. Photodetachable Adhesion. *Advanced Materials*, 31(6):1806948, 2019.

[302] Mélanie Despeisse and Simon Ford. The Role of Additive Manufacturing in Improving Resource Efficiency and Sustainability. In Shigeki Umeda, Masaru Nakano, Hajime Mizuyama, Hironori Hibino, Dimitris Kiritsis, and Gregor von Cieminski, editors, *Advances in Production Management Systems: Innovative Production Management Towards Sustainable Growth*, IFIP Advances in Information and Communication Technology, pages 129–136, Cham, 2015. Springer International Publishing.

[303] Malte Gebler, Anton J. M. Schoot Uiterkamp, and Cindy Visser. A global sustainability perspective on 3D printing technologies. *Energy Policy*, 74:158–167, November 2014.

[304] Margaret E. Prendergast and Jason A. Burdick. Recent Advances in Enabling Technologies in 3D Printing for Precision Medicine. *Advanced Materials*, 32(13):1902516, 2020.

[305] Elia A. Guzzi and Mark W. Tibbitt. Additive Manufacturing of Precision Biomaterials. *Advanced Materials*, 32(13):1901994, 2020.

[306] David Chimene, Roland Kaunas, and Akhilesh K. Gaharwar. Hydrogel Bioink Reinforcement for Additive Manufacturing: A Focused Review of Emerging Strategies. *Advanced Materials*, 32(1):1902026, 2020.

[307] Florian Hartmann, Melanie Baumgartner, and Martin Kaltenbrunner. Becoming Sustainable, The New Frontier in Soft Robotics. *Advanced Materials*, 33(19):2004413, 2021.

[308] Paul Bazylewski, Ranjith Divigalpitiya, and Giovanni Fanchini. In situ Raman spectroscopy distinguishes between reversible and irreversible thiol modifications in l -cysteine. *RSC Advances*, 7(5):2964–2970, 2017.

[309] Rosaria Ciriminna and Mario Pagliaro. Biodegradable and Compostable Plastics: A Critical Perspective on the Dawn of their Global Adoption. *ChemistryOpen*, 9(1):8–13, 2020.

[310] Jian Hu, Takayuki Kurokawa, Tasuku Nakajima, Zi Liang Wu, Song Miao Liang, and Jian Ping Gong. Fracture Process of Microgel-Reinforced Hydrogels under Uniaxial Tension. *Macromolecules*, 47(11):3587–3594, June 2014.

[311] Jian Hu, Takayuki Kurokawa, Tasuku Nakajima, Tao Lin Sun, Tiffany Suekama, Zi Liang Wu, Song Miao Liang, and Jian Ping Gong. High Fracture Efficiency and Stress Concentration Phenomenon for Microgel-Reinforced Hydrogels Based on Double-Network Principle. *Macromolecules*, 45(23):9445–9451, December 2012.

[312] Victoria G. Muir, Taimoor H. Qazi, Junwen Shan, Jürgen Groll, and Jason A. Burdick. Influence of Microgel Fabrication Technique on Granular Hydrogel Properties. *ACS Biomaterials Science & Engineering*, February 2021.

[313] Jinhua Li, Chengtie Wu, Paul K. Chu, and Michael Gelinsky. 3D printing of hydrogels: Rational design strategies and emerging biomedical applications. *Materials Science and Engineering: R: Reports*, 140:100543, April 2020.

[314] Takayuki Nonoyama, Yong Woo Lee, Kumi Ota, Keigo Fujioka, Wei Hong, and Jian Ping Gong. Instant Thermal Switching from Soft Hydrogel to Rigid Plastics Inspired by Thermophile Proteins. *Advanced Materials*, 32(4):1905878, 2020.

[315] Mike Ashby. Hybrid Materials to Expand the Boundaries of Material-Property Space. *Journal of the American Ceramic Society*, 94(s1):s3–s14, 2011.

ALVARO CHARLET

E-mail: alvaro.charlet@epfl.ch
Cell: + 41 (0)79 249 45 09

PROFILE

- **PhD on Soft Materials at EPFL**
- **Multicultural skills (3 fluent languages + long stays in different countries & continents)**
- **Interdisciplinary thinking**

BIRTH: June 4, 1993, Basel (Switzerland). German mother and French father.
French & German Citizenship

LANGUAGES: English (fluent), French and German (mother tongues)
Italian (B2), Swedish (A2)

ADDRESS: Chemin François-de-Lucinge 3, CH-1006 Lausanne

EDUCATION

2014-2017 Master Diploma in Materials Science Engineering, *EPFL Lausanne, Switzerland*
2011-2014 B.Sc. in Materials Science Engineering, *EPFL, Lausanne, Switzerland (thesis: Powder Metallurgy)*
2009-2011 Lycée International, AbiBac Diploma (French / German), with Distinction, *Grenoble, France*
2008-2009 Lowell High School, *San Francisco, California, USA*

RESEARCH EXPERIENCE

2017-present Mechanical reinforcement of hydrogels through physical crosslinks and double network granular architecture, *PhD at the Laboratory of Soft Materials under the supervision of Esther Amstad, EPFL Lausanne, Switzerland*
2016-2017 A bio-inspired double network hydrogel, *master thesis at the Laboratory for Bio-inspired Interfaces under the supervision of Niels Andersen-Holten, MIT, Boston, USA*
2015-2016 Nano-gratings for novel optic based anti-counterfeiting and solar energy harvest applications, *9 months research internship at CSEM SA under the supervision of Benjamin Gallinet, Basel, Switzerland*
2015 (summer) Computational molecular surface simulations "The Pyrite Case", *voluntary summer research project at the Laboratory of Geological Molecular Science, under the supervision of Kideok Kwon, KNU, Chuncheon, S. Korea*
2014-2015 SOLAR Association Board Member, *an international cross-disciplinary student competition (SolarDecathlon) to build and operate a full-scaled solar-powered house, Fribourg-Geneva-Lausanne*
2015 (spring) Electronic and transport properties of two-dimensional materials using Wannier functions, *Research semester project at the THEOS group under the supervision of Nicola Marzari, EPFL*
2014 (autumn) Tuning the wettability of surfaces using micro-particles, *Research semester project at the Laborytory of Soft Materials under the supervision of Esther Amstad, EPFL*
2014 (spring) Characterisation of graphite grades for the sintering of powder metallurgy steels, *bachelor thesis under the supervision of Eduard Hryha, Chalmers Institute of Technology, Gothenburg Sweden*

SKILLS Technical know-how in Rheology, Raman, Thin Films, Microfluidics, Soft Matter
Public speaking, TEDx speaker, coding in python, bash scripting

PERSONNAL INTERESTS
Art : *Industrial Design, Architecture, Artisanal Craftsmanship*
Sport : *Sailing, Climbing, Tennis, Ski Touring*


SMaL